DISSERTATION

Charge Separation and Transport in Organic Solar Cells Studied by Electron Paramagnetic Resonance Spectroscopy

Im Fachbereich Physik der Freien Universität Berlin
eingereichte Dissertation zur Erlangung des Grades eines

Doktors der Naturwissenschaften (Dr. rer. nat.)

vorgelegt von

M. SC. KEN FELIX KRAFFERT

aus Cuxhaven

eingereicht am
15. August 2017

Freie Universität Berlin

THIS IS A CUMULATIVE WORK CONTAINING THE FINDINGS OF THE ARTICLES LISTED IN "LIST OF PUBLICATIONS".

1. Gutachter:
Prof. Dr. Jan BEHRENDS
2. Gutachter:
Prof. Dr. Martin WEINELT
3. Gutachter:
Prof. Dr. Karl LEO

Tag der Disputation:
09. April 2018

Summary

Charge Separation and Transport in Organic Solar Cells Studied by Electron Paramagnetic Resonance Spectroscopy

by M. Sc. Ken Felix KRAFFERT

This thesis presents a comprehensive study of organic solar cells (OSCs) by electron paramagnetic resonance (EPR) techniques. Magnetic resonance techniques use the spin of charged particles as a probe to measure interactions of the excitations relevant for organic solar cells such as spin-$\frac{1}{2}$ polarons, charge-transfer (CT) states, spin-1 triplets and spin-2 quintet states. EPR spectroscopy is a powerful method to discover processes within solid state molecular materials. Time-resolved EPR techniques allow observation of dynamic molecular processes such as electron transfer from a donor to an acceptor molecule and spin-dependent processes such as hopping transport or charge-carrier recombination. This thesis focuses on the spin states generated during charge separation from an initial photo-excited exciton into separated (free) polarons. Intermediate states such as CT states and higher spin states including triplets or quintets are extensively studied. To observe and investigate these states, various organic semiconductors were explored in the form of thin films or bulk-heterojunction blends with time-resolved EPR and electrically detected magnetic resonance (EDMR).

Firstly, in this thesis we develop a semi-analytical simulation code for multi-frequency EPR spectra of CT states. This code involves both dipolar and exchange coupling between the polarons. In combination with multi-frequency experiments the simulations show that it is generally necessary to include exchange as well as dipolar interactions for CT state simulations. We apply rate equation models in combination with EPR spectrum simulations to study the generation of triplet excitons in low-bandgap organic photovoltaic materials. We investigate interfacial triplets appearing in donor:acceptor blends based on the much sought after non-fullerene acceptors.

Secondly, building on this insight on triplet signatures EPR is used on highly interesting singlet fission materials to prove the occurrence of weakly and strongly exchange coupled triplets generated by singlet fission.

Additionally, this work contains technique developments: We introduce a new method called transient EDMR (trEDMR), a combination of time resolved EPR and electrical detection known from EDMR. The method demonstrates how short-lived EPR signatures influence the macroscopic conductivity of a complete solar cell. A miniaturized encapsulated OSC design was developed that fits into commercial EPR resonators to enable EDMR measurements of oxygen-sensitive OSCs. This setup was also applied to complex organic tandem solar cells which were investigated with pulsed EDMR methods. We visualize that a triplet-exciton quenching process occurring within the acceptor domains of a high-efficient tandem solar cell influences its photo-conductivity.

Finally, in a combined optical, electrical and EPR study we show that the new p-type dopant, the Lewis acid BCF, reliably, stably, and efficiently dopes an organic semiconductor and thereby massively increases the conductivity of the doped layer.

These studies open up new perspectives for subsequent investigations of OSCs by magnetic resonance techniques.

Zusammenfassung

Ladungstrennung und -transport in Organischen Solarzellen untersucht mit Elektronenspinresonanz-Spektroskopie

von M. Sc. Ken Felix KRAFFERT

Die vorgestellte Doktorarbeit ist eine umfassende Studie zu organischen Solarzellen (OSZ) basierend auf Elektronspinresonanz Spektroskopie (ESR). Diese nutzt den Spin der geladenen Teilchen als Sonde, um Ladungsträgerinteraktionen von relevanten angeregten Zuständen zu untersuchen, wie z.B. Polaronen (Spin-$\frac{1}{2}$), Ladungstransferzustände (LTZ), Triplett-Exzitonen (Spin-1) oder Quintett-Exzitonen (Spin-2). ESR ist eine vielseitige Methode um molekulare Prozesse in Festkörpern und Molekülen zu analysieren. Zeitaufgelöste ESR-Techniken ermöglichen hierbei auch die Beobachtung von dynamischen molekularen Prozessen, wie den Elektronentransfer von einem Donator- zu einem Akzeptormolekül oder spinabhängige Prozesse, wie Ladungsträger-Hüpftransport oder -Rekombination. Unser Fokus liegt auf Spin-Zuständen, die während des Ladungstrennungsprozesses von Exziton auftreten, beispielsweise LTZ, Triplett- und Quintett-Zustände. Um diese zu analysieren wird eine Vielzahl von organischen Halbleitern mittels zeitaufgelöster ESR und elektrisch detektierter magnetischer Resonanzspektroskopie (EDMR) untersucht.

Der erste Teil dieser Arbeit behandelt die Entwicklung eines teilweise analytischen Simulationscodes um LTZ in mehreren ESR-Frequenzen spektral zu beschreiben. Die Simulation beinhaltet sowohl dipolare als auch Austauschkopplungen. Die Kombination von ESR-Messungen in zwei Frequenzen und den dazugehörigen LTZ-Simulationen konnte zeigen, dass es im Allgemeinen notwendig ist, beide Kopplungen zu berücksichtigen. Weiterhin untersuchen wir den Entstehungsmechanismus von Triplett-Exzitonen in organischen Mischsystemen, die vielversprechende Halbleiter mit kleiner Bandlücke enthalten, indem wir spektrale Simulationen von Experimenten mit einem Ratenmodell verknüpfen. Ein angegliedertes Projekt befasst sich mit Grenzflächen-Tripletts in Donator-Akzeptor-Mischzellen, die auf aktuell stark nachgefragten Fulleren-freien Akzeptoren basieren.

Im zweiten Teil nutzen wir erlangtes Wissen über Tripletts in der ESR-Spektroskopie, um viel diskutierte "Singlet-Fission" (SF) Materialien zu untersuchen. Wir weisen nach, dass SF in TIPS-Tetracen auftritt und sowohl schwach- als auch stark-gekoppelte Triplett-Exzitonen erzeugt. Wir beschreiben die Neuentwicklung einer transiente EDMR genannten Methode, die eine Kombination der transienten ESR und elektrischer Detektion ist. Hierdurch kann der Einfluss von kurzlebigen ESR-Signaturen auf die Leitfähigkeit von Solarzellen gezeigt werden. Ein miniaturisiertes Design für verkapselte OSZ wird vorgestellt, dass EDMR-Messungen an kompletten OSZ innerhalb eines ESR-Resonators ermöglicht. Dieses Design wird in der Folge auch für komplexere organische Tandemsolarzellen (OTSZ) verwendet. Gepulste EDMR zeigt den Einfluss von Triplett-Exzitonen-Vernichtungsprozessen auf den Photostrom in effizienten OTSZ.

Im dritten Teil wird eine Kooperationsstudie vorgestellt, in der optische, elektrische und ESR-Messungen kombiniert werden, um einen neuen p-Dotanten, die Lewis-Säure BCF, für organische Halbleiter zu charakterisieren.

Schließlich zeigt die Arbeit neue Perspektiven für zukünftige Untersuchungen von organischen Solarzellen mit Elektronspinresonanz auf.

List of Publications

This sections lists, in order of appearance, FELIX KRAFFERT's publications:

[FK1] F. Kraffert, R. Steyrleuthner, S. Albrecht, D. Neher, M. C. Scharber, R. Bittl, and J. Behrends. "Charge Separation in PCPDTBT: PCBM Blends from an EPR Perspective". In: *Journal of Physical Chemistry C* 118.49 (2014), pp. 28482–28493. DOI: 10.1021/jp509650v.

[FK2] M. Schubert, B. A. Collins, H. Mangold, I. A. Howard, W. Schindler, K. Vandewal, S. Roland, J. Behrends, F. Kraffert, R. Steyrleuthner, Z. H. Chen, K. Fostiropoulos, R. Bittl, A. Salleo, A. Facchetti, F. Laquai, H. W. Ade, and D. Neher. "Correlated Donor/ Acceptor Crystal Orientation Controls Photocurrent Generation in All-Polymer Solar Cells". In: *Advanced Functional Materials* 24.26 (2014), pp. 4068–4081. DOI: 10.1002/adfm.201304216.

[FK3] F. Kraffert, R. Steyrleuthner, C. Meier, R. Bittl, and J. Behrends. "Transient electrically detected magnetic resonance spectroscopy applied to organic solar cells". In: *Applied Physics Letters* 107.4 (2015), 43302(1–5). DOI: 10.1063/1.4927446.

[FK4] L. R. L. Weiss, S. L. S. Bayliss, F. Kraffert, K. K. J. Thorley, J. E. J. Anthony, R. Bittl, R. H. R. Friend, A. Rao, N. N. C. Greenham, and J. Behrends. "Strongly exchange-coupled triplet pairs in an organic semiconductor". In: *Nature Physics* 13 (2017), pp. 176–181. DOI: 10.1038/nphys3908.

[FK5] P. Pingel, M. Arvind, L. Kölln, R. Steyrleuthner, F. Kraffert, J. Behrends, S. Janietz, and D. Neher. "p-Type Doping of Poly(3-hexylthiophene) with the Strong Lewis Acid Tris(pentafluorophenyl)borane". In: *Advanced Electronic Materials* 2.10 (2016), 1600204(1–7). DOI: 10.1002/aelm.201600204.

[FK6] R. Steyrleuthner, Y. Zhang, L. Zhang, F. Kraffert, B. P. Cherniawski, R. Bittl, A. Briseno, J.-L. Bredas, and J. Behrends. "Impact of Morphology on Polaron Delocalization in a Semicrystalline Conjugated Polymer". In: *Physical Chemistry Chemical Physics* 19.5 (2017), pp. 3627–3639. DOI: 10.1039/C6CP07485E.

[FK7] F. Kraffert and J. Behrends. "Spin-correlated doublet pairs as intermediate states in charge separation processes". In: *Molecular Physics* 115.19 (2017), pp. 2373–2386. DOI: 10.1080/00268976.2016.1278479.

[FK8] F. Kraffert, D. Bahro, C. Meier, M. Denne, A. Colsmann, and J. Behrends. "Transport-related triplet states and hyperfine couplings in organic tandem solar cells probed by pulsed electrically detected magnetic resonance spectroscopy". In: *Journal of Magnetic Resonance* 282 (2017), pp. 10–17. DOI: 10.1016/j.jmr.2017.06.015.

Contents

1 Introduction

Climate change has been widely recognized, mandating a more responsible use of fossil fuels.[1] As a result, there has been a global shift towards renewable energy sources, with wind and solar power becoming more predominant in today's energy mix.[2] Different models show that a high share of renewable energy sources is feasible.[3] Furthermore, the price for the renewable energy production by photovoltaics and wind power plants has decreased during recent years.[4] It is even believed that in the long term the shift towards renewable sources will lead to a cost reduction of energy production as techniques get refined and new technologies are commercialized,[5] for example organic photovoltaics, which this thesis focuses on. The energy cost prediction for 2022 published recently by the U.S. Energy Information Administration estimates the levelized energy costs of photovoltaic plants to be 58.1 $/MWh, comparable to those of natural gas 58.6 $/MWh.[6]

After the initial development of silicon solar cells, they became the most successful commercialized *first generation* solar cell technology in the early nineties. Some years later a technology based on thin films arose such as poly-crystalline silicon, copper indium diselenide and amorphous silicon. The reduced material costs by eliminating silicon wafers have created a *second generation* of photovoltaics which has supported the growth of the photovoltaic industries.[7] For industrial production the most important parameter is the power per unit price. This requires both the optimization of the power-conversion efficiency and cost per square meter of the solar cells. This sparked again the next generation of solar cells. While the *first generation technology* is still the most efficient (best PCEs over 25%[8]) and the *the second generation* (best PCEs over 20%[9,10]) is comparable cheap, the idea of a *third generation* came up which could beat conventional loss limits and use entirely new material system not based on silicon.

Third generation solar cells aims to use the high and low energy solar photons more efficiently. Tandem solar cells, singlet fission based solar cells (multiple electron-hole pair generations per incident photon) and thermoelectric approaches are all being considered.[7] Additionally, new molecular-based material systems, e.g. dye-sensitized solar cells and organic solar cells (OSCs), are being investigated, which may realize some of these new concepts.

Organic solar cells are the main focus of this thesis, thus the following section provides an overview of organic solar cells.

1.1 State of the Art of Organic Solar Cells

Organic semiconductors already play an important role in the semiconductor industry because of their comparably low production costs,[11] their mechanical flexibility,[12] and their amazing variety in emitting and absorbing colors in contrast to silicon based devices. One very successful product based on organic semiconductors are organic light-emitting diodes (OLEDs). OLEDs are elements of many smartphone and TV screens and are famous for their intensive colors, very thin and flexible screens and low power consumption.[13] OSCs are more or less the opposite of OLEDs but

are not yet on the market. They have undergone a strong increase of their power-conversion efficiencies during the last decade. OSCs have exceeded certified efficiencies of 13%,[14,15] which makes them interesting for industrial applications. The German company *BELECTRIC* already implemented a first roll-to-roll printing setup to automatically produce solar cell panels. They were awarded for their product line "OPVIUS" with the price for *architecture and building*.[16] Another market leader of organic photovoltaic (OPV)-panels *HELIATEK* specializes in vacuum evaporation deposition and also has a first roll-to-roll production line.[17] Their market concept is to promote OSCs in application areas which are not accessible to classical photovoltaics, like shadowed building facades or roofs of cars and trucks. Despite these first industrial successes, many basic processes in OSCs are still unknown. Unfortunately, OSCs are not yet stable and efficient enough to have large-scale commercial application.

Most record efficiencies have been achieved on solar cells that were empirically optimized. Targeted improvements were not possible because of a missing understanding about the fundamental loss mechanisms. One major reason for this lack of knowledge is the evolution of the materials to more complicated and disordered soild-state structures.[15] Therefore, one key question within our investigations is to figure out fundamental reasons why some of the developed materials show low and others high performances. In some cases the power-conversion efficiency of a solar cell differs by a factor of two, although just one single atom in the donor polymer is exchanged.[FK1,18]

An important issue in the further improvement of OSCs is to find an alternative acceptor that outperforms the widely-used fullerene derivatives. Fullerenes have been the dominant acceptors for OSCs during the last decade while improvements of donor molecules and polymers have been the main reason for OPV efficiency enhancements. Many different acceptors with electron-transport properties better than those of fullerenes were tried during the last years (one example is given in [FK2]) but could not compete with fullerene-derivatives. Just very recently OSCs based on non-fullerene acceptors yielded extremely high power-conversion efficiencies (above 11 % for single junctions).[19–21] Nevertheless, PCBM (a fullerene with side chain) is still the dominant acceptor on the market. The very efficient charge separation on donor:fullerene interfaces[1] often compensates lower electron mobilities. Therefore, good knowledge of the molecular charge-separation processes is an important research interest. One key question that remains is the importance of charge-transfer (CT) states in OSCs.[22–27] Some people found low solar-cell efficiencies to be connected with long-lived CT states that show a low dissociation yield.[28] Other studies define low energetic CT states as unimportant and emphasize vibrational excited (*hot*) CT states as the crucial states for the charge separation.[29–33] In contrast, other groups report on efficient charge separation independent of the excitation energy and thus prove the importance of CT states which are in the vibrational ground state.[34–36] These ambiguous results show that processes in OSCs are system-dependent and that not an overall description can be determined. Therefore, it is important to develop good characterization procedures to investigate various OSC materials.

A variety of optical and electrical spectroscopic methods have been applied to investigate charge-transfer states. Unfortunately, it can be difficult to distinguish between CT states and e.g. triplet excitons or free polarons by optical spectroscopy such

[1] The term *donor:fullerene* describes a bulk-heterojunction of a donor material blended with a fullerene derivative.

as transient absorption (TA),[27,30,37] photoinduced absorption (PIA),[22,38] electroluminescence (EL),[22,39] and photoluminescence (PL) spectroscopy[40–43] due to their overlapping signatures. A detailed knowledge of the spectral signatures of CT-state formation and dissociation is therefore necessary to identify CT states unambiguously.

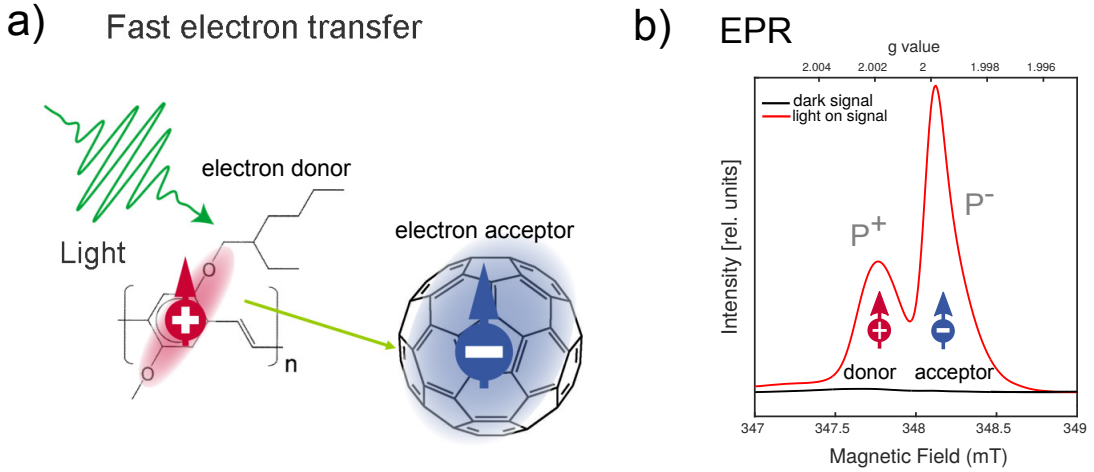

Figure 1.1.1: a) Visualization of fast electron transfer from an electron donor (MEH-PPV) to an electron acceptor (C_{60}) first observed in 1992 by Sariciftci *et al.* [44]. b) Integrated cwEPR measurement on up-to-date low band gap polymers (donor) blended with a fullerene derivative (acceptor). The experiment shows the separated positive and negative polarons located on the donor and the acceptor.

Electron paramagnetic resonance spectroscopy (EPR) uses the paramagnetic properties – the spin (S) – of the charge carrier, e.g. an electron or polaron ($S = \frac{1}{2}$), to distinguish between weakly coupled electron-hole pairs such as CT states, strongly coupled electron-hole pairs such as triplet excitons or strongly coupled triplet pairs (quintet states). All these states can be distiguished by EPR spectroscopy because of their unambiguous EPR signatures. EPR has previously successfully been applied to investigate triplet excitons and CT states in a research field similar to organic photovoltaics, the investigation of photosynthetic reaction centers and organic crystals.[45–48] Building on this knowledge, Sariciftci *et al.* [44] performed one of the first OPV-related EPR experiments. They measured a photoinduced electron transfer from a conducting polymer to a fullerene with EPR (visualized in Fig. 1.1.1a). Figure 1.1.1b shows two EPR spectra: one with the OPV absorber blend kept in dark (black line) and another one under continuous illumination. The light continuously generates free charges in the absorber. The spectral separation of the electron signal located on the acceptor (negative polaron P^-) and a hole on the donor (positive polaron P^+) is clearly visible in the measurement. Their experiments lay the foundation for many follow-up studies of organic semiconductors by EPR.

1.2 About this Thesis

This doctoral thesis studies the charge-excitation and separation processes in OSCs with a variety of EPR methods. It also includes the development of a new electrically-detected magnetic resonance (EDMR) technique to study the influence of spin-dependent processes on the photocurrent of OSCs.
Within this thesis, EPR spectroscopy is used in organic photovoltaics

- to investigate photoinduced charges on different organic solar cell materials (see [FK1, 49–56]),
- to determine hyperfine couplings between polarons and nuclei (see [FK6, 57, 58]),
- to count charge densities in doped organic semiconductors (see [FK5, 59]),
- to determine delocalization lengths of polarons on organic semiconductors, (see [FK6, 58]),
- to observe weakly coupled CT states (see [FK1, FK3, FK7, 60, 61]),
  strongly coupled triplet excitons (see [FK1, FK2, FK8, 56, 62]),
  as well as quintet states (see [FK4, 63]).

The following EPR methods have been especially decisive for analyzing CT states, triplet excitons and for determining inter-charge couplings like polaron-polaron and polaron-nuclear couplings:

- pulsed electron nuclear double resonance (see [FK6, 57, 58]),
- out-of-phase electron spin echo envelope modulation (OOP-ESEEM) (see [64]),
- transient EPR and time-resolved pulsed EPR spectroscopy (see [FK1, FK3, 56, 60, 61, 65, 66])

More recently, the electrical detection scheme of EDMR is used to measure spin-dependent transport and recombination in OSCs (see [FK3, FK8, 62, 67–70]). In addition, we combine EPR and EDMR measurements to correlate spin-dependent effects on the photocurrent to signatures determined by conventional EPR in full solar-cell architectures (see [FK3]).

This cumulative work combines the findings of the publications listed in "List of Publications" to an interconnected story. The thesis focuses on three core themes:

1. *Charge separation in organic donor-acceptor materials*
2. *Exceeding the conventional efficiency limits of OSCs*
3. *Determining charge-carrier delocalization and concentration*

It is structured in the following way:

Chapter 2 gives an introduction to the fundamentals of OSCs and EPR. This chapter starts with a description of OSCs and continues with general charge-separation processes. In the second part the principles of EPR and EDMR are introduced.

Chapter 3 constitutes the heart of this work. This chapter presents the *charge separation in donor-acceptor materials* and is composed of four publications. It starts with an overview of charge-separation pathways based on [FK1] and afterwards focuses on the formation of CT states investigated in [FK3, FK7]. Further on, it contains the development of the new technique transient EDMR. The second part of this chapter describes triplets in OSCs, which were studied in [FK1] and [FK2].

Chapter 4 presents a complementary research direction: *exceeding the conventional efficiency limits of OSCs* and *determining charge-carrier delocalization and concentration*. This chapter is composed of three publications [FK4, FK5, FK8]. It shows results from singlet-fission materials published in [FK4] and continues with a study about EDMR effects in organic tandem solar cells published in [FK8]. Finally, a new doping material for p-type doping in organic semiconductors is investigated with different spectroscopic methods. This study was published in [FK5].

Chapter 5 delivers a summary and a conclusion of the most relevant findings from chapters 3 and 4. Furthermore, an outlook for future work is provided.

Appendix A contains an overview of the experimental setups used for EPR and EDMR spectroscopy.

Appendix B contains the full publications which form this thesis.

2 Fundamentals

2.1 Organic Solar Cells

Organic solar cells mimic mechanisms from biological photosystems in order to convert solar energy into usable energies like electrical or chemical energy. The name "organic solar cells" is used in contrast to "inorganic solar cells" like crystalline silicon or "thin-film" solar cells, because of the π-conjugated small molecules and polymers which form their absorber layers. Within this thesis we mainly investigated donor polymers in combination with fullerene acceptors.

2.1.1 Exemplified Structure of an Organic Solar Cell

Figure 2.1.1 shows a simplified layer structure of an OSC. A polymer-fullerene solar cell contains a transparent substrate, for example a quartz glass or a thin transparent plastic foil. The upper side of the glass substrate is covered by a transparent conducting oxide (TCO), often indium tin oxide (ITO). This layer forms the front electrode (cathode). On top of this conducting layer an optional interlayer (e.g. PEDOT:PSS[1]) can be placed for the reduction of shunts and adjustment of the work-function. The following active layer (absorber) consists either of a double layer structure with one donor and one acceptor layer or a blend, i.e. a mixture of the donor and acceptor material (bulk heterojunction). On top of the cell a metal is evaporated acting as the back electrode (anode).

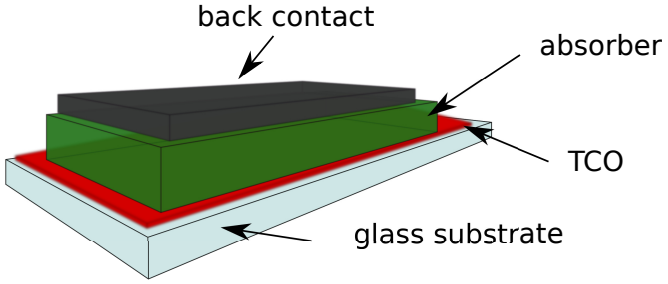

Figure 2.1.1: Model of an organic solar cell. An OSC can contain a transparent glass as carrier substrate. Next, a layer of a transparent conductive oxide (TCO), in most cases indium tin oxide (ITO) is used as front electrode. The layer above is the active medium, also called absorber that appears mainly in two different structures, the blend and the bi-layer structure. The electronic back contact is realized by a metal layer (e.g. aluminum). The cell is illuminated through the glass substrate.

Most of the measurements presented within this work are based on blend-structured absorbers. In the last decade several organic materials were investigated or developed for the use in organic solar cells leading to rapid power-conversion efficiency increase. In order to understand the underlying mechanisms, we studied many different blends as well as fully-processed solar cells in fruitful cooperation with our collaborator from the university of Potsdam,[FK1,FK2,FK5,FK6] the Fraunhofer IAP,[FK5] the university of Cambridge,[FK4] and the Karlsruhe Institute of Technology.[FK8] All

[1]Poly(3,4-ethylenedioxythiophene) poly(styrenesulfonate)

investigated materials and systems are described in the experimental details of these publications.

2.1.2 The Charge Separation within Organic Solar Cells

The investigation of the charge separation within OSCs is one main topic of this work. The following section contains technical terms printed in bold letters that are explained in more detail in Sec. 2.1.3.

After the initial generation of an excited state in an OSCs, several deactivation pathways are possible. The pathway for an ideal or highly efficient solar cell is demonstrated in Fig. 2.1.2. The most relevant alternative routes are described later in Sec. 2.1.3.

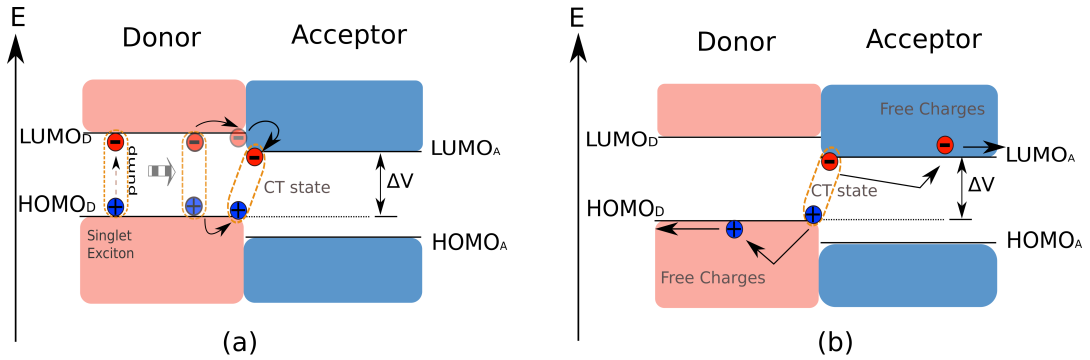

Figure 2.1.2: Schematic representation of the efficient charge-separation mechanism in OSCs. (a) A singlet **exciton** is generated by photon absorption and moves to a donor-acceptor interface. An electron is transferred to the acceptor and forms a CT state. (b) The CT state dissociates into two free charges, which can be extracted at charge specific electrodes. The energy levels LUMO$_D$ and HOMO$_D$ correspond to the donor material, and LUMO$_A$ and HOMO$_A$ to the acceptor molecule. The maximal possible potential of a solar cell with this combination of donor and acceptor is given by ΔV.

If a photon is absorbed by the donor, an electron is excited via an electronic transition from the HOMO level of the donor into its LUMO level and forms a strongly coupled **exciton** (see Fig. 2.1.2a). Note that an **exciton** can also be formed after photon absorption in the acceptor. For charge separation the **exciton** has to reach the donor-acceptor interface by diffusion. This requires the lifetime and the corresponding diffusion length of the **exciton** to be larger than the distance between the **exciton** creation and dissociation locations. Typical lifetimes for singlet **excitons** in organic semiconductors are approximatively 1 ns at room temperature.[71] If this criterion is not fulfilled, geminate recombination will occur and the absorbed energy will be lost to heat or radiation.

When a donor-acceptor interface is reached, the electron is transferred to the acceptor and a **CT state** arises (see Fig. 2.1.2b). This **exciton** dissociation only takes place, if the energy of the **exciton** is larger than the energy of the emerging **CT state** (also called weakly coupled **polaron** pair) after the electron transfer.[71] Therefore, a distinct energetic difference between both LUMOs and HOMOs levels is necessary. This charge-transfer process is stated to be extremely fast – in the range of femtoseconds at room temperature.[72,73]

After the **CT state** dissociation into free uncoupled **polarons**, a positively charged quasi-particle in the donor material and a negatively charged quasi-particle in the acceptor material can be transported to the selective electrodes. In the case of organic

non-crystalline molecules this transport takes place, in general, by hopping from one localized state to the next one. The mobility and charge-carrier concentration of organic semiconductors are lower than those of silicon-based solar cells. This results in shorter diffusion lengths of charges in the organic absorber materials.[74] To avoid non-geminate recombination of charges that are not able to reach an electrode, very thin absorber layers are required in comparison to silicon solar cells ($d_{\text{OSC}} \sim 100$ nm[75] versus $d_{\text{Si-Solar cell}} \sim 100 - 500\,\mu\text{m}$[76,77]).

This charge separation process is valid for both bi-layer structured OSCs and bulk-heterojunction OSCs. A bi-layer structured solar cell consists of a donor and an acceptor layer that are stacked on top of each other without an overlapping or intermixed region. The bulk heterojunction concept, mentioned before, is more suitable for organic solar cells.[71] The blend morphology enables very short distances between the **exciton** creation and dissociation. Unfortunately this also results in lower conductivities for the charge-carrier extraction into the electrodes due to the low crystallinity of the phases.

A quantum-mechanical description of triplet **excitons** and **CT states** in a magnetic field, based on their spin-interaction Hamiltonian of these states, will be given in Sec. 2.2.3 and Sec. 2.2.5, respectively. A description of the charge separation from an EPR point of view will be presented in chapter 3.

2.1.3 The Physics of Organic Solar Cells

This section presents an overview on the most important processes and states occurring in OSCs that are relevant for our EPR studies. More details about the physical effects of solar cells in general are well described in the book "Third Generation Photovoltaics" by Martin Green.[7] Another well-written book that is more focused on OSCs and organic semiconductors is the book "Electronic Processes in Organic Semiconductors" by Anna Köhler and Heinz Bässler.[74]

States in OSCs

Organic solar cells provide several different quantum-mechanical configurations of charges, states, that differ e.g. by their inter-charge interaction or by their spin multiplicity. In the following, I introduce the three most important states that appear during the charge-separation process of OSCs.

An exciton is a strongly bound electron-hole pair which is located in a single material phase and has a certain binding radius. An exciton can be either in a singlet ($S = 0$) or a triplet spin state ($S = 1$), since electrons and holes are both spin-$\frac{1}{2}$. Due to the selection rule for electronic transitions $\Delta S = 0$, only singlet excitons (EPR silent) can be created out of a singlet precursor state. Singlet excitons can also be converted into triplet excitons (EPR active) by **intersystem crossing** or by **singlet fission**. The EPR signatures of triplet excitons are discussed in detail in Sec. 2.2.3.

A CT state is a weakly bound polaron pair coupled by Coulomb interaction. The binding energy of a CT state is in general smaller than 0.5 eV, which describes the lower limit of the binding energy of excitons.[78] Such a polaron pair is created, if the electron or the hole has already been transferred to the acceptor or donor material, respectively, but is still coupled by Coulomb interaction (see Fig. 2.1.2).[71] For a fast charge separation the dissociation time of the CT state has to be very quick. The Polaron pair dissociation is described by the Braun-Onsager model,[79,80] which gives the

dissociation probability $P(E)$ as

$$P(E) = \frac{k_d(E)}{k_d(E) + k_r}, \tag{2.1.1}$$

with the electric field E, the recombination rate of the polaron pair k_r and the electric field-dependent dissociation rate $k_d(E)$.[71] The EPR signatures of CT state are discussed in detail in Sec. 2.2.5.

A polaron is a charged quasi-particle (hole or electron) that deforms the energetic environment of the charge. Crucially, in organic molecules an additional charge deforms the whole structure and strongly influences the electronic transport properties of the molecule. The EPR signatures of polarons are discussed in detail in Sec. 2.2.6.

Relaxation Processes

After the excitation of an electron into a higher electronic singlet state (singlet exciton) with an excited vibrational level, several types of relaxation can occur before the exciton either reaches a donor-acceptor interface or is completely relaxed to the ground state. Fig. 2.1.3 visualizes the Jablonski diagram for the deactivation pathways of e.g. a pure donor material in absence of an acceptor.[81] In case of a pristine donor material all excited states decay finally to the ground state. If an acceptor is available, e.g. in a blend structure, recombination is competing with charge separation. In order to produce solar cells with a high charge-separation yield, a good knowledge about possible recombination mechanisms is important.

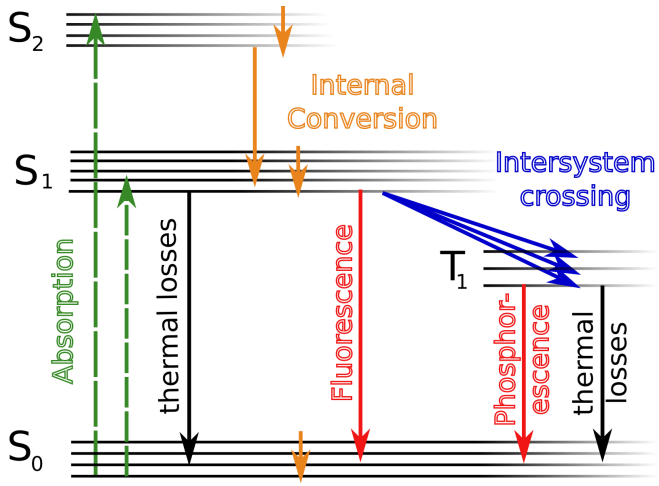

Figure 2.1.3: Jablonski scheme of possible deactivation pathways of e.g. a pristine donor material. The relaxation process from the first excited S_1 state or even from S_2 may occur in different ways.The probability of intersystem crossing to T_1 is small compared to the probability of other processes as described in the text. One can observe a modulation of the absorption- and fluorescence transition by the vibrational modes. Transitions with small ΔE are naturally faster than transitions with large energy differences. Thermal losses are part of non-radiative recombination.

Internal conversion describes the process of intermolecular energy exchange of an excited charge with its environment caused by collisions, e.g. polaron-phonon interaction. This process occurs for relaxations from higher vibrational states to lower ones, because smaller energy steps are preferred and the energy difference between vibrational states is less than between electronic states. Therefore, the transition rates are on the order of 10^{12}-$10^{13}\,\mathrm{s}^{-1}$, much faster than the other relaxation processes shown in Fig. 2.1.3.

Charge-carrier recombination is one of the major problems of organic solar cells. Low charge-carrier mobilities in organic molecules result in short diffusion lengths. Thus, charge-carrier recombination can occur before the charge separation is achieved. There are two types of recombination, radiative and non-radiative. The radiative recombination is much less deleterious to the cell performance because the emitted radiation can be absorbed again by the active layer. In contrast, non-radiative recombination always causes a loss in power-conversion efficiency.

Intersystem crossing (ISC) is the relaxation of the S_1 state to the T_1 triplet state, which is a possible but not favorable process.[82] An unpaired electron spin is flipped and the multiplicity of the state is changed. Spin-orbit coupling allows ISC to violate the selection rule $\Delta S = 0$. Thus ISC is usually much slower than singlet-singlet transitions. This relaxation process is non-radiative and a large overlap between the transition states is required because no or only little energy has to be gained or lost by vibrations. Since this process is driven by spin-orbit coupling, heavy atoms like iodide or bromide or even silicon in the surrounding can increase the probability of ISC. The ISC times for polymers are in the range of nanoseconds.[83] The radiative decay of a triplet state into a singlet ground state is called phosphorescence and is orders of magnitudes slower than fluorescence, which would appear in case of a singlet-singlet radiative decay.

Back electron-transfer (BET) is an alternative mechanism to generate triplet excitons. Here, triplets are populated by back electron-transfer over the interface during CT-state recombination. This alternative relaxation from a CT state is observed in different types of material systems: e.g. zeolites,[84] photosynthetic reaction centers,[47,85] and also organic polymers.[FK1,86,87] This back transfer can be energetically favorable, if the CT-state dissociation into free charge carriers is blocked and the initial singlet CT state interconverts to a triplet CT state. A triplet exciton generated by BET has an unambiguous EPR signature and can be distinguished from an ISC-triplet exciton by EPR as explained in Sec. 2.2.4. A EPR study of BET in organic photovoltaics is presented in Sec. 3.2.2 ([FK1]).

Singlet fission describes a process in which one singlet exciton splits into two triplet excitons under energy conservation. The singlet exciton needs roughly twice the energy of the resulting triplets and another singlet ground state has to be in close proximity. This process can be used for solar cells to lift the external quantum efficiency above 100%. For this purpose one incoming photon has to generate a high-energy singlet exciton that undergoes singlet fission, creating two triplet excitons, which dissociate into two holes and two electrons.[88,89] Triplet excitons populated by singlet fission have the same triplet shapes in EPR as BET triplets (see Fig. 2.2.4). The singlet-fission process is discussed in more detail in Sec. 4.1.1 ([FK4]).

2.2 Electron Paramagnetic Resonance (EPR)

Electron paramagnetic resonance spectroscopy is a method to investigate the interaction between the electron's magnetic moment and an external magnetic field. The following section deals with the physical aspects and effects for a spin-$\frac{1}{2}$ (e.g electrons, holes, polarons) and spin-1 (triplet excitons) state in a magnetic field. More detailed information can be found in EPR textbooks, e.g. [90–93], on which the following section is based.

2.2.1 Electron-Zeeman Splitting

The electron-Zeeman interaction describes the interaction between an electron spin and an external magnetic field. The Zeeman effect was discovered by Pieter Zeeman in 1896 and is the fundamental effect for all magnetic resonance measurements. Zeeman observed a splitting in optical spectra, when an external magnetic field is applied. For his important discovery he received the Nobel Prize in physics in 1902.[94] About twenty years later, Otto Stern[2] and Walther Gerlach observed the spin quantization of an electron. Their experiment demonstrated that particles possess an intrinsic angular momentum that can only have certain quantized values. In 1925, Goudsmit and Uhlenbeck defined this quantum mechanical angular momentum with no classical analogon as *the spin*.

A century later, these basic findings about the Zeeman splitting still form the foundation of all modern magnetic resonance spectroscopy methods. We used the spin properties of charge carriers, e.g. electrons or holes, in all our investigations [FK1–FK8] to gain information about the charge-carrier surroundings, the charge-carrier interactions and even to quantify the charge-carrier densities in our samples. The following text describes how the Zeeman effect can be used to distinguish between two polarons with different microscopic spin environments.

If a particle with a spin, e.g. a polaron on a polymer, is placed inside an external magnetic field $\mathbf{B_0}$, its spin precesses with the Larmor frequency around the magnetic field, thus only the component parallel to $\mathbf{B_0}$ is an observable. The Larmor frequency is given by:

$$\omega_0 = -\gamma \left|\mathbf{B_0}\right| \tag{2.2.1}$$

with $\gamma = \frac{g\mu_B}{\hbar}$ being the gyromagnetic ratio. The energy of a dipole in a magnetic field is given by:

$$E = -\boldsymbol{\mu}\mathbf{B_0} \tag{2.2.2}$$

with $\mathbf{B_0} = (0, 0, B_0)$ the static external magnetic field, pointing along the z-axis by convention. The magnetic dipole moment $\boldsymbol{\mu}$ is composed of the spin operator $\mathbf{S}$, the Bohr magneton $\mu_B = \frac{e\cdot\hbar}{2m_e} = 9.2740097(2) \cdot 10^{-24}\,\mathrm{JT}^{-1}$, the reduced Plank constant $\hbar$ and the g-factor, which describes the relation between the spin angular momentum and the magnetic moment (for free electrons $g_e = 2.002319315$):

$$E = -\boldsymbol{\mu}\mathbf{B_0} = \frac{g\mu_B}{\hbar}\mathbf{S}\mathbf{B_0}. \tag{2.2.3}$$

Due to spin-orbit coupling g can also be a matrix (see Sec. 2.2.2) For a paramagnetic species with a spin-$\frac{1}{2}$, e.g. an electron, located inside a magnetic field just two spin

[2] Nobel Prize awarded for the development of the discovery of the magnetic moment of protons.[95]

states $m_s = \pm\frac{1}{2}$ are possible. The transition energy between these two states is given by:

$$\Delta E_{eZ} = g\mu_B B_0 \tag{2.2.4}$$

with ΔE_{eZ} the electron Zeeman splitting energy. The energetic splitting is proportional to the strength of the magnetic field B_0 (see Fig. 2.2.1). This effect is used to spectrally separate two paramagnetic species, e.g. polarons (spin-$\frac{1}{2}$), with different g-factors along the magnetic field axis. For the quantum mechanical description of the Zeeman interaction of electrons, the Hamiltonian is defined as:

$$\mathcal{H}_{eZ} = \frac{g\mu_B}{\hbar} B_0 s_z \tag{2.2.5}$$

with s_z being the z-component of the spin operator $\mathbf{s}$.

Figure 2.2.1 visualizes that electromagnetic radiation (photons) with the energy $E = h\nu$ can drive a transition between $|\uparrow\rangle$ and $|\downarrow\rangle$ (spin-$\frac{1}{2}$ system). This occurs, if the frequency of the magnetic component $\mathbf{B_1(t)}$ of the incident radiation is in resonance with the Larmor frequency of the spin. This resonance condition is dependent on the g-factor of the paramagnetic species, which differs for charges occurring in different donor and acceptor materials. Hence, EPR signatures can be used to distinguish positive polarons in a donor material from negative polarons in an acceptor material because their g-factors often differ. More information about g-factors in general, are given in Sec. 2.2.2.

This effect is used among others for the investigation of polarons in organic semiconductors.[96] The typical magnetic fields used in EPR spectroscopy are in the range of 0.3 T (X-band), the corresponding electromagnetic radiation has a frequency of 9 GHz (microwaves). EPR transitions observed for unpaired polarons are absorptive (positive, see Fig. 2.2.1), for spin states with a spin-level (e.g. spin up and spin down) population in accordance to the Boltzmann equilibrium. This means that the majority of probed spins are lifted by the resonant microwave transition from the lower energetic spin state (spin down) to the higher energetic spin state (spin up). In contrast, an emissive (negative) EPR signal means that the majority of probed spins resides in the higher energetic spin state until they are stimulated by resonant microwave irradiation. They then emit photons with energies $h\nu$ while flipping their spin state from spin up to spin down.

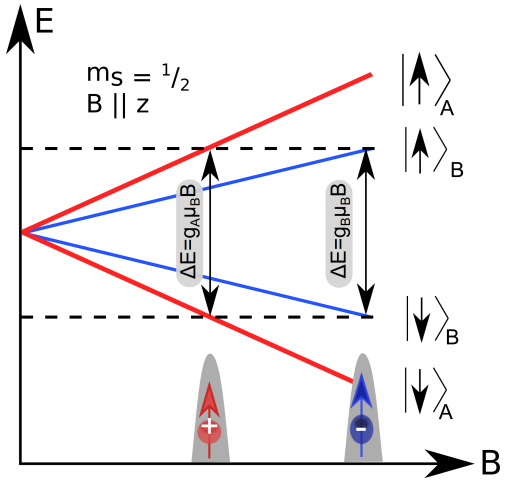

Figure 2.2.1: Zeeman splittings of two independent particles (red and blue line) with a spin-$\frac{1}{2}$ and different g-factors g_A and g_B. The resonant spin transitions lead to microwave absorption, in case of a spin system with spin levels populated in accordance to a Boltzmann equilibrium. For a fixed microwave frequency, the EPR transitions of particle A and B with g_A and g_B occur at different magnetic fields.

2.2.2 g-factor and g-matrix

The g-factor of a paramagnetic particle is often used as a microscopic fingerprint in order to distinguish between different species and particle surroundings. We used this property, e.g. in [FK1] or [FK3] to separately probe charges in either the acceptor or the donor material or to attribute EPR signals to specific layers in complex solar cell devices [FK3]. This is possible, since the magnetic field in the surroundings of a spin species depends in general not only on the external magnetic field but is also influenced by local magnetic fields and screening effects. The effective magnetic field has to be considered as the sum of both fields:

$$\mathbf{B_{eff}} = \mathbf{B_0} + \mathbf{B_{local}}. \tag{2.2.6}$$

The local magnetic field $\mathbf{B_{local}}$ originates from a magnetic-field-dependent and a permanent part that is only orientation dependent.[90] The measurement of the exact magnetic field $\mathbf{B_{eff}}$ is impossible, thus these deviations of the magnetic field are included in the g-factor. This results in a difference between the sample's g-factor and the g-factor of the free electron (g_e). $\mathbf{B_{eff}}$ is defined as:

$$\mathbf{B_{eff}} = \frac{\mathbf{g B_0}}{g_e}. \tag{2.2.7}$$

If the g-factor is dependent on the orientation of the spin species (e.g. molecule, medium) in the magnetic field then it is called anisotropic g-factor or g-matrix (3×3). Anisotropic g-values can be determined in a powder or solid sample but not in solution, since there the anisotropy is averaged due to molecular rotations.[90] Most of the charges in organic semiconductors possess an anisotropic g-matrix that is not resolvable in X-band (9.6 GHz). Often higher frequency bands like Q-band (34 GHz, see [FK1]) or W-band (94 GHz, see [FK5]) are useful to determine detailed information about the particles' surrounding. In general, one differentiates between three types of g-matrices: isotropic, axial and rhombic.

In the case of an unpaired electron in an isotropic medium, g is a scalar constant and the Hamiltonian is given by:

$$\mathcal{H} = g\beta_e(B_x s_x + B_y s_y + B_z s_z). \tag{2.2.8}$$

In this case the g-factor is called isotropic g-factor with $\beta_e = \frac{\mu_B}{\hbar}$.

If the spin-symmetry is reduced along one axis (e.g. by stress), one has to distinguish between $g_\parallel$ and $g_\perp$. The g-factor is not isotropic anymore, but axial and thus dependent on the field orientation. The corresponding Hamiltonian is given by:[90]

$$\mathcal{H} = \beta_e \cdot [B_x\, B_y\, B_z] \cdot \begin{bmatrix} g_\perp & 0 & 0 \\ 0 & g_\perp & 0 \\ 0 & 0 & g_\parallel \end{bmatrix} \cdot \begin{bmatrix} s_x \\ s_y \\ s_z \end{bmatrix} \tag{2.2.9}$$

$$= \beta_e \mathbf{B}^T \mathbf{g} \mathbf{S}. \tag{2.2.10}$$

The most complex local symmetry is the rhombic one, where $g_x \neq g_y \neq g_z$. The rhombic Hamiltonian is given by:

$$\mathcal{H} = \beta_e \cdot [B_x\, B_y\, B_z] \cdot \begin{bmatrix} g_x & 0 & 0 \\ 0 & g_y & 0 \\ 0 & 0 & g_z \end{bmatrix} \cdot \begin{bmatrix} s_x \\ s_y \\ s_z \end{bmatrix} \tag{2.2.11}$$

2.2.3 The EPR Spectrum of Triplet States

Figure 2.2.1 showed a spin systems with a total spin-$\frac{1}{2}$. Spin systems with higher spins have more complex EPR signature. The following subsection is focused on spin systems with a total spin-1 (triplet excitons) but the description can be analogously extended to other spin systems, e.g. quartets or quintets. As mentioned in Sec. 2.1.3 triplet excitons (hereafter referred to as triplets) often occur in organic semiconductors. Investigations of triplets played a crucial role in many of our studies, e.g. [FK1, FK2, FK4, FK8], therefore it is important to be able to formally describe these types of spin states.

The electron Zeeman operator $\mathcal{H}_{eZ}$ of a two spin system (spin $\mathbf{A}$,$\mathbf{B}$) is:

$$\mathcal{H}_{eZ}^{\mathbf{A},\mathbf{B}} = \sum_{n=\mathbf{A},\mathbf{B}} g_n \mu_B s_{nz} B_0. \tag{2.2.12}$$

The Zeeman operator alone is not enough to describe a spin system with two spins since it does not consider any interaction between the spins. Two spins at a finite distance from each other will show spin-spin interactions. These interactions are described by the spin-interaction Hamiltonian $\mathcal{H}_{SS}$, which contains an isotropic part $\mathcal{H}_{SS}^{ex}$ and an anisotropic part $\mathcal{H}_{SS}^{dd}$. The isotropic part is determined by the overlap of the wave functions of the electrons and the anisotropic part originates from the magnetic dipole-dipole interaction. The isotropic interaction Hamiltonian is also often called **exchange Hamiltonian** $\mathcal{H}_{SS}^{ex}$ and is given by:

$$\mathcal{H}_{SS}^{ex} = -2J\, \mathbf{s_A} \cdot \mathbf{s_B} = \mathbf{S_A J S_B} \tag{2.2.13}$$

with J being the coupling constant of the overlap. The overlap of the wave functions forces the spins to stay strictly antiparallel and leads to a spin quantum number for the system equal to zero. The kinetic exchange between both spins makes the singlet state ($S = 0$) more favorable than the triplet state ($S = 1$). The electrostatic potential (exchange interaction) due to the repulsive Coulomb interaction can be described by the exchange integral J_{AB} between the spins $\mathbf{A}$ and $\mathbf{B}$:

$$J_{\mathbf{AB}} = \langle \Psi_A(\mathbf{A}) \Psi_B(\mathbf{B}) | \, \frac{e^2}{2\epsilon_0 h r_{\mathbf{AB}}} \, | \Psi_A(\mathbf{B}) \Psi_B(\mathbf{A}) \rangle \tag{2.2.14}$$

with the elementary charge e, the vacuum permittivity ϵ_0 and the distance r_{AB} between the spins along the dipolar axis between spin A, B. The electrostatic potential part makes the triplet state more favorable due to the repulsive force.

The anisotropic **dipole-dipole interaction** $\mathcal{H}_{SS}^{dd}$ can be calculated using the classical electro-dynamic interaction between two dipoles:

$$\mathcal{H}_{SS}^{dd} = \frac{\mu_0}{2h} g_{\mathbf{A}} g_{\mathbf{B}} \mu_B^2 \left(\frac{\mathbf{s_A s_B}}{r_{\mathbf{AB}}^3} - \frac{3(\mathbf{s_A r_{AB}})(\mathbf{s_B r_{AB}})}{r_{\mathbf{AB}}^5} \right) \tag{2.2.15}$$

with μ_0 being the magnetic vacuum permeability. As the interaction between two localized spins is directly proportional to r^{-3}, this relation enables the determination of the inter-spin distance.

Alternatively, this interaction is often described using the dipolar coupling matrix $\mathbf{D}$:

$$\mathcal{H}_{SS}^{dd} = \mathbf{S_A D S_B} \tag{2.2.16}$$

with $\mathbf{S_{A,B}}$ the spin operator for $\mathbf{A}, \mathbf{B}$ and $\mathbf{D}$ the dipole–dipole coupling matrix. The dipolar coupling matrix is traceless and can be diagonalized. The matrix only depends on two independent coupling parameters D and E, which are called zero-field coupling parameters. D is defined by the principal value D_{zz} of the diagonalized matrix $\mathbf{D}$: $D = -3/2\ D_{zz}$, while E is dependent on the principal values D_{xx} and D_{yy}: $E = -1/2$ (D_{xx}-D_{yy}).

If E=0, the dipolar coupling matrix $\mathbf{D}$ shows axial symmetry. The resulting dipolar component of the Hamiltonian is:

$$\mathcal{H}_{SS}^{dd} = \frac{1}{2} D_{zz} (3\, s_{\mathbf{Az}} s_{\mathbf{B}z} - \mathbf{s_A s_B}) \tag{2.2.17}$$

Taking both interaction Hamiltonians and the electron-Zeeman Hamiltonian together one derives for two interacting spins:

$$\mathcal{H} = \mathcal{H}_{eZ} + \mathcal{H}_{SS}^{ex} + \mathcal{H}_{SS}^{dd} \tag{2.2.18}$$

$$= g_{\mathbf{A}} \mu_B B_0 s_{\mathbf{A}z} + g_{\mathbf{B}} \mu_B B_0 s_{\mathbf{B}z} - 2J \mathbf{s_A s_B} + \frac{1}{2} D_{zz} (3\, s_{\mathbf{A}z} s_{\mathbf{B}z} - \mathbf{s_A s_B}). \tag{2.2.19}$$

This Hamiltonian can also be described in a matrix representation. Therefore, one has to find a proper basis set. In order to define a high-spin system, a product basis can be used for weak spin-spin couplings ($J, D < \Delta g B_0$), e.g. for CT states.[FK7,97] For weak couplings this basis is an eigenbasis and therefore leads to a diagonal Hamiltonian. For a two-spin system it is defined by four eigenstates:

$$|\uparrow\uparrow\rangle, |\downarrow\downarrow\rangle, |\downarrow\uparrow\rangle, |\uparrow\downarrow\rangle \tag{2.2.20}$$

Additionally, one can introduce a second basis for the strong coupling regime ($J, D \gg \Delta g B_0$), the singlet-triplet basis. This basis set is often used for the description of triplet excitons. The singlet-triplet basis leads to a diagonal Hamiltonian for the strong coupling regime. The eigenstates of this basis are:

$$|\mathrm{T}_+\rangle = |\uparrow\uparrow\rangle \tag{2.2.21}$$

$$|\mathrm{T}_0\rangle = \frac{1}{\sqrt{2}} (|\uparrow\downarrow\rangle + |\downarrow\uparrow\rangle) \tag{2.2.22}$$

$$|\mathrm{T}_-\rangle = |\downarrow\downarrow\rangle \tag{2.2.23}$$

$$|\mathrm{S}\rangle = \frac{1}{\sqrt{2}} (|\uparrow\downarrow\rangle - |\downarrow\uparrow\rangle) \tag{2.2.24}$$

The resulting Hamiltonian $\mathcal{H}$ can be written in the matrix representation as:

$$\mathcal{H} = \begin{array}{c} \begin{array}{cccc} |\mathrm{T}_+\rangle & |\mathrm{S}\rangle & |\mathrm{T}_0\rangle & |\mathrm{T}_-\rangle \end{array} \\ \begin{pmatrix} \hbar\omega_0 - J/2 + \frac{D_{zz}}{2} & 0 & 0 & 0 \\ 0 & 3J/2 & \hbar\Delta\omega & 0 \\ 0 & \hbar\Delta\omega & -J/2 - d & 0 \\ 0 & 0 & 0 & \hbar\omega_0 - J/2 + \frac{D_{zz}}{2} \end{pmatrix} \end{array} \tag{2.2.25}$$

with $\omega_0 = 1/2 \mu_B \hbar^{-1} B_0 (g_{\mathbf{A}} + g_{\mathbf{B}})$ and $\Delta\omega = 1/2 \mu_B \hbar^{-1} B_0 (g_{\mathbf{A}} - g_{\mathbf{B}})$.[91]

If $g_A = g_B = g_e$ are quantized along the magnetic axis and the electron Zeeman interaction is the dominant interaction, the dipole-dipole interaction can be approximated for the high-(magnetic-)field range ($g B_0 \gg D$). Thus only terms parallel to

the static magnetic field can participate at the spin-spin interaction. In this case the eigenstates are given by $|\mathrm{T}_+\rangle$, $|\mathrm{T}_0\rangle$, $|\mathrm{T}_-\rangle$.

In contrast, for the low-(magnetic-)field range as well as for zero field the quantum states are connected to the molecular orientations x, y and z and are given by $|\mathrm{T}_x\rangle$, $|\mathrm{T}_y\rangle$, $|\mathrm{T}_z\rangle$. A transformation between the low-field and high-field representation of a triplet is applied e.g. in [FK1] to distinguish between zero-field populated ISC triplets and high-field populated BET triplets. More information about their spectral difference are given in Sec. 2.2.4.

For a triplet in the high-field representation, $\mathcal{H}_{SS}^{dd}$ is reduced to:

$$\mathcal{H}_{SS}^{dd} = \frac{\mu_0 \mu_B^2}{2hr_{\mathbf{AB}}^3} g_e^2 \cdot (3\cos^2\theta - 1) \tag{2.2.26}$$

with θ being the angle between the magnetic field and the dipolar connection axis of both spins. The projection on the z-axis becomes $z = r \cdot \cos\theta$ (point-dipole approximation).

The resulting spin-1 energy levels are depicted in Fig. 2.2.2 for the case of a single-crystalline sample presenting the three Cartesian molecular orientations. The level plot is separated into the low-field range (left) and the high-field range (right). Triplets that are generated within the zero-field (low-field) representation can be described with $|\mathrm{T}_x\rangle$, $|\mathrm{T}_y\rangle$, $|\mathrm{T}_z\rangle$. These states are populated by e.g. ISC. In contrast, triplets generated by a high-field process, e.g. singlet fission, show direct population in the $|\mathrm{T}_+\rangle$, $|\mathrm{T}_0\rangle$, $|\mathrm{T}_-\rangle$ states and cannot be described by $|\mathrm{T}_x\rangle$, $|\mathrm{T}_y\rangle$, $|\mathrm{T}_z\rangle$. The article [FK4] presents EPR measurements of such single-crystalline samples which show high-field triplet excitons populated by singlet fission. An example for an ISC triplet-exciton occurring in a crystalline sample is discussed in Sec. 3.2.1.

The width of the EPR triplet spectrum (magnetic field range between both corresponding transitions) depends on the orientation of the molecular dipolar coupling axis with respect to the main magnetic field (Fig. 2.2.2, right). The energy levels for the three Cartesian molecular orientations of the triplet exciton wave function are plotted versus the main magnetic field. The bottom plot summarizes the six transitions for these three orientations with normalized transition intensities. The resulting intensities and transition directions depend on the population differences between the two contributing states.

The corresponding triplet spectrum of a crystalline or amorphous powder containing all molecular orientations is visualized in Fig. 2.2.3 and 2.2.4. Since it is more probable that the dipolar coupling axis is perpendicular to the main magnetic field than parallel, the triplet signature is typically a Pake pattern. Triplets revealing Pake patterns are published in [FK1, FK4, FK8].

A good knowledge of triplet generation mechanisms in OSC is crucial since triplets can occur as loss mechanisms in the devices (see Sec. 2.1.3). A detailed study of different population mechanisms of triplet excitons is published in [FK1].

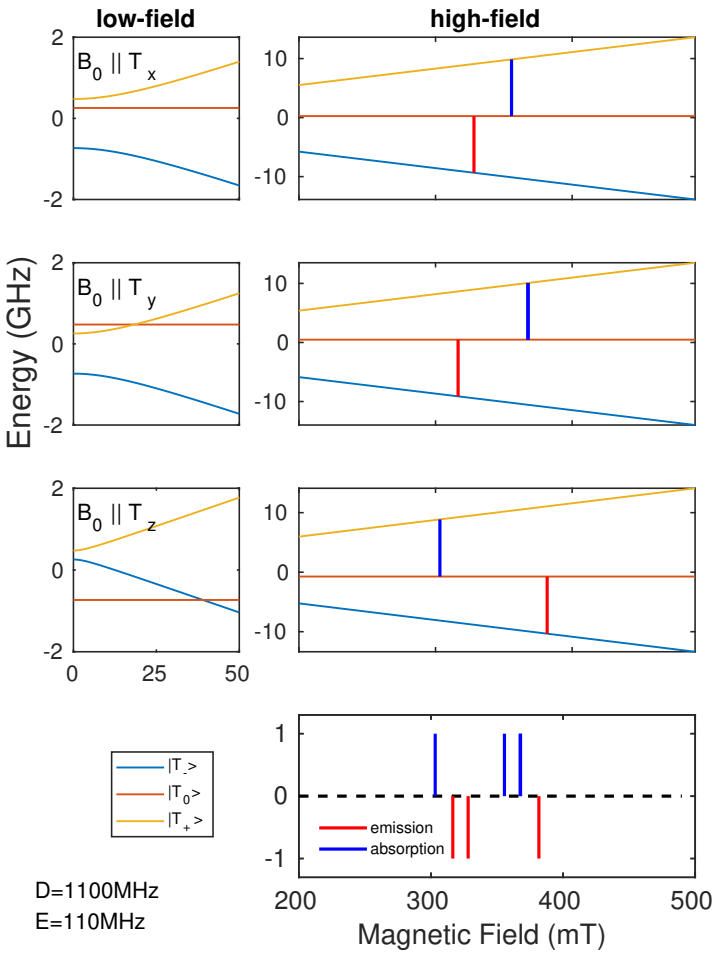

Figure 2.2.2: Zeeman splitting for a spin-1. The energetic levels of a triplet state in an external magnetic field $\mathbf{B_0}$ is depicted. The selected Cartesian molecular orientation of the dipolar axis versus $\mathbf{B_0}$ are depicted in three first rows for the zero-field ($\mathbf{B_0} \approx 0\,\mathrm{T}$) region (left) and the high-field (right). For a disk shaped density function of the triplet exciton, the energy level of $|\boldsymbol{T_z}\rangle$ is below the energy levels of $|\boldsymbol{T_x}\rangle$ and $|\boldsymbol{T_y}\rangle$ in the zero-field range. The transition direction depends on the population of the states and can either be absorptive or emissive. The bottom plot combines the transitions for the three outstanding orientations with a population of $[|\boldsymbol{T_-}\rangle\ |\boldsymbol{T_0}\rangle\ |\boldsymbol{T_+}\rangle]$=[0 1 0].[a]

[a] The energy levels were determined by the EASYSPIN toolbox[98] for Matlab (MathWorks, Natick, MA, USA).

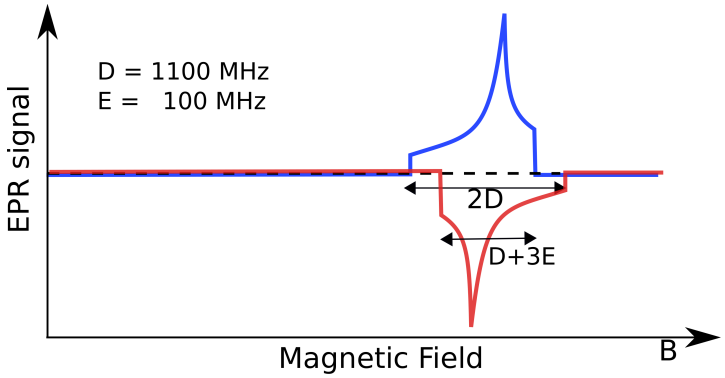

Figure 2.2.3: Visualization of the EPR transitions of a triplet exciton ($S = 1$) in a powder or amorphous sample assuming a dipolar-coupling between the spins. The dipolar coupling parameter D depends directly on the distance between the coupled spins and is marked in the diagram. The blue line depicts the absorptive transitions and the red line the emissive ones. The final triplet spectrum is generated by the summation of all transitions.

2.2.4 ISC Triplets versus BET Triplets

In order to determine the spectral shape of a triplet exciton, not only the energetic splitting but also the population of the states are important. Triplet excitons can be generated by a population transfer from different precursor states[3], e.g. a single singlet exciton or a charge-transfer state. The precursor state of a triplet significantly influences the shape of the triplet-exciton EPR spectrum. A good knowledge about different triplet precursor states was necessary for our studies [FK1, FK2, FK4]. Triplets populated via a high-field process, like BET from a CT state or via singlet fission, can only result in a very distinct EAAEEA- or AEEAAE-pattern[4] as shown in Fig. 2.2.4. In contrast, triplets formed via ISC can result in a large variety of different triplet signatures. The reasons for these differences are that the spin ensemble populates varying sets of triplet sublevels.

Triplet excitons formed by BET or singlet fission directly populate the high-field spin states $|T_+\rangle$, $|T_-\rangle$ and $|T_0\rangle$. In contrast, ISC triplets are generated by spin-orbit coupling which acts on the molecular zero-field states $|T_x\rangle$, $|T_y\rangle$ and $|T_z\rangle$. The population of these zero-field states is then translated to a mixed population of the $|T_+\rangle$, $|T_-\rangle$ and $|T_0\rangle$ states depending on the energetic order and population at zero-field (see Fig. 2.2.2). Two exemplary ISC-triplet signatures are depicted in Fig. 2.2.4. More information about triplets formed by BET versus ISC can be found in [FK1].

Triplets that lost their spin-polarization convert into thermalized triplets for which the precursor state can no longer be determined. An example for a thermalized triplet is published in [FK8] and another one shown in Fig. 2.2.4.

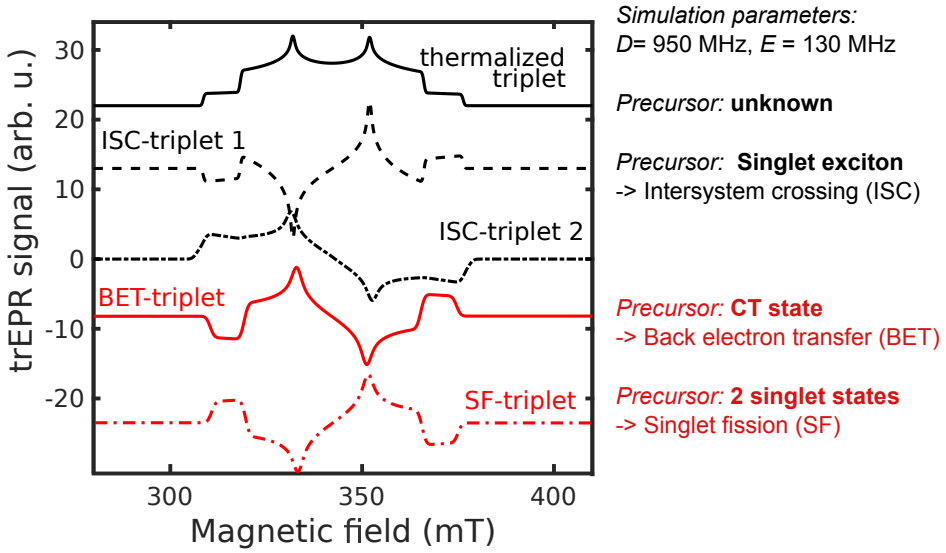

Figure 2.2.4: This plot shows different triplet simulations with the same set of coupling parameters D and E but different populations and precursors. The thermalized triplet signature (black solid curve) is based on zero-field states $|T_x\rangle$, $|T_y\rangle$ and $|T_z\rangle$ that are populated in accordance to a Boltzmann equilibrium, while the ISC triplets 1 and 2 (black dashed curves) are simulated with arbitrary populations of $|T_x\rangle$, $|T_y\rangle$ and $|T_z\rangle$. A state population which is not in accordance with a Boltzmann distribution occurs because of laser excitation leading to a polarization of spin states. BET & SF triplets have a pure high-field precursor (e.g. CT state) and thus show the unambiguous triplet EAAEEA- or AEEAAE-patterns[4] (red curves).

[3] A precursor state is the initially populated spin state that fills the emerging spin state.

[4] "E" meaning emissive and "A" absorptive part of the EPR signal, the order is by convention from low to high-field.

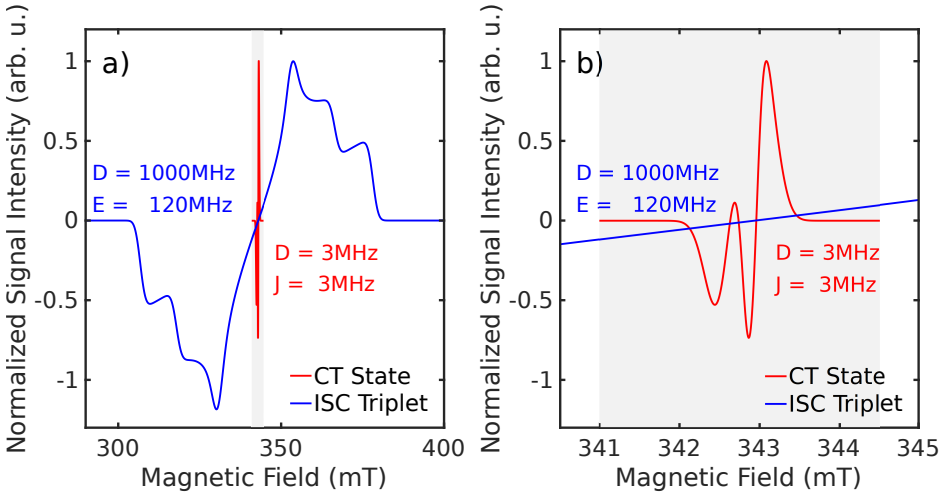

Figure 2.2.5: Charge-transfer states versus triplet states. This plot visualizes the difference in EPR spectra between strongly coupled triplet excitons and weakly coupled CT states. The triplet simulation is based on the EASYSPIN[98] for Matlab. The CT-state simulation is based on a semi-analytical calculation published in [FK7].

2.2.5 The EPR Spectrum of CT States

EPR spectroscopy can unambiguously distinguish between CT states (weakly coupled polaron pairs) and triplet excitons (strongly coupled electron-hole pair) within organic semiconductors because of their different EPR signatures depicted in Fig. 2.2.5a. This is an important feature of EPR spectroscopy for OPV investigations, since it is difficult to distinguish between both states with optical spectroscopy. Therefore, triplet excitons and CT states are sometimes mixed up in literature as mentioned in the introduction and discussed in [FK1].

The simulation in Fig. 2.2.5 illustrates the difference between the spectral width of triplet excitons and CT-state EPR signatures. The simulation contains a typical ISC triplet with a dipolar coupling of 1000 MHz and a CT state with a dipolar coupling of 3 MHz. The grayish area in Fig. 2.2.5b is a magnification of the simulation in Fig. 2.2.5a for a small magnetic field range. Due to the large difference in the spectral width (ca. 3 orders of magnitude), triplet excitons are typically invisible in measurements optimized for CT states.

The process of the generation and dissociation of a CT state from an EPR point of view is schematically shown in Fig. 2.2.6. In general, the CT-state sublevels are populated by a singlet precursor (Fig. 2.2.6a) like a singlet exciton. The transfer of the electron from a donor to an acceptor leads to an EAEA-pattern in the EPR spectroscopy (depicted in Fig. 2.2.5b) and implies that the CT-state spin eigenstates are not in thermal equilibrium (see Fig. 2.2.6b).[99,100]

This originates in the angular momentum conservation that leads to a filling of the singlet-triplet mixed states $|2\rangle$ and $|3\rangle$. Afterwards, the CT state dissociates into free polarons (Fig. 2.2.6c) and reveals the signature of free polarons described in the next Sec. 2.2.6.

The quantum mechanical description of the CT state is given by the Hamiltonian:

$$\begin{aligned}\mathcal{H}_0 = \frac{\mu_B}{h}\mathbf{B_0 g_A S_A} + \frac{\mu_B}{h}\mathbf{B_0 g_B S_B} + \mathbf{S_A J S_B} + \mathbf{S_A D S_B} \\ + \sum_i \mathbf{S_A}\,\mathbf{A_{Ai}}\,\mathbf{I_i} + \mathbf{S_B}\,\mathbf{A_{Bi}}\,\mathbf{I_i}\end{aligned} \tag{2.2.27}$$

as reported in [FK7, 45, 97] with $\mathbf{J}$ being the exchange coupling tensor and $\mathbf{D}$ the dipole–dipole coupling tensor. The hyperfine coupling between the i-th nuclear spin $\mathbf{I_i}$ and the electron spins $\mathbf{A}$ and $\mathbf{B}$ is described by the hyperfine tensors $\mathbf{A_{Ai}}$ and $\mathbf{A_{Bi}}$, respectively.

A detailed description of the theory and more information on CT-state EPR signatures as a function of the coupling parameters $\mathbf{J}$ and $\mathbf{D}$ are reported in [FK7].

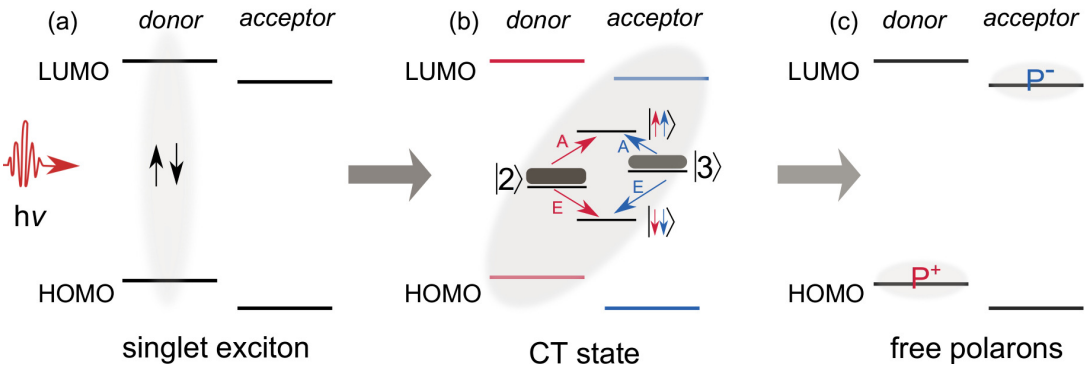

Figure 2.2.6: "Charge-transfer state at the donor/acceptor interface. (a) A singlet exciton is generated by the absorption of a photon in the donor material. (b) Upon reaching the donor/acceptor interface by diffusion, the exciton is split up into a SCPP [spin-correlated polaron pair] with the positive polaron (P^+) residing in the donor and the negative polaron (P^-) residing in the acceptor phase. The resulting CT state comprises four energy eigenstates with four allowed EPR transitions. (c) The CT state dissociates into two separated polarons that contribute to the photocurrent in solar cells with absorber layers made from the donor:acceptor blend. HOMO and LUMO refer to the highest occupied and the lowest unoccupied molecular orbitals, respectively." The figure and caption are taken from [FK7].

2.2.6 The EPR Spectrum of Free Polarons

A purely absorptive signal, evoked by resonant microwave absorption of a spin, is called "free polaron signal" throughout this thesis if the observed spin ensemble is in a Boltzmann equilibrium. These "free polaron signals" are measurable by different EPR methods. The notation is used analogously to Sariciftci *et al.* [44] and Dyakonov *et al.* [96] who observed two light-induced cwEPR signals in a MDMO-PPV[5]:PCBM[6].[7] They stated that these free polarons are charge-separated states and their signal originates from two decoupled spins. This convention is adapted in several publications, e.g. [55, 101–104]. An example for an EPR spectrum of free polaron signals is depicted in Fig. 1.1.1 & 2.3.3. Note that free polaron signals are commonly depicted as their derivatives causing them to look very similar to a trEPR "EA"-pattern even though they are not.

Free polaron signals result from a Boltzmann population of spin states, which can be calculated if the energetic splitting and the temperature are known. Therefore, a spin quantification is easily possible (see [92]) and can be used for the determination of charge-separation efficiency (see [FK1]) as well as doping efficiencies of dopants for organic semiconductors.[FK5] Hereby, the spin is used as probe for a charge with spin-$\frac{1}{2}$, e.g. an electron, to determine the charge-carrier density.

[5] poly[2-methoxy-5-(3',7'-dimethyloctyloxy)-1, 4-phenylenevinylene]
[6] phenyl-C61 -butyric acid methyl ester
[7] Their exact notation was mobile polarons.

2.3 Experimentals

The following section describes the layout and preparation of the various types of samples which were investigated within this thesis. It continues with an overview of the EPR and EDMR methods relevant to this thesis.

2.3.1 Sample Preparation

We use three types of EPR/EDMR samples (see Fig. 2.3.1):

EPR inner wall samples (Fig. 2.3.1a) consist out of a thick film of organic semiconductors that covers the inner wall of an EPR quartz tube. They are prepared by loading dissolved organic material into an EPR tube and evaporating the solvent under vacuum. This results in a thick film preferable for measurements with good signal-to-noise ratio. These type of samples were used in most of our publications [FK1, FK3–FK7].

Substrate (thin film) samples (thickness between 30 nm to 400 nm) are prepared by spincoating from solutions onto quartz substrates. They show comparable film morphologies to real solar cells (Fig. 2.3.1a, right) and are useful to study ordering and crystallinity effects of thin organic semiconductor layers. Thin film samples were used in [FK1, FK2, FK4, FK6].

The third type of samples is made specially for EDMR measurements and is shown in Fig. 2.3.1c). EDMR spectroscopy needs a more complex structure because contacts are necessary for current measurements. The preparation of the layered structure for a single-junction solar cell is visualized in b), while c) is a picture of a miniaturized complete solar cell with all necessary layers and contacts. The development of an encapsulated miniaturized solar cell especially was a major part of this PhD work. Several steps (visualized in Fig. 2.3.1b) had to be developed in our labs before we were able to build cells compatible with standard EPR resonators. As a first step, nano-structured ITO substrate (transparent front electrode) had to be designed, which was achieved in cooperation with Micheal Eckhard (AG Harneit). Two spin-coaters, one for the hydrous PEDOT:PSS solution (workfunction adjustment of the ITO) and one for the organic absorber inside an inert atmosphere Glovebox, were taken into operation. A new evaporation Glovebox System (MBraun ECOVAP 5) was installed and adjusted for the evaporation of the metal back electrode. An encapsulation system was developed in order to avoid degradation of the organic semiconductor.

The degradation of organic semiconductors (e.g. P3HT, PCBM, PCPDTBT) in air was studied in addition to this thesis by Helen Wolfson (HZB summer student 2013/2014). Several doping series of organic semiconductors connected to this thesis were investigated in the bachelor theses of Christian Northe (2013), Kelvin Yao (2014) and Charlotte Beck (2016). In order to improve the design of our solar cells and to investigate organic field effect transistors Adrià Gràcia Condal performed his master thesis.

Detailed descriptions of sample preparation for doping series or of EDMR samples are covered in the aforementioned bachelor and master theses as well as in the attached publications.[FK3,FK8]

2.3.2 Continuous Wave EPR (cwEPR)

Continuous wave EPR is the most common EPR technique. It is used for preliminary investigations of new materials in all our studies to determine material-characteristic features like g-values. Thus cwEPR spectra are presented in several of our publications

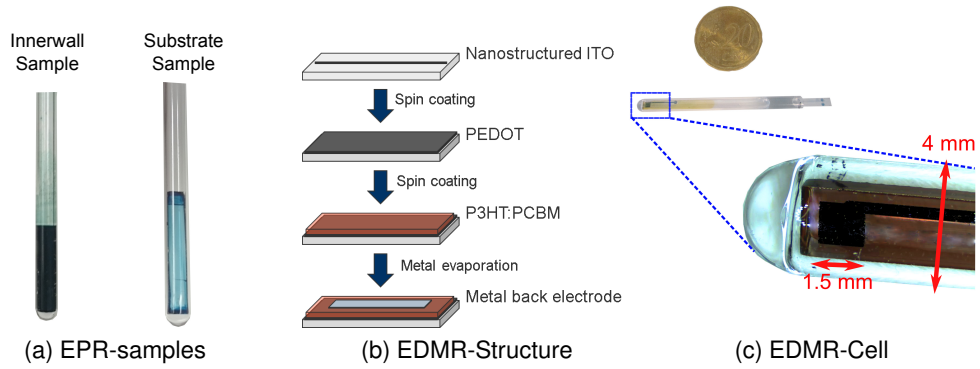

Figure 2.3.1: Overview of various types of investigated samples. (a) inner-wall (left) and substrate samples (right) of pristine organic semiconductors and blends used for EPR measurements. (b) flow-chart diagram of the preparation of a miniaturized solar cell for EDMR. (c) working miniaturized solar cell encapsulated in a 4 mm EPR tube for EDMR and EPR measurements. The graph in c) belongs to [FK3].

[FK1, FK5–FK7]. For cwEPR measurements a sample is placed inside an EPR resonator and is continuously irradiated with microwaves. The resonator is placed inside a He-flow cryostat within a sweepable magnet. Nearly all EPR techniques use resonators to spatially separate the electric and magnetic component of the microwaves and to enhance the B_1-field at the sample position as well as the sensitivity to microwave absorption. More information on the setup is given in the appendix A.

The magnet generating the main magnetic field B_0 is used to force the Zeeman splitting of the spin states. The continuous microwave irradiation of the sample leads to a Boltzmann equilibrium of the spin states. If the resonance criterion mentioned in Sec. 2.2.1 is fulfilled, a spin transition occurs and a microwave absorption is measured. The intensity of the signal depends on the population difference between the two Boltzmann spin states and thus on the temperature. In order to increase the signal-to-noise ratio of cwEPR a field-modulation in combination with a lock-in detection is applied. Therefore, most of the published cwEPR spectra show a derivative spectrum as depicted in Fig. 2.3.2 (dashed line). Another route to improve the signal-to-noise ratio in cwEPR is to measure at low temperatures at which the deviation of the spin-state population is increased in accordance with the Boltzmann distribution.

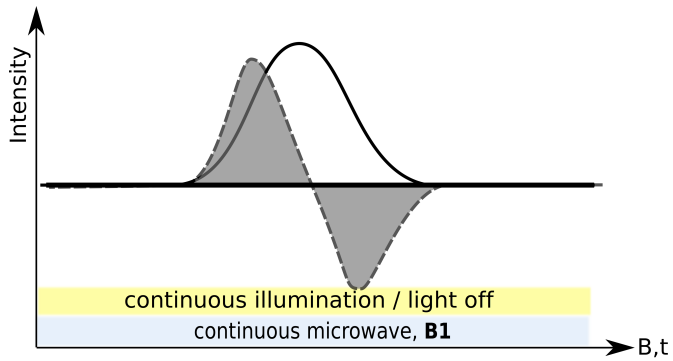

Figure 2.3.2: Schematic of a light-induced lock-in detected cwEPR spectrum. In general, field-modulated cwEPR spectra are recorded as the first derivative (dashed curve) of the absorptive spectrum (solid line).

Two typical light-induced cwEPR (li-cwEPR) spectra of organic absorber blends are shown in Fig. 2.3.3a. The graph contains two different blends (blue and red), measured with the same continuous illumination as well as a reference spectrum without

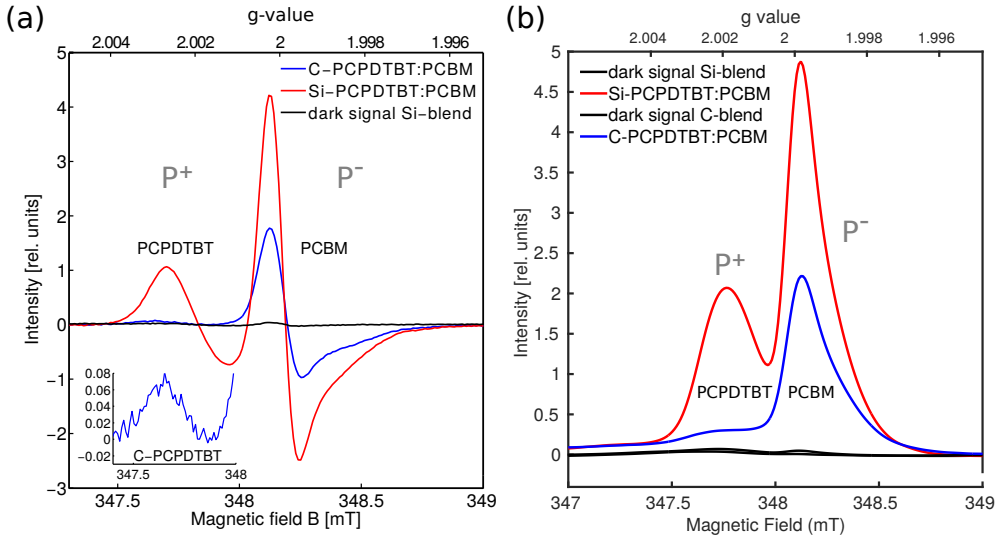

Figure 2.3.3: Light induced lock-in spectra of organic semiconductor blends. a) shows typical derivative spectra taken from [FK1]. b) shows the integrated spectra from a). Both blends show separated signals from the positive and negative polarons.

illumination. To make sure that the EPR signals contain only light-induced components, a dark reference spectrum[8] (sample background) has to be acquired and subtracted from all spectra determined for the illuminated samples. This is necessary because cwEPR is also sensitive to non-light induced signals from the sample, the sample tubes or the resonator. The graph also demonstrates that EPR is able to separate signals from different spin species, like the positive and negative polarons marked in the plot. Fig. 2.3.3b shows the integrated signals from (a). All observed signals are absorptive (positive in the first integral) and can be used for a comparison of the signal intensities. An absolute quantification of the number of investigated spins is possible in a calibrated cwEPR setup.

EPR measurements can be performed at different microwave frequencies (bands). The most frequently used band is the X-band at ∼10 GHz, but cw- and pulsed EPR spectrometers for S-band (3 GHz), Q-band (34 GHz), W-band (94 Ghz) and 263 GHz are commercially available as well. A higher frequency band often leads to a better spectral resolution of anisotropic g-values and thus is a powerful tool to distinguish between spin species with very similar EPR signatures.

2.3.3 Pulsed EPR (pEPR)

In contrast to cwEPR, pulsed EPR uses short (nanosecond) microwave pulses to flip spin states and to measure, e.g. spin coherence times, inter-spin couplings etc. via pulse sequences and echo detection. In general, echo detection is necessary for EPR measurements because the dead time of the detection system almost always prohibits a direct detection. The most basic pEPR sequence is the Hahn echo sequence (see Fig. 2.3.4a).

A Hahn echo sequence performed at different magnetic field positions is called a field-sweep echo (FSE) which will result in a standard EPR spectrum (an absolute spectrum, zero harmonic, not a derivative spectrum). Standard FSE are published in

[8]The sample is kept in the dark resonator before and during the measurement.

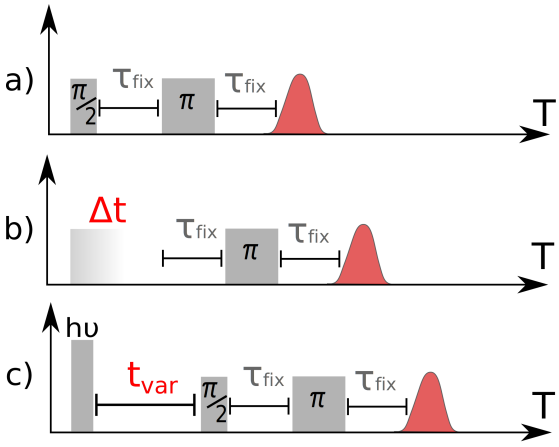

Figure 2.3.4: A selection of pEPR sequences are shown in this graph. The grey boxes symbolize the pulse durations, τ the waiting times between the pulses, and the red curve is the detected echo. $\pi/2$- or π-pulses are used to describe a 90° or 180° spin flip. This means that the magnetic dipole moment $\boldsymbol{\mu}$ is moved from $\boldsymbol{\mu} \parallel \mathbf{B_0}$ to $\boldsymbol{\mu} \perp \mathbf{B_0}$ or to $\boldsymbol{\mu}$ antiparallel to $\mathbf{B_0}$. a) depicts the Hahn echo sequence, which is the read-out sequence for most pEPR methods. b) shows one possible Rabi-nutation sequence and c) laser-flash correlated Hahn-echo sequence.

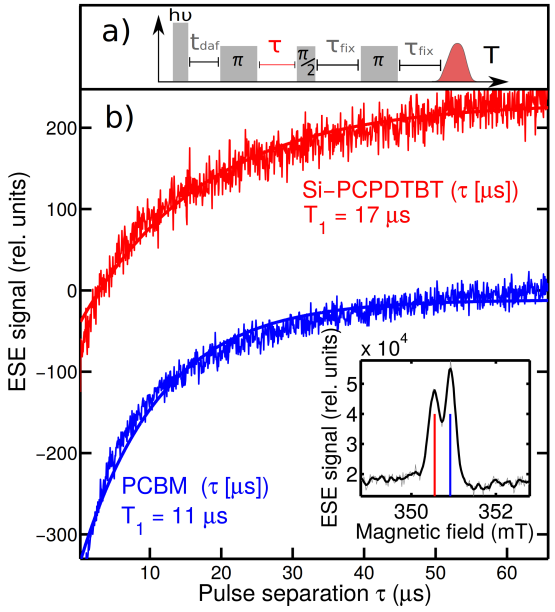

Figure 2.3.5: Example for laser flash correlated field-sweep echo and inversion recovery measurement of an organic semiconductor blend. a) depicts the used pulse sequence and b) shows the inversion recovery at the magnetic field position of the P^+ and P^- state. The inversion recovery is used to determine the spin-lattice relaxation time. The graph is taken from [FK1].

[FK4, FK6] to visualize the EPR spectra of the donor and acceptor polaron or of triplet excitons.

A field-sweep echo sequence can also be triggered by a laser flash (see Fig. 2.3.4c), which excites charges in the sample. The time between the laser flash and the Hahn-echo sequence t_{var} can be varied in order to investigate *spin state snap shots* – EPR spectra for certain delays after flash (daf).

These measurements are similar to trEPR spectra even though they have some advantages and disadvantages which we discuss later. One example of laser-correlated FSE measurement is shown in the inset of Fig. 2.3.5 . The main graph depicts a laser correlated inversion recovery measurement, which can be used to determine the spin-lattice relaxation time T_1, together with the used pulse sequence. The figure is published in [FK1] to compare spin-lattice relaxation times (T_1) of the donor material Si-PCPDTBT and the acceptor material PCBM. The laser-correlated FSE visualizes the magnetic field position of the spin on the donor (red) and acceptor (blue) material.

Over time, many different advanced pulse sequence were developed to determine spin–spin distances between electrons or between electrons and nuclei together with advanced phase-cycling steps to avoid artifacts overlapping with the echo. Another basic pulse sequence that is helpful to determine the optimal pulse lengths but also to discriminate between spins with different spin multiplicities is the Rabi sequence

depicted in Fig. 2.3.4 b. A Rabi sequence (see Fig. 2.3.4b) was used, e.g. in [FK4] to prove the appearance of quintet states in the singlet-fission material TIPS-tetracene. Another one, modified for EDMR, was used in [FK8] to separate triplet exciton signals from polaron signals. Rabi nutations measure the spin flip-angle in dependence on the applied pulse length.

2.3.4 Transient EPR (trEPR)

Transient EPR uses a similar setup as cwEPR with continuous microwave irradiation, but is a time sensitive measurement method. Transient microwave absorption after an initial trigger signal (laser flash) is recorded with a fast oscilloscope or transient recorder depicted in Fig. 2.3.6a. The advantage of trEPR measurements compared to laser-correlated pEPR measurements is that with one laser shot a whole time trace is recored, whereas for the pEPR experiment each laser flash delivers only a single transient point. Additionally, less microwave power is applied to the sample resulting in a higher spectral resolution in comparison to most time resolved pEPR spectra, which are often power-broadened. The main advantage of laser-correlated pEPR measurements is that they are not directly dependent on spin–spin and spin–lattice relaxation which is one of the main drawbacks of trEPR. In trEPR it is difficult to evaluate the real dynamics of spin state decays because it is convoluted with spin relaxations. Laser correlated FSE spectra contain always just a fixed degree of spin relaxation independent of the daf. For trEPR measurements lasers, with ∼10 ns pulses, pulse energies between 1 µJ and several mJ, and shot repetition times between some seconds up to 100 Hz are possible in our setup.

Transient EPR is the most applied method within my PhD thesis and was used to study CT states, triplet excitons and free polarons. At the beginning of my thesis we reactivated and improved (higher time resolution by mixer detection) the Q-band (34 GHz) detection of the trEPR setup to enable direct comparisons between X-band (9.6 GHz) and Q-band measurements. These comparisons help to differentiate between J, D couplings and Δg effects of CT states. This work will be published soon.

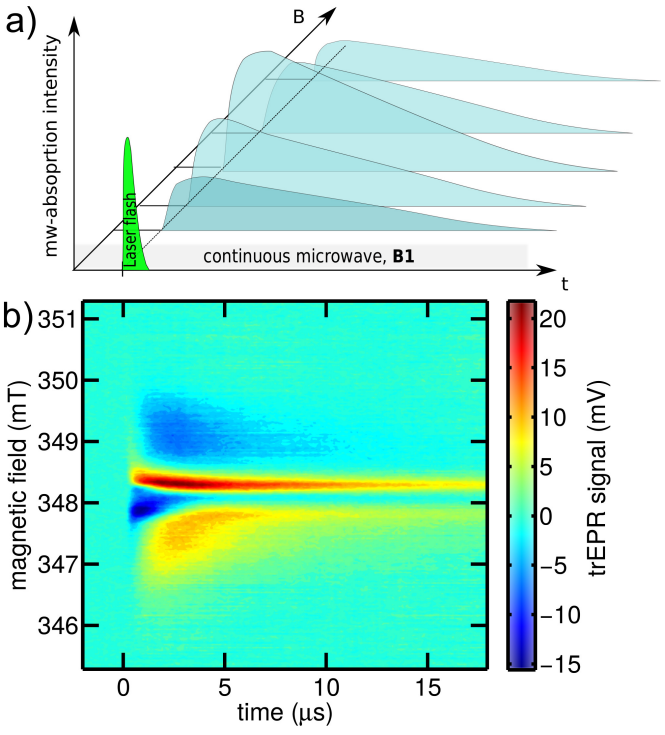

Figure 2.3.6: The trEPR spectrum. a) depicts trEPR time traces recorded at different magnetic fields. The transients are correlated to the laser excitation of a ns-pulse laser. The microwave irradiation is continuously applied. b) shows a 2D-trEPR spectrum after background correction (off-resonant background is subtracted). The dynamic change of the microwave absorption can be observed. In many cases, field slices for a certain daf are plotted to depict a complete EPR spectrum for a fixed daf.

In Fig. 2.3.6b a trEPR measurement of an organic blend is plotted that reveals the dissociation of a CT state into free polarons. For visualization purpose, the off-resonant background, generated by interaction of the electrical component of the microwave with the charges generated within the sample, is subtracted from every transient. As minimizing the off-resonant background increases the signal-to-noise-ratio it is helpful to optimize the measurement conditions with respect to the position and geometry of the light absorbing sample within the modes of the resonator.

2.3.5 EDMR versus EPR

The preceding sections were focused on EPR methods that are suitable for the investigation of the microscopic environment of paramagnetic centers in organic semiconductors. Furthermore, time-resolved EPR is capable of studying charge-carrier processes and excited state pathways in solar cells. However, EPR is limited by its low detection sensitivity (minimum 10^{11} spins) and it is often not possible to connect findings from EPR to the electrical properties for complex device structures like solar cells, transistors or light emitting diodes.

One approach to combine an appropriate sample observable, the sample conductivity, with the electron spin manipulation of localized paramagnetic centers is called electrically detected magnetic resonance (EDMR). EDMR was firstly published in the nineteen-sixties.[105,106] The main reason for the higher sensitivity of EDMR compared to EPR is based on the different detection scheme: EDMR probes the resonant photoconductivity changes $\Delta\sigma/\sigma$ of a sample which is influenced by population transfer between triplet and singlet yields of a spin pair (transition energies up to 1 eV[107]). By contrast, EPR observes the resonant microwave absorption of spin transitions, which translates into a five orders of magnitude lower quantum energy ($\sim$ µeV) for EPR transitions.

All effects that are observable in EDMR are based on at least two interacting spins. The observation of a single spin as in EPR is not possible. For the description of a spin pair including two spin-$\frac{1}{2}$ a Hamiltonian with four eigenstates can be applied. It contains two pure triplet states $|\mathrm{T}_+\rangle$ and $|\mathrm{T}_-\rangle$ and two mixed states, wherefore the mixing ratio ϕ is dependent on inter spin coupling strength J, D.

These eigenstates are:

$$|1\rangle = |\mathrm{T}_+\rangle = |\uparrow\uparrow\rangle \tag{2.3.1}$$

$$|2\rangle = \cos\phi\,|\mathrm{S}\rangle + \sin\phi\,|\mathrm{T}_0\rangle \tag{2.3.2}$$

$$|3\rangle = \sin\phi\,|\mathrm{S}\rangle + \cos\phi\,|\mathrm{T}_0\rangle \tag{2.3.3}$$

$$|4\rangle = |\mathrm{T}_-\rangle = |\downarrow\downarrow\rangle \tag{2.3.4}$$

$$\text{with } |\mathrm{T}_0\rangle = |\uparrow\downarrow\rangle + |\downarrow\uparrow\rangle \wedge |\mathrm{S}\rangle = |\uparrow\downarrow\rangle - |\downarrow\uparrow\rangle\,. \tag{2.3.5}$$

If ϕ is equal to zero, the spins are in the strong coupling regime and $|2\rangle = |\mathrm{S}\rangle$ and $|3\rangle = |\mathrm{T}_0\rangle$ are good eigenstates. For weak coupling between the spins ($J, D \ll \Delta g B_0$) the mixing ratio $\phi \sim \pi/4$ and $|2\rangle = |\downarrow\uparrow\rangle$, $|3\rangle = |\uparrow\downarrow\rangle$ become appropriate eigenstates.

Transitions between these states rely on spin-selection rules. Resonant microwave absorption can drive transitions between the different states and shift population from state $|1\rangle$ & $|4\rangle$ to $|2\rangle$ & $|3\rangle$ and therefore influence the EDMR observable, the sample conductivity. The conductivity σ of a semiconductor with electron and hole contributions is described by:

$$\sigma = e[n_e\mu_e + n_h\mu_h], \tag{2.3.6}$$

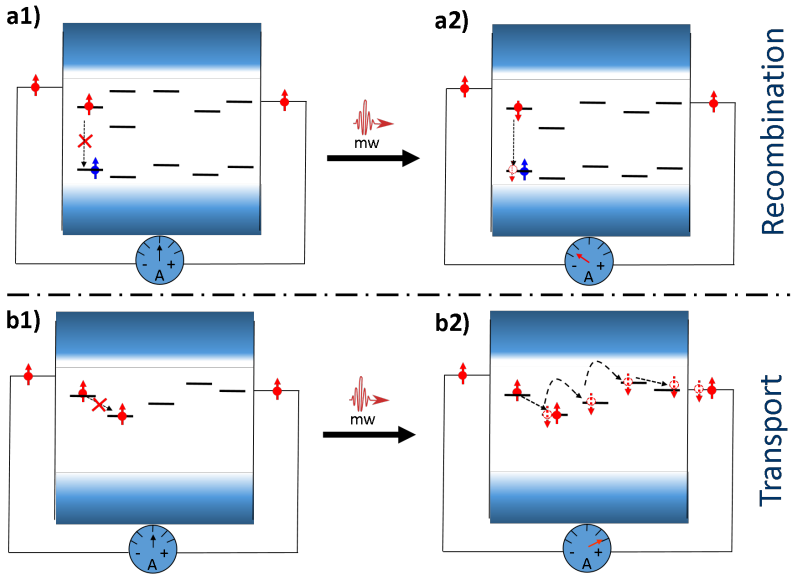

Figure 2.3.7: The two basic EDMR effects, spin dependent recombination a) and transport b) are visualized. a1) recombination of the excited electron (red) with a hole is not possible in a triplet configuration because of the Pauli exclusion principle. a2) the absorption of a microwave photon changes the spin state to a singlet state which allows recombination. A recombined free charge carrier leads to a decrease of the sample conductivity. b1) depicts an electron that cannot move via hopping to the next state because of a Pauli blockade. b2) a spin flip after microwave absorption changes the triplet state to a singlet state and opens the path for the electron towards the electrode, the conductivity is increased.

with e being the elementary charge, n_e, n_h the electron and hole concentration and μ_e, μ_h the electron and hole mobility. By resonant microwave absorption and consequent spin manipulation, the charge-carrier concentration can be reduced by spin dependent recombination. In addition the charge carrier mobility can also be influenced by spin-dependent hopping transport. These two basic spin effects lead to a change of the sample conductivity and thus to a resonant change of the photocurrent. Both effects are visualized in Fig. 2.3.7.

More detailed information about EDMR can be found in [108–110].

2.3.6 Transient EDMR (trEDMR)

Transient EDMR is a new technique, first described in [FK3], that combines the time resolution of trEPR with the electrical detection of EDMR.

In principle, it uses the same setup as trEPR spectroscopy with a pulsed laser for charge excitation and continuous microwave irradiation for the subsequent spin manipulation. In contrast to trEPR samples, EDMR samples need electrical contacts (see Fig. 2.3.1) to probe the influence of the spin manipulation on the photocurrent. A bias voltage can be applied to the sample, resulting into a constant "DC" current. The final signal is measured on the AC channel of a current voltage amplifier. In case of a trEDMR experiment an AC photo-transient appears subsequent to the excitation laser flash in addition to the DC current .

The advantage of the setup, schematically shown in Fig. 2.3.8, is the possibility of simultaneously detecting EDMR and EPR signals. Hence, a direct correlation between signals arising in trEDMR and trEPR measurements is possible. Such a combined experiment is presented in Sec. 3.1.2.

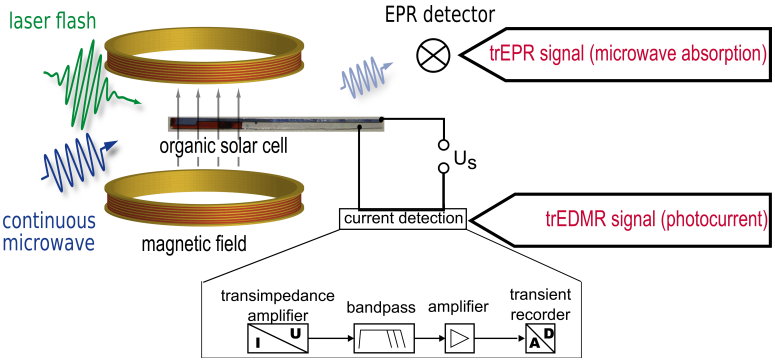

Figure 2.3.8: This schematic is an illustration of a combined trEDMR and trEPR experiment which was developed within this thesis. The shown schematic is a part of figure 1 in [FK3].

Similar to trEPR, also trEDMR measurements have a strong off-resonant background – the laser induced current transient – that has to be subtracted from each recorded transient in order to receive a visible resonant signal. In general, the resonant EDMR effect is ∼1% of the off-resonant photo transient (see 2.3.9). Note that it is important to correlate the sign of the resonant current change with the sign of the off-resonant current. In contrast to trEPR, trEDMR is inherently quantitative.

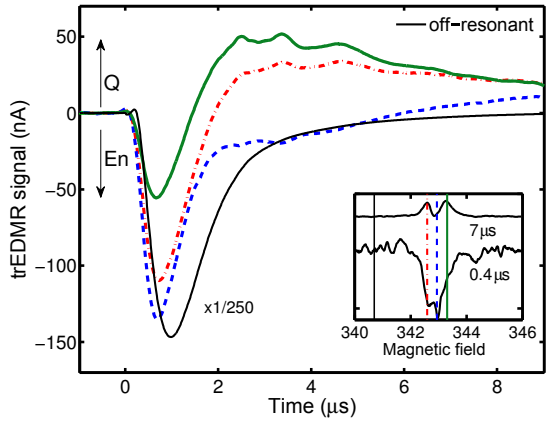

Figure 2.3.9: The graph shows three resonant EDMR transients together with the off-resonant background (black solid line) that is already subtracted from all recorded transients. The inset visualizes two slices along the magnetic field for two daf. The field positions of the shown current transients are marked within the inset. The off-resonant background trace is taken in the field region far away from the resonance signals. The shown figure is published in [FK3].

2.3.7 Pulsed EDMR (pEDMR)

Pulsed EDMR is a technique that uses short microwave pulses in a certain sequence to drive spin transitions and detects their influence on the current of the device. In contrast to pEPR, pEDMR is not limited by detection dead times and thus allows the most simple pulse sequence of a single π pulse (180° pulse, flipping the spin state from up to down or vise versa). The resulting resonant conductivity change is measured with a transient recorder that is connected via a current-voltage amplifier to the sample electrodes, analogously to the trEDMR setup. Again the AC signal of the amplifier is measured while the DC signal gives the DC current of the sample in dependence on the bias voltage. An example pEDMR measurement with different bias conditions performed with an organic tandem solar cell under illumination is shown in Fig. 2.3.10. The graph shows different features from several layers and contains triplet states and doublet states. A bias-dependency of all signals can be observed. More information on these signatures is given in [FK8].

Similar to pEPR, many advanced pulse sequences can be adapted to pEDMR to determine, e.g. electron–electron or electron–nucleus (hyperfine) interactions. These pulse sequences need an additional $\pi/2$ pulse at the position at which the echo would appear. This read-out pulse moves the magnetization parallel to the magnetic z-axis.

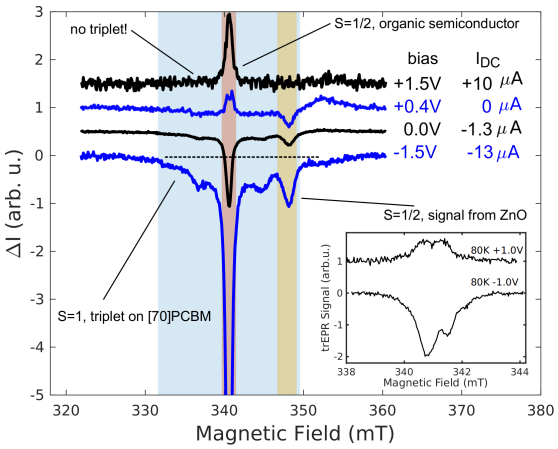

Figure 2.3.10: Pulsed EDMR measurements of organic tandem solar cell at 5 K were performed under continuous illumination with white light (Schott Lamp Setting 4D and Franke amplifier). Different spectral components are highlighted with colored areas. More information on these signatures are given in [FK8]. Several bias voltages were applied. The measurement show field slices for 2 µs after the microwave π-pulse. The inset shows a measurement with a higher field resolution of the central peak revealing two EDMR signatures. The shown figure is taken from [FK8].

Pulsed EDMR measurements are used in [FK8] to investigate polaron-triplet as well as polaron-nucleus interactions in organic tandem solar cells.

3 Charge Separation from an EPR Point of View

In this chapter we discuss charge separation in OSCs and in particular, the role of different spin states such as free polarons, CT states and triplet excitons. It summarizes our publications in this field.

- [FK1]: Kraffert *et al.*, *Charge Separation in PCPDTBT: PCBM Blends from an EPR Perspective* published in the Journal of Physical Chemistry C (2014).
- [FK7]: Kraffert *et al.*, *Spin-correlated doublet pairs as intermediate states in charge-separation processes* published in the Journal of Molecular Physics (2017).
- [FK3]: Kraffert *et al.*, *Transient electrically detected magnetic resonance spectroscopy applied to organic solar cells* published in the Journal of Applied Physics Letters (2015).
- [FK2]: Schubert *et al.*, *Correlated Donor/Acceptor Crystal Orientation Controls Photocurrent Generation in All-Polymer Solar Cells* published in the Journal of Advanced Functional Materials (2014).

Overview of EPR signatures within charge-generation

Figure 3.0.1 provides an overiew of charge-separtion in OSCs, showing the different deactivation pathways in OSCs after initial electron excitation. The schematic connects the occuring spin states such as CT states or triplet excitons with their trEPR signatures. This overview is published and described in detail in [FK1].

After an initial photon absorption in the organic blend, an EPR silent singlet exciton ($S = 0$) is generated either in the donor or acceptor material (here demonstrated for absorption in the donor). If the singlet exciton reaches a donor-acceptor interface by diffusion, it can dissociate into a singlet CT state (sometimes called "weakly coupled polaron pair") with the positive polaron P^+ (hole) located on the donor and the negative polaron P^- (electron) located on the acceptor. The CT state can further dissociate into free separated charge carriers. This pathway would be the most straight forward charge-separation process which lead to an efficient and fast charge separation. The intermediate charge-transfer state and the two separated polarons are all visible in EPR with the EPR signatures shown in Fig. 3.0.1. A combined experimental and theoretical study about the CT-state signatures in EPR is published in [FK7] and discussed in Sec. 3.1.1. An extensive material study about the binding energies within coupled polaron pair states is in preparation.

A second pathway starting at the singlet exciton is *intersystem crossing* (ISC) (see Sec. 2.1.3), a comparably slow process ($t_{\mathrm{ISC}} \gg$ns[83]) driven by spin-orbit coupling, which leads to a triplet exciton (for more information see Sec. 2.1.3). ISC happens in many organic materials if there is no donor-acceptor interface available for dissociation. Some organic semiconductors that show ISC are discussed in Sec. 3.2. Triplet excitons are strongly coupled states which have a very broad EPR signature due to

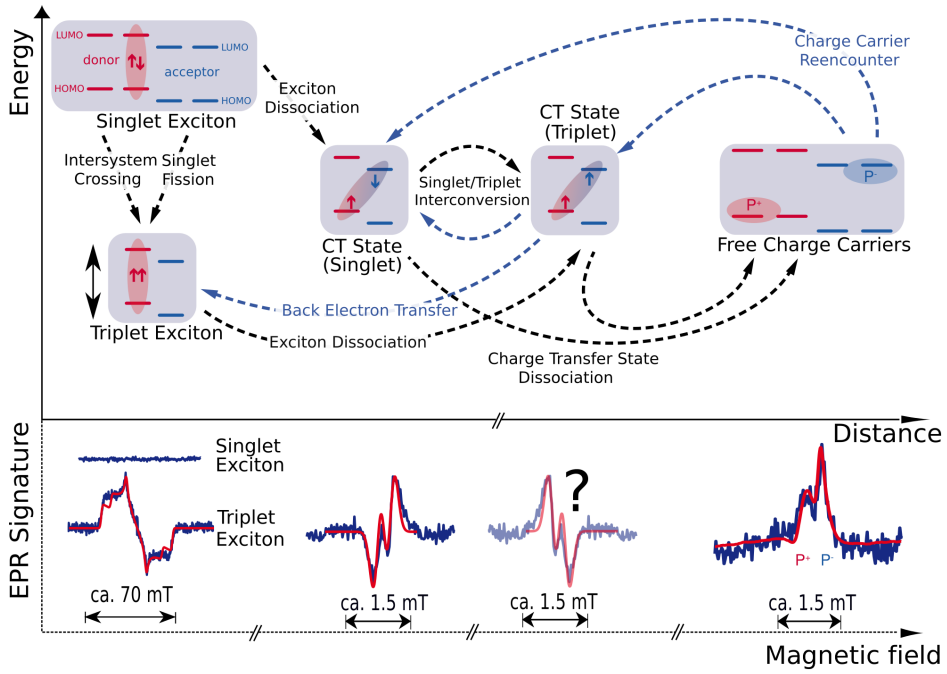

Figure 3.0.1: Charge-Transfer Pathways investigated by trEPR spectroscopy (This figure is published in [FK1]): The upper part of this schematic illustrates the most important spin states, which are potentially involved in charge separation along with their possible excitation transfer pathways. The lower part connects these states with their unambiguous EPR signatures. These signatures can be distinguished by their shape and spectral width which is dependent on the inter charge-carrier distances.

the strong dipolar coupling between the spins (see Fig. 3.0.1 bottom). These states can also be generated by a *singlet fission* process. This process is the splitting of one singlet exciton into two triplet excitons under energy conservation. Singlet fission is a process that can only occur within semiconductors with special energy levels but is much faster than ISC (see Sec. 2.1.3 for more information). A study about strong exchange coupled triplet excitons taking part in the singlet fission process is presented in Sec. 4.1 and published in [FK4].

A third pathway to generate triplets can occur if a singlet CT state converts to a triplet CT state and populates triplet excitons directly via a *back electron-transfer* (BET) pathway. One material compound which exhibit BET processes is C-PCPDTBT:PCBM. A detailed trEPR study about this phenomena is also published in [FK1].

One major drawback of trEPR spectroscopy but also of other optical methodes such as transient absorption or photoluminescence spectroscopy is that they are not able to distinguish whether or not the detected free charge carriers can contribute to the photocurrent of the solar cell. For example, it is possible that the detected states belong to trapped charges which are not able to reach their electrodes and produce a photocurrent. Therefore we developed a new method called transient electrically detected magnetic resonance (trEDMR) spectroscopy to combine the electrical sensitivity of EDMR spectroscopy with the time resolution of trEPR spectroscopy (more information are provided in Sec. 3.1.2). This new method allows us to investigate the microscopic influence of the spin states on the macroscopic photocurrent (process influencing spin tronics). A first combined study of trEPR and trEDMR applied to a working OSC is published in [FK3] and is discussed as well in Sec. 3.1.

3.1 Charge Transfer States in Organic Solar Cells

The scope of these studies is to understand the role of CT states for the charge separation and to investigate the characteristic properties of CT states – e.g. coupling strength, dipolar versus exchange coupling, polaron pair distances, influence on the photocurrent – in different organic solar cell blends. We start with a publication about a theoretical description of CT-state signatures in EPR.

3.1.1 Spin-Correlated Doublet Pairs as Intermediate States in Charge-Separation Processes

This section summarizes the article [FK7] published in the Journal of Molecular Physics (2017). The whole article is attached in appendix B.7.

My contribution within this article is the development of the semi-analytical Matlab code for CT-state spectral simulations. I performed all cwEPR and trEPR measurements. The results and analysis were discussed with Jan Behrends. I wrote the article with support from Jan Behrends and generated all figures.

Here, we developed a simulation tool for CT states measured by time-resolved EPR. Earlier CT simulations were either based on isotropic couplings and g-values or refer to some fixed symmetries between the coupled spin pair. Our main achievement is a semi-analytical approach (for more information see Sec. B.7) that can simulate polaron pairs with anisotropic dipolar and exchange couplings for an ensemble of all relative molecular orientations between both participating polarons in a reasonable calculation time. The simulations are compared with X- and Q-band EPR spectra of a model OSC blend to distinguish exchange versus dipolar coupling. The theoretical description is foundational for all our following CT-state analyses. Figure 3.1.1 visualizes our approach to generate a validated simulation based on parameters that are determined by independent EPR measurements. We use these simulations to extract CT-state couplings from experimental data.

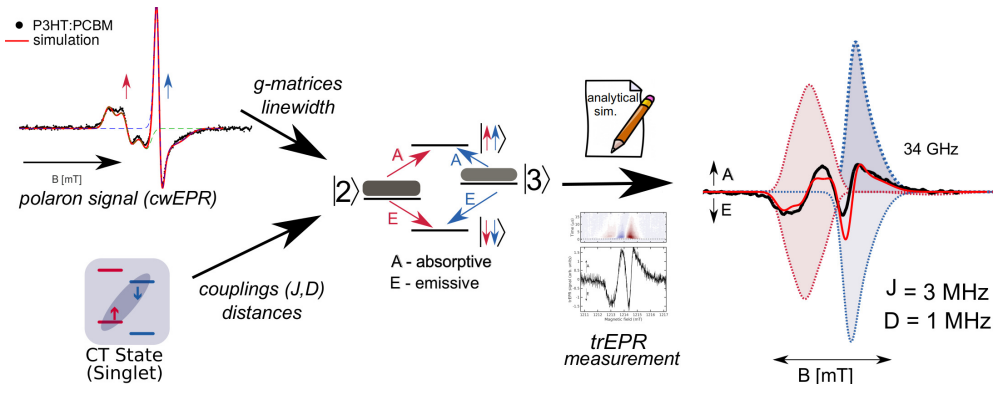

Figure 3.1.1: This figure depicts the road-map of how to create a proper trEPR spectral simulation of a CT state. Continuous wave EPR is applied to determine g-matrices and line widths of the contributing polarons which are used together with dipolar (D) and exchange coupling (J) parameters as input for the semi-analytical simulation of the CT state. This schematic is taken from [FK7].

Abstract

"Spin-correlated charge-carrier pairs play a crucial role as intermediate states in charge separation both in natural photosynthesis as well as in solar cells. Using transient electron paramagnetic resonance (trEPR) spectroscopy in combination with spectral simulations, we study spin-correlated polaron pairs in polymer:fullerene blends as organic solar cells materials. The semi-analytical simulations presented here are based on the well-established theoretical description of spin-correlated radical pairs in biological systems, however, explicitly considering the disordered nature of polymer:fullerene blends. The large degree of disorder leads to the fact that many different relative orientations between both polarons forming the spin-correlated pairs have to be taken into account. This has important implications for the spectra, which differ significantly from those of spin-correlated radical pairs with a fixed relative orientation. We systematically study the influence of exchange and dipolar couplings on the trEPR spectra and compare the simulation results to measured X- and Q- band trEPR spectra. Our results demonstrate that assuming dipolar couplings alone does not allow us to reproduce the experimental spectra. Due to the rather localized nature of polarons in conjugated organic semiconductors, a significant isotropic exchange coupling needs to be included to achieve good agreement between experiments and simulations." cited from [FK7].

3.1.2 Transient Electrically Detected Magnetic Resonance Spectroscopy Applied to Organic Solar Cells

This subsection presents the article [FK3] published in the Journal of Applied Physics Letters (2015). The whole article is attached in the appendix B.3.

The development of the new method called *transient electrically detected magnetic resonance spectroscopy* is one main project of this thesis. This project is embedded in the priority program "New Frontiers in Sensitivity for EPR Spectroscopy: From Biological Cells to Nano Materials" (SPP1601). More information on the electrical detection are given in Sec. 2.3.5. My contribution within this article is the development of micro-solar cells suitable for EPR resonators. The development includes the design of ITO structured substrates and sealing of the sample in an inert atmosphere. The production of the solar cells was support by Robert Steyrleuthner. I carried out all trEPR and trEDMR measurements. The results and analysis were discussed with all authors. I performed the spectral simulations of the polarons and CT states. I wrote the article with support from Jan Behrends and generated all figures.

The article describes the first application of trEDMR in which a fully-processed OSC is investigated. The method is developed to investigate the correlation between trEPR signals, e.g. CT states, triplet excitons or free polarons, and their influence on the device property, the photocurrent. Especially the role of the free polarons (detected by trEPR) for the solar cell performance was unclear before. In essence, based on the EPR spectrum alone it is impossible to distinguish between the signals from i) separated, non-interacting thermalized polarons and ii) Boltzmann-populated coupled polaron pairs with a to weak coupling strength to be resolved in the EPR spectrum. All signals that appear after two or three spin-lattice relaxation constants cannot be distinguished to be either interacting or non-interacting states. In [FK3] we showed with a combination of trEDMR and trEPR that the free polaron signal from trEPR could be correlated with current influencing states.

In our setup trEPR and trEDMR measurements can be carried out simultaneously. Figure 3.1.2 shows such a combination of a trEPR and trEDMR measurement performed at the same OSC. It demonstrates that the microscopic spin states measured by trEPR (Fig. 3.1.2a) have an influence on the photocurrent (Fig. 3.1.2b) in the OSC. This finding was quite important for all our trEPR measurements. Furthermore, the study reveals that CT states also appear in fully processed solar cells and not just in isolated organic blends and they live at least for 1 µs at 80 K. Within a recent review article by J. Niklas *et al.* [111] our results from [FK3] are described in context of validating the role of free polaron states in EPR as: "This controversy on the applicability of EPR for understanding the influence of light-induced paramagnetic states on the photo-current generated in solar cells has been partially solved by the breakthrough achieved by Behrends and co-wokers."

Abstract

"The influence of light-induced paramagnetic states on the photocurrent generated by polymer:fullerene solar cells is studied using spin-sensitive techniques in combination with laser-flash excitation. For this purpose we developed a setup that allows for simultaneous detection of transient electron paramagnetic resonance as well as transient electrically detected magnetic resonance (trEDMR) signals from fully-processed and encapsulated solar cells. Combining both techniques provides a direct link between photoinduced triplet excitons, charge

transfer states and free charge carriers as well as their influence on the photocurrent generated by organic photovoltaic devices. Our results obtained from solar cells based on poly(3-hexylthiophene) and a fullerene-based electron acceptor show that the resonant signals observed in low-temperature ($T = 80\,\mathrm{K}$) trEDMR spectra can be attributed to positive polarons in the polymer as well as negative polarons in the fullerene phase, indicating that both centers are involved in spin-dependent processes that directly influence the photocurrent." cited from [FK3].

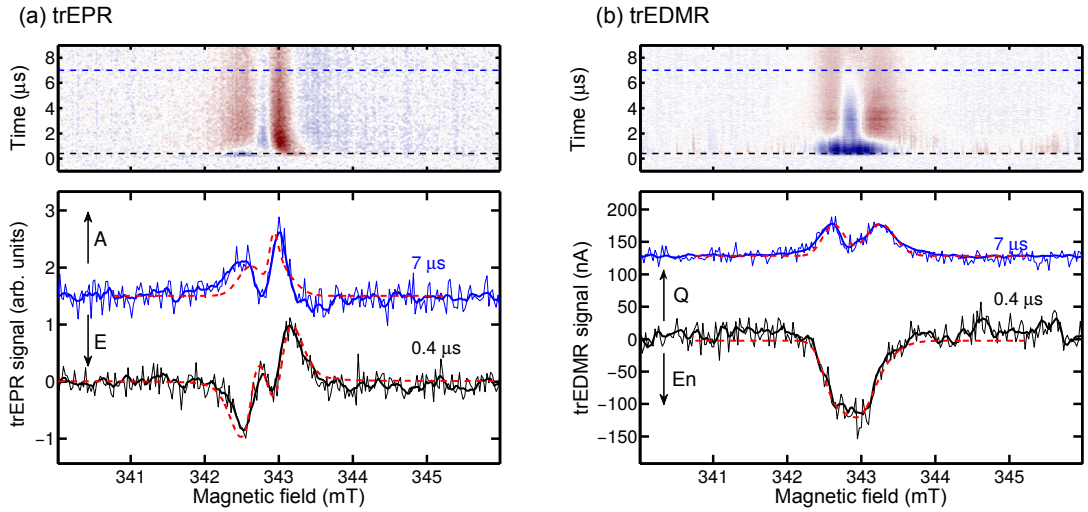

Figure 3.1.2: Transient EPR measurement (a) and trEDMR measurement (b) taken under identical conditions at T=80 K. The trEPR signal for short delays after the excitation (black curve) exhibit a clear CT-state signature with an EAEA-pattern (E – emissive, A – absorptive transition). For longer delays (blue curve) a signal arising from purely absorptive separated P^+ (342.5 mT) and P^- (343 mT) can be observed. The red dashed lines are simulations for the CT state and the free polarons based on g-matrices reported in literature. The upper plot shows the complete time dependence of the trEPR spectrum. The trEDMR measurement has a purely photocurrent enhancing signal (En) for short delays which can be well simulated with the same set of g-values used for simulations of the EPR spectra, just with a different line width. For 7 µs delay after the excitation a current quenching signal (Q) is observed that can be simulated with the whole anisotropic g-matrix of the P^+ and the z-component of the g-matrix of the P^-. The figure is taken from [FK3].

3.2 Triplets in Organic Solar Cells

Within this section different trEPR studies about triplet excitons in OSC are presented and their role for solar cell processes are discussed. We start with an unpublished overview about triplet EPR-signatures for several archetypal pristine organic semiconductors in order to show how diverse these signatures can be. This study emphasizes that trEPR is a good tool to resolve the origin, morphology and generation process of triplet excitons especially in samples with various materials. We are looking in general at systems comprising several materials. Therefore, good references for the shape and spectral width of triplet excitons are very helpful to link signatures to their specific material phase for all our trEPR investigations.

3.2.1 Intersystem Crossing Triplets in Pristine OPV Materials

Many OPV materials exhibit triplet excitons if there does not exist a donor-acceptor interface that enables a fast exciton dissociation. The EPR signature arises of these ISC-crossing triplets varies with the population of the triplet sub-levels and the dipolar coupling strength. Figure 3.2.1 depicts four different organic semiconductors spin-coated on a quartz substrate, where four show a triplet exciton state. [60]PCBM, a C_{60}-fullerene with a side chain, shows a triplet with a relatively weak dipolar coupling strength and therefore reveals a narrow triplet signature. Other polymers like P3HT and PCPDTBT show a much broader signature because of a stronger triplet coupling strength. All three materials show a powder pattern of a triplet which is typical for an amorphous or polycrystalline material that show all molecular orientation with respect to the magnetic field. The polymer, N2200 from Polyera (POLYERA CORPORATION), is more crystalline and therefore exhibits not a complete triplet powder spectrum but only two orientation dependent transitions. The widths of these spectra are dependent on the orientation of the substrate surface in correlation to the magnetic field axis. The plot gives good overview about the various shapes of triplets. In summary a detailed analysis of triplet spectra allows to determine the coupling strength, the population of the triplet sub-levels and the molecular orientation of the triplet itself. More information about analysis of triplets in EPR are given in Sec. 2.2.3.

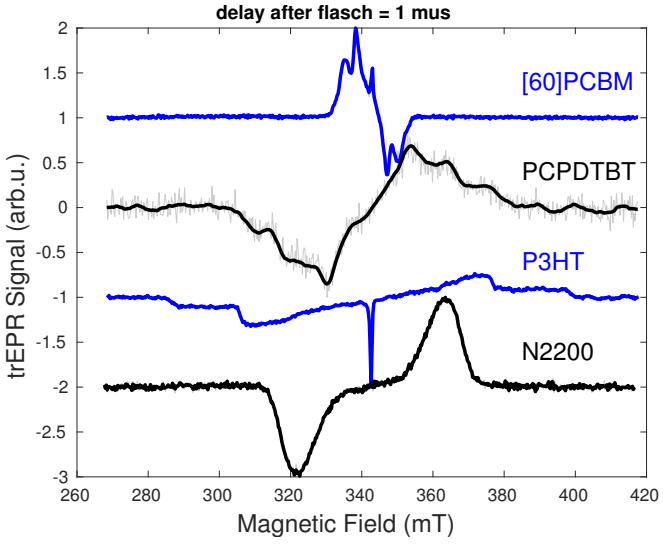

Figure 3.2.1: Transient EPR measurements shown for different pristine organic semiconductors. All samples are thin films of about 100 nm spin-coated on a quartz substrate. The measurements were performed at T=80 K. All materials show an ISC-triplet signal differing in their dipolar coupling strength. In contrast to the upper three triplets , the lowest one reveals a signature of a crystalline sample instead of a powder sample.

3.2.2 Charge Separation in PCPDTBT:PCBM Blends from an EPR Perspective

This subsection contains a summary of [FK1] published in the Journal of Physical Chemistry C (2014). The whole article is attached in the appendix B.1.

My contribution within this article is the development of the Matlab code for dynamic simulation of the BET triplets with state populations based on rate equations. The samples were produced by Steve Albrecht and encapsulated by me. I carried out all cwEPR, pEPR and trEPR measurements. I analyzed all the data. The results and analysis were discussed with all authors. I wrote most of the article supported by Jan Behrends and generated all figures.

The article presents a direct comparison of two donor derivatives, C-PCPDTBT and Si-PCPDTBT, blended with PCBM, that show an enormous difference in their power-conversion efficiency. The only difference between both PCPDTBT polymers is one atom in the conjugated system which is either Silicon (efficient polymer) or Carbon (non-efficient polymer). This study about charge separation within organic blends containing two promising low-bandgap polymers describes the most relevant charge-transfer pathways in OSCs. We demonstrate that not just the observable spin states but also the precursors can often be determined if a good knowledge about spectral shapes is available. The concluding schematic (Fig. 3.2.2) visualizes that Si-PCPDTBT:PCBM blend reveals efficient charge separation, while C-PCPDTBT:PCBM offers a major loss channel via BET to triplet excitons. Why this loss channel just appears for the C-bridged polymer is not yet clear. There are two possible reasons for explanation. Both blends offer different crystallinity and different energy levels of the triplet excitons. This may effect the dissociation yield of the CT state towards free charge carriers.

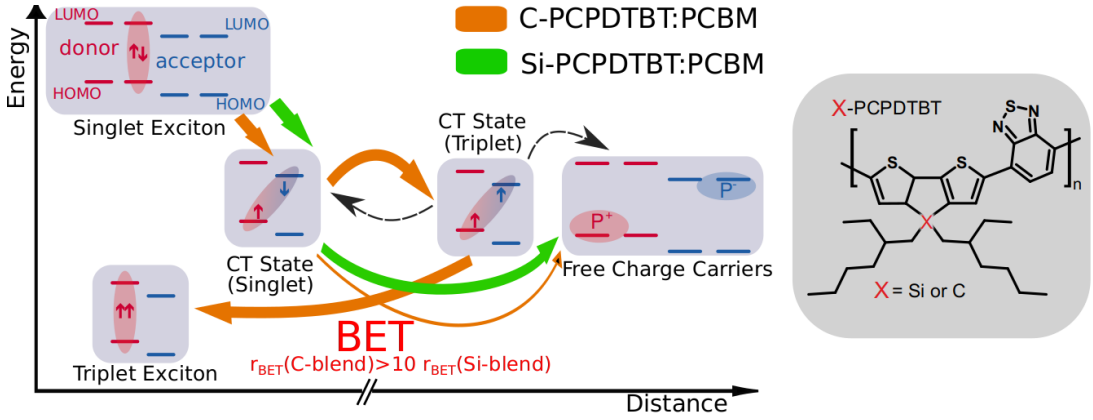

Figure 3.2.2: Visualization of charge-transfer pathways in C-PCPDTBT:[60]PCBM and Si-PCPDTBT[60]PCBM. The more efficient Si-blend exhibit a direct charge separation via a singlet CT state to free charge carriers while the C-blend generates less free charge carriers but has a loss channel via a triplet CT state to a triplet exciton populated by BET. This figure is taken from [FK1] and the chemical structure is added for reference.

Abstract

"Using time-resolved electron paramagnetic resonance (EPR) spectroscopy in conjunction with optical excitation we study charge separation in conjugated polymers blended with [6,6]-phenyl C61-butyric acid methyl ester (PCBM). A direct comparison between samples comprising poly[2,6-(4,4-bis-(2-ethylhexyl)-4H-cyclopenta[2,1-b;3,4-b']-dithiophene)-alt-4,7-(2,1,3-benzothiadiazole)] (C-PCPDTBT) and their analogues containing poly[(4,4'-bis(2-ethylhexyl)dithieno[3,2-b:2',3'-d]silole)-2,6-diyl-alt-(4,7-bis(2-thienyl)-2,1,3-benzothiadiazole)-5,5'-diyl] (Si-PCPDTBT) reveals a remarkable influence of the bridging atom (carbon vs. silicon) in the polymer on the EPR spectra. While the EPR signatures of photogenerated positive polarons in C- and Si-bridged PCPDTBT are virtually identical, significant differences are observed with respect to the spin-relaxation behavior. The spin-lattice relaxation time of positive polarons in C-PCPDTBT at low temperature (T = 80 K) is found to be more than two orders or magnitude longer than in the Si-bridged polymer derivative. This surprisingly slow relaxation can be rationalized by polarons trapped in defect states that seem to be absent (or are present in a substantially smaller concentration) in blends comprising Si-PCPDTBT. Transient EPR signals attributed to charge-transfer (CT) states and separated polarons are smaller in the blends with C-PCPDTBT as compared to those with the silicon-bridged polymer. We propose that triplet formation occurs via the CT state, thus diminishing the probability that the CT state forms free charge carriers in blends of C-PCPDTBT with PCBM. This hypothesis is confirmed by direct detection of triplet excitons in C-PCPDTBT:PCBM blends. The shape of the transient EPR spectra reveals that the triplet excitons are, in contrast to those formed in pristine polymer films, not generated by direct intersystem crossing, but result from back electron-transfer through CT-state recombination. The strong triplet signal is not observed in blends containing the Si-bridged polymer, indicating efficient singlet exciton splitting and subsequent charge-carrier separation at the Si-PCPDTBT/PCBM interface." cited from [FK1]. The whole charge-separation pathway for both donor polymers is visualized in Fig. 3.2.2.

3.2.3 Triplets in All-Polymer Solar Cells

This subsection presents our contribution to the article [FK2] published in Advanced Functional Materials (2014). Many groups shared and discussed their results for this article coordinated by Marcel Schubert (formerly from AG Neher, University of Potsdam).

Our contribution within this report are the trEPR measurements shown in [FK2]. I carried out all EPR measurements and triplet simulations. I discussed the results with Jan Behrends and Marcel Schubert. Marcel Schubert generated the final plots for the article.

The donor/acceptor copolymer P(NDI2OD-T2) (N2200 from Polyera Cooperation) is an alternative for a fullerene acceptor that reveals very high charge mobilities [112]. High charge mobilities are preferable, because charge extraction at the electrodes always competes with non-geminate recombination. If the charge needs too long to reach an electrode, it recombines. Fullerenes were the most successful electron acceptors for the last decade, while the increase of the power-conversion efficiency of OSCs is only based on the development of new donor materials. Therefore, the properties of fullerene acceptors are limiting current solar-cell efficiencies. Non-fullerene acceptor based organic solar cells showed very recently that they can achieve higher power-conversion efficiencies than fullerene based ones. All recent world records of organic single junction solar cells rely on small molecule acceptors.[19–21]

In [FK2] a large morphology dependency of the charge-separation process in P3HT:P(NDI2OD-T2) is studied in a cooperation project by several methods such as EQE measurements, transient absorption measurements, photothermal deflection spectroscopy, energy-filtered transmission electron microscopy, X-ray diffraction methods and trEPR. It could be shown that a proper orientation of the crystalline domains in all polymer solar cells is necessary for an electron-hole pair dissociation. This provides a possible explanation for the low quantum efficiency of P(NDI2OD-T2) compared to fullerene based acceptors.

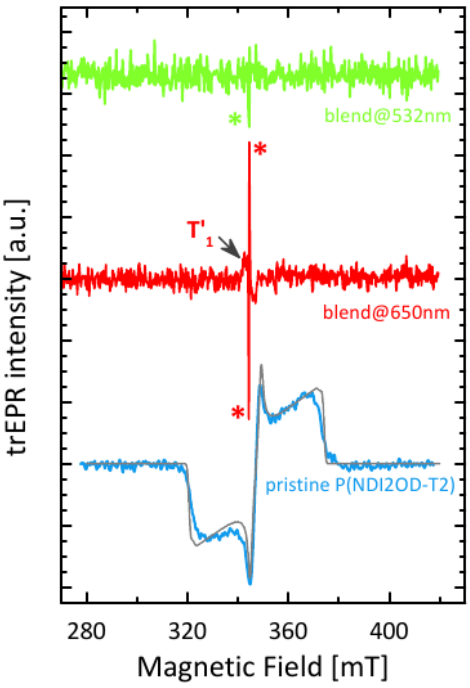

Figure 3.2.3: trEPR spectra of pristine P(NDI2OD-T2) films (blue) including an ISC-triplet simulation (grey line) and a morphology-optimized P3HT:P(NDI2OD-T2) blend after excitation at 650 nm (red) and 532 nm (green). The signal from the (bulk) triplet is quenched in the blend. The CT states occurring in the blends are marked with an asterisk. It is assumed that an interface triplet causes the signal marked with T'$_1$. The figure is taken from [FK2].

TrEPR was used within this article to directly detect triplet states in the pure P(NDI2OD-T2) films and optimized blends. We could measure a strong ISC triplet in the pristine film, which did not occur in the optimized blend (see Fig. 3.2.3). The blend optimization was performed by adjusting the spin-coating process with different compositions of organic solvents and additives. Instead of the triplet, a CT state (marked with an asterisk) occurred independently of the excitation wavelength (532 nm absorbed by the donor, 650 nm absorbed by the acceptor). In case of the excitation of the donor we found an additional signal of a long-lived interface triplet T'_1 which may be originated in ISC of singlet excitons (see Fig. 3.2.3). Photoluminescence quenching efficiency (PQE) measurements showed that just 50% of the singlet excitons generated in the P(NDI2OD-T2) domains reach the heterojunction. ISC may enhance the diffusion length of these formerly singlet excitons and thus generate long-lived interface triplets. Further information can be found in the supplementary information of [FK2].

4 Efficiency Enhancing Systems for OSCs studied by EPR

This chapter represents the second part of my thesis that focuses on efficiency enhancement systems for OSCs. It contains results from the following publications:

- [FK4]: Weiss *et al., Strongly exchange-coupled triplet pairs in an organic semiconductor* published in Nature Physics (2017).
- [FK8]: Kraffert *et al., Transport-related triplet states and hyperfine couplings in organic tandem solar cells probed by pulsed electrically detected magnetic resonance spectroscopy* published in the Journal of Magnetic Resonance (2017).
- [FK5]: Pingel *et al., p-Type Doping of Poly(3-hexylthiophene) with the Strong Lewis Acid Tris(pentafluorophenyl)borane* published in the Advanced Electronic Materials (2016).

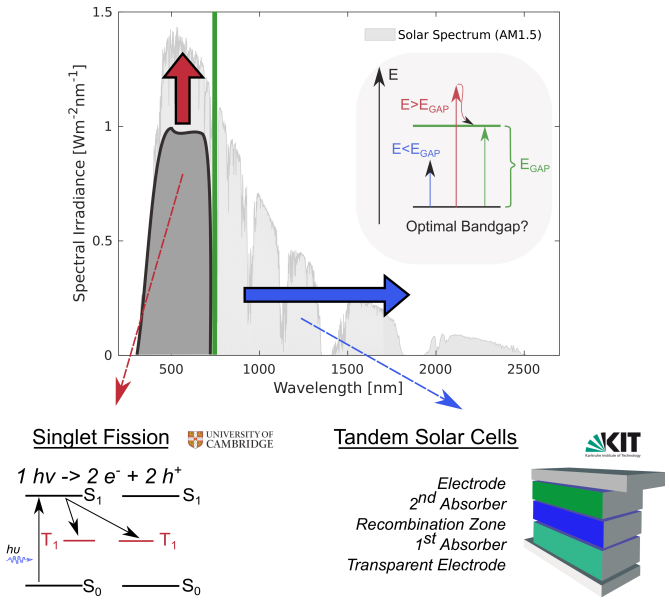

Figure 4.0.1: The power-conversion efficiency of a solar cell is dependent on how many photons from the sun spectrum can be effectively converted to electrical power. E_{gap} stands for the bandgap of the solar cell. Two major loss mechanisms (thermalization and transmission) are visualized in this schematic together with two approaches to reduce these losses. The singlet-fission approach studied by trEPR is published in [FK4]. Tandem solar cells are investigated in collaboration with Daniel Bahro and Alexander Colsmann from the KIT published in [FK8]. The shown sun spectrum under AM1.5 condition is based on data from the National Renewable Energy Laboratory (NREL).[15]

The power-conversion efficiency of a solar cell under realistic conditions is strongly dependent on absorbance of the solar spectrum on the earth (AM1.5) and how efficient it can convert the incoming photon energy to electrical energy. With a single p-n-junction solar cell the theoretical limit of power-conversion efficiencies is about 30% (E_{gap} = 1.1 eV) calculated by Shockley and Queisser for inorganic solar cells.[113] Note the Shockley-Queisser limit can only be applied to OSCs after adding empirical corrections for the difference between the transport and absorption bandgap.[114] Figure 4.0.1 demonstrates that even a solar cell with an optimal bandgap has some major

losses. On the one hand low energy photons, with energies below the bandgap, can not be absorbed (blue arrows). On the other hand photons with energy higher than the bandgap lose their excess energy above the bandgap because of relaxation processes (thermalization, arrows). To avoid these losses, two promising approaches are presented here. Singlet fission, which hinders the loss of thermalization, and tandem solar cells, which are able to use also low energy photons for the charge separation. It has been shown that the solar cells with efficient singlet fission can have external quantum efficiencies above 100% for pentacene:fullerene solar cells.[88,89] The excess energy of high energetic photons from the solar spectrum can such be more efficiently used in the power-conversion process.

Within a collaboration with the University of Cambridge we investigate the singlet-fission process that allows to generate two triplet excitons from one incoming high energetic photon. A detailed trEPR study of the singlet fission in TIPS-tetracene is published in Nature Physics in [FK4] and is presented in Sec. 4.1.

In a collaboration with the Karlsruhe Institute of Technology (KIT) and the group of Alexander Colsmann we studied fully processed micro organic tandem solar cells. Tandem solar cells use two absorber layers to access low and high energy photons more efficiently. A pEDMR study of organic tandem solar cells is published in the Journal of Magnetic Resonance in [FK8] and presented in Sec. 4.1.

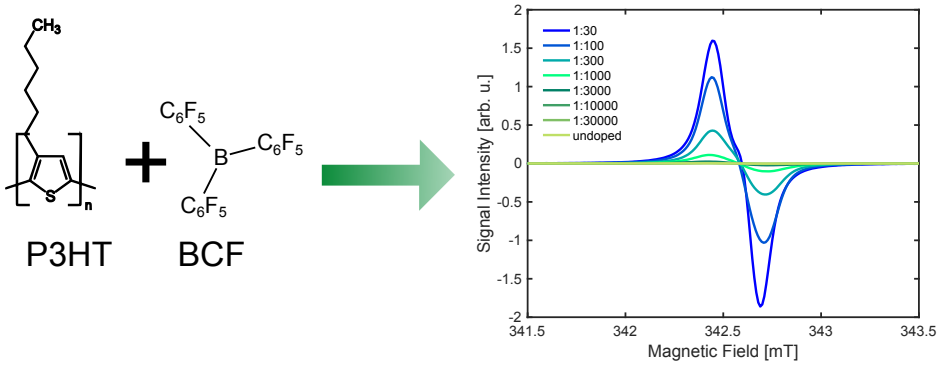

Figure 4.0.2: In [FK5] it was shown for the first time that the Lewis acid tris(pentafluorophenyl)borane (BCF) is an efficient dopant for our reference material P3HT. The charge-carrier density increase in the semiconductor with higher doping ratio can be observed in the cwEPR measurement. The sample preparation (at RT) was done by Charlotte Beck (Bachelor Student in the group of Jan Behrends).

A major drawback of organic semiconductors in contrast to Silicon is the low mobility for electrons and holes. These low mobilities lead to short diffusion lengths and therefore limit the maximum domain/phase size (distance between CT state dissociation and charge extraction) of the donor and acceptor materials . Instead of further optimizing the Π-conjugated backbone and the crystallinity of the phases by synthesizing new polymers, one can also increase the charge-carrier density by doping in analogy to doping in silicon. In section 4.2 a study about doping of organic semiconductors due to a Lewis acid will be presented. Quantitative cwEPR enables to measure charge-carrier densities in organic semiconductors as it is demonstrated in Fig. 4.0.2. The change of the doping ratio directly influence the EPR signal intensity. The amount of acceptor molecules (P3HT) was kept constant for the whole series. The whole study combines a variety of different methods published in [FK5].

All articles have in common that they describe methods to enhance the performance of organic semiconductors or in particular OSCs which are studied by EPR techniques.

4.1 Singlet Fission and Tandem Solar Cells

In the following section we present two projects that deal with approaches to enhance the external quantum efficiency of OSCs: First, a singlet-fission system based on a pure TIPS-tetracene sample investigated as a small single crystal and a thin film sample. Second, an advanced organic tandem solar device with various layers each specialized for different properties. Both systems have in common that they belong to the "third generation" of OSCs and triplet excitons are important for their main process.

4.1.1 Strongly Exchange-Coupled Triplet Pairs in an Organic Semiconductor

This section is a summary of the article [FK4] published in Nature Physics (2017). The whole article can be found in the appendix B.4. All measurements published within this article are achieved in our labs (AG Bittl/AG Behrends) at the Freie Universität Berlin. Together with Leah Weiss and Sam Bayliss I performed most of the published pEPR and trEPR measurements. Leah Weiss and Sam Bayliss evaluated the data and wrote the manuscript. I generated the figure about the rise time of the trEPR signal published in the supplementary information. All authors discussed and improved the manuscript.

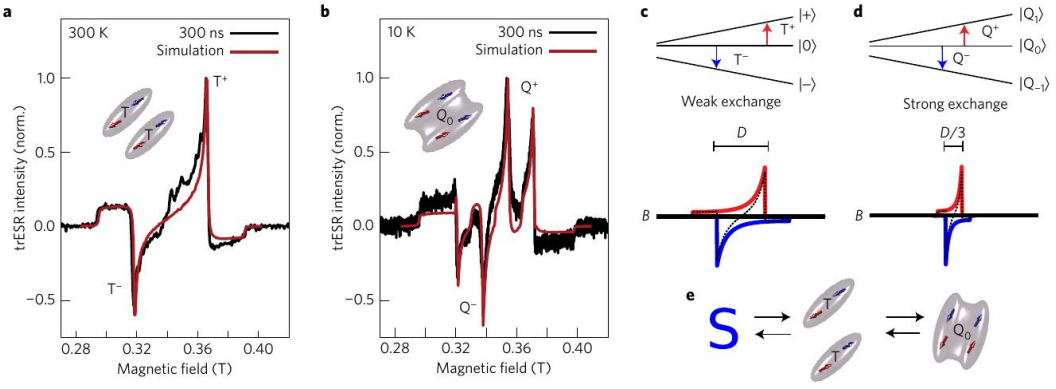

Figure 4.1.1: This schematic shows weakly and strongly coupled pairs formed by singlet fission in TIPS-tetracene. (a) trEPR spectrum of a TIPS-tetracene thin film sample which exhibit a non-interacting triplet signature generated by singlet fission at room temperature. (b) shows a trEPR spectrum of the same film measured at 10 K. Two additional peaks Q^+ and Q^- appeared which can be attributed to strongly interacting triplet pair with inter-triplet exchange coupling (Quintet state). In (c) and (d) the components of the low temperature spectrum which belong to the weakly and strongly exchange coupled triplet pairs are shown. The schematic is published in [FK4].

In our experiments we investigate thin film and micro-crystalline TIPS-tetracene samples in order to understand the role of different spin states during and after the singlet-fission process. Transient EPR measurements at room temperature in combination with simulation prove the existence of weakly interacting triplets generated by the singlet fission process. Due to the triplet shape we can exclude that these triplets arise via intersystem crossing. Further information about triplet shapes are given in the Fundamentals Sec. 2.2.4. In low temperature measurements below 100 K two additional peaks appear in both types of samples. We perform Rabi nutation experiments in a pulsed EPR setup to determine the spin state of the different features. Figure 4.1.2 shows that the Rabi nutation frequency differs by $\sqrt{3}$ between the outer and inner peaks ($T^{\pm}$ vs. $Q^{\pm}$ see Fig. 4.1.1) and by a factor of $\sqrt{2}$ between the outer peaks and

the central component corresponding to a $S = \frac{1}{2}$ species (mainly visible in pEPR measurements). This measurement justifies the assumption that the inner peaks belong to strongly coupled triplet excitons ($S = 2$, quintet transition) and the outer ones to weakly coupled triplet excitons. Note that the finding of weakly and strongly coupled triplet pairs (triplet exciton vs. quintet state) is comparable to weakly and strongly coupled polaron pairs (CT state vs. triplet exciton). An additional fit of the ratio between the triplet peak and the singlet peak intensities in a detailed temperature series helps us to determine the activation energy of 4.2 meV which can be understood as the thermal energy required to escape from the strongly coupled quintet state. This energy provides a good estimate for the exchange parameter J of the strongly coupled triplet state.

The observation of quintet states formed via singlet fission is of high interest for optimizing the singlet fission (down-conversion) and also triplet-triplet annihilation (up-conversion) processes in solar cells and light emitting diodes.

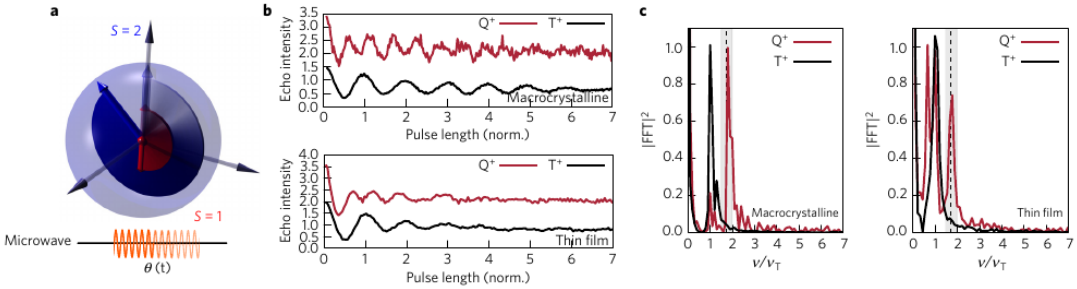

Figure 4.1.2: *"Rabi oscillations of weakly and strongly interacting triplets.* ***a****, Vector model representation of the dependence of the Rabi nutation on total spin in which the nutation frequency increases with S.* ***b****, Echo intensity measured as a function of initial pulse length (Rabi oscillations), resulting in distinct oscillation frequencies at the peak triplet (T^+) and quintet (Q^+) transitions in both the thin-film (bottom) and macrocrystalline samples (top).* ***c****, Fast Fourier transform (FFT) of Rabi oscillations in b, revealing a frequency component at the quintet peak corresponding to a factor of $\sqrt{3}$ higher frequency than the triplet transition, within the error shown in grey. This frequency corresponds to the $\Delta m_s = \pm 1$ transitions of the $|Q_0\rangle$ pair state. Note that peak amplitudes are normalized, and that the Q^+ transition in the disordered film also exhibits a Fourier component corresponding to an $S = \frac{1}{2}$ species ($\nu/\nu_T = 1/\sqrt{2}$) due to the presence of non-light-induced charges as well as an $S = 1$ species due to overlapping transitions of weakly coupled triplet states"* taken from [FK4].

Abstract

"From biological complexes to devices based on organic semiconductors, spin interactions play a key role in the function of molecular systems. For instance, triplet-pair reactions impact operation of organic light-emitting diodes as well as photovoltaic devices. Conventional models for triplet pairs assume they interact only weakly. Here, using electron spin resonance, we observe long-lived, strongly interacting triplet pairs in an organic semiconductor, generated via singlet fission. Using coherent spin manipulation of these two-triplet states, we identify exchange-coupled (spin-2) quintet complexes coexisting with weakly coupled (spin-1) triplets. We measure strongly coupled pairs with a lifetime approaching 3 µs and a spin coherence time approaching 1 µs, at 10 K. Our results pave the way for the utilization of high-spin systems in organic semiconductors. " published in [FK4].

4.1.2 Transport-Related Triplet States and Hyperfine Couplings in Organic Tandem Solar Cells Probed by Pulsed Electrically Detected Magnetic Resonance Spectroscopy

This subsection contains an overview of the article [FK8] published in the Journal of Magnetic Resonance (2017). The complete article can be found in the appendix B.8. The underlying project was handled in a cooperation with the KIT who have a great expertise in the production of organic tandem solar cells.

My contribution within this article is the development of the EPR capable tandem micro solar cells together with Daniel Bahro. Daniel Bahro and Maximilian Denne produced all investigated tandem solar cells including the final contacting and encapsulation as well as the solar cell characterization. I carried out all pEDMR measurements with support by Christoph Meier for the electrically detected hyperfine sublevel correlation experiment (ED-HYSCORE). The results and analysis were discussed with all authors. I performed the spectral simulations of the triplet state and HYSCORE spectrum. I wrote the article, except for the paragraphs about the materials and sample preparation. I generated all figures.

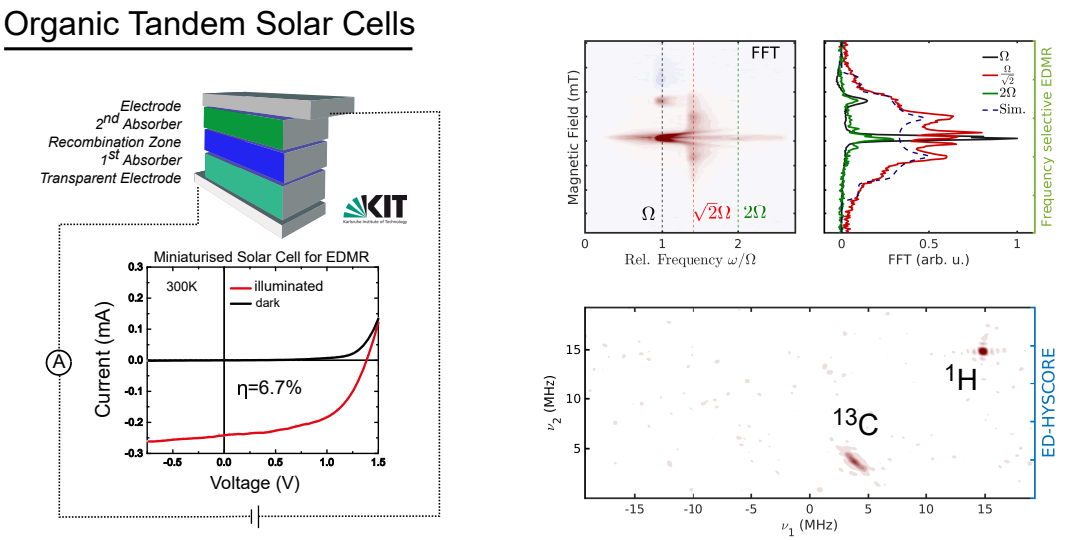

Figure 4.1.3: (Left) current-voltage measurements for an organic tandem solar cells produced and measured by Daniel Bahro at the KIT. All measurements were performed on miniaturized solar cells. The power-conversion efficiency of 6.7% is comparable to those of normal sized cells. The graphs on the right side depict overviews of our results. The graph was taken from [FK8].

In this study we investigate fully processed tandem solar cells in a miniaturized setup in order to make them fitting to a conventional EPR resonator. We can produce and measure complete tandem solar cells with all necessary layers for high open circuit voltage (V_{OC}) above 1.2 V and efficiencies of 6.7%. Our scope is to better understand the functionality of the recombination layers in the cell. These layers are required for a loss-less recombination of electron and holes to increase the open circuit potential of their compensating charge. We try to understand the influence of triplet formation at the interface on the recombination process.

We see spin-dependent transport and recombination in our organic tandem solar cells and can identify several spin centers contributing to the photocurrent at low temperatures: weakly coupled polarons (spin-$\frac{1}{2}$) in the organic blend, triplets localized in the fullerene ([70]PCBM) phase and charges ($S = \frac{1}{2}$) in the ZnO layer.

This first approach to tackle the complex devices processes of organic tandem solar cells with EDMR methods paves the way for further studies. One promising follow up study would be to construct sub cells of the tandem cell with different interfaces to identify the conditions for triplets occurrences. Furthermore, a better knowledge about the spin states at the recombination layer interface would be helpful to increase the rate of lossless recombination at the recombination layer.

Abstract

"Tandem solar cells constitute the most successful organic photovoltaic devices with power-conversion efficiencies comparable to thin-film silicon solar cells. Especially their high open-circuit voltage – only achievable by a well-adjusted layer stacking – leads to their high efficiencies. Nevertheless, the microscopic processes causing the lossless recombination of charge carriers within the recombination zone are not well understood yet. We show that advanced pulsed electrically detected magnetic resonance techniques such as electrically detected (ED)-Rabi nutation measurements and electrically detected hyperfine sublevel correlation spectroscopy (ED-HYSCORE) help to understand the role of triplet excitons in these microscopic processes. We investigate fully working miniaturised organic tandem solar cells and detect current-influencing doublet states in different layers as well as triplet excitons located on the fullerene-based acceptor. We apply ED-HYSCORE in order to study the nuclear spin environment of the relevant electron/hole spins and detect a significant amount of the low abundant ^{13}C nuclei coupled to the observer spins." cited from [FK8].

4.2 Doping & Mobilities

As introduced in the beginning of chapter 4, low mobilities of organic semiconductors are one of their main disadvantages. This issue can be compensated by doping as it is well known from inorganic semiconductors. The following section presents a combined optical, electrical and EPR study about a new p-type doping agent, the Lewis acid BCF[1]. This investigation connects contact-less quantitative charge-carrier density measurements with electrical mobility measurements, shown in Fig. 4.2.1. It shows the capability of quantitative EPR (qEPR) to extend the sensitivity range of optical and electrical measurements to determine charge carrier concentrations. qEPR spectroscopy was the main method of most of the Bachelor students who were supervised during my PhD project. Thus, the calibration and improvement of the setup and the evaluation routine was always an important part of my project. This study presents an overview of our qEPR setup, its capability and the importance of the supporting multi-frequency preliminary study.

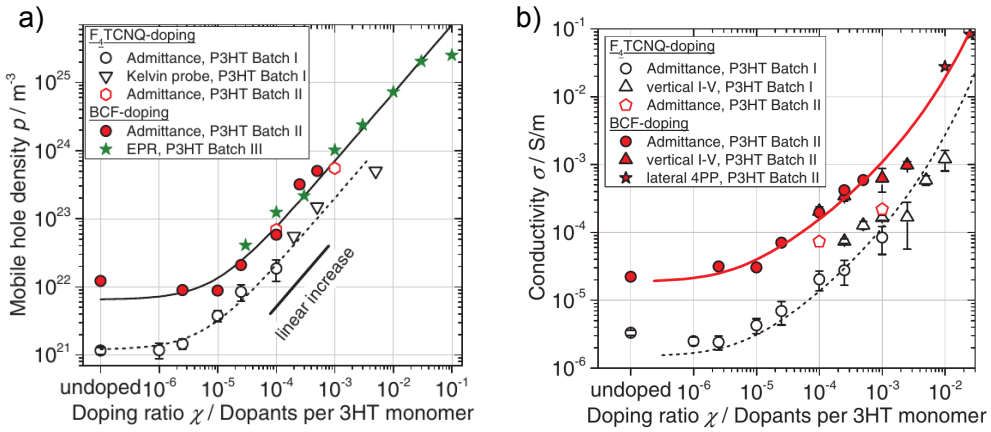

Figure 4.2.1: (a) shows the hole density versus the doping ratio of BCF per 3HT monomer unit. This plot shows a direct comparison between three different independent measurement methods, Kelvin probe spectroscopy, Admittance spectroscopy and EPR spectroscopy, probing the same materials. (b) displays the resulting conductivity dependence of P3HT on the doping ratio. This shows the parallel increase of the charge-carrier mobility and conductivity of P3HT with increasing doping concentration of BCF.[FK5]

4.2.1 P-Type Doping of Poly(3-Hexylthiophene) with the Strong Lewis Acid Tris(Pentafluorophenyl)Borane

This subsection presents the article [FK5] published in the Journal of Advanced Electronic Materials (2016). The whole article can be found in the appendix B.5.

My contribution within this article is the calibration scheme of our cwEPR machine for qEPR together with Christian Teutloff and Christopher Engelhard. The calibration was improved within several foregoing Bachelor projects which were connected to this thesis. Christopher Engelhard developed the applied spin-counting toolbox for Matlab. The production and qEPR mesurements of the doped samples were carried out by Charlotte Beck. I performed the spectral deconvolution of the EPR signals by X-band, Q-band and W-band measurements including necessary simulations and the final plots within the supplementary information of the article. The results and

[1] tris(pentafluorophenyl)borane

analysis were discussed with all authors. I wrote all passages about EPR within the article and the supplementary information with support from Robert Steyrleuthner.

Within this article it is shown that the strong Lewis acid BCF can effectively dope the well known P3HT polymer with a doping efficiency of about 18%. The resulting mobile hole density is comparable with the densities reached with the widely used dopant F_4TCNQ. In both cases the charge-carrier density increases linearly with the dopant ratio (see Fig. 4.2.1a and Fig. 4.2.2). Quantitative EPR measurements extend the observable doping range beyond the one accessible with electrical measurements and showed a convincing agreement in the overlapping range with admittance and Kelvin probe measurements. Analogous to the strong increase of the mobile hole density upon increasing doping ratio, the electrical conductivities of the doped samples also increase significantly. The conductivities are found to be three times higher than the conductivities determined for the established dopant F_4TCNQ at the same doping ratios.

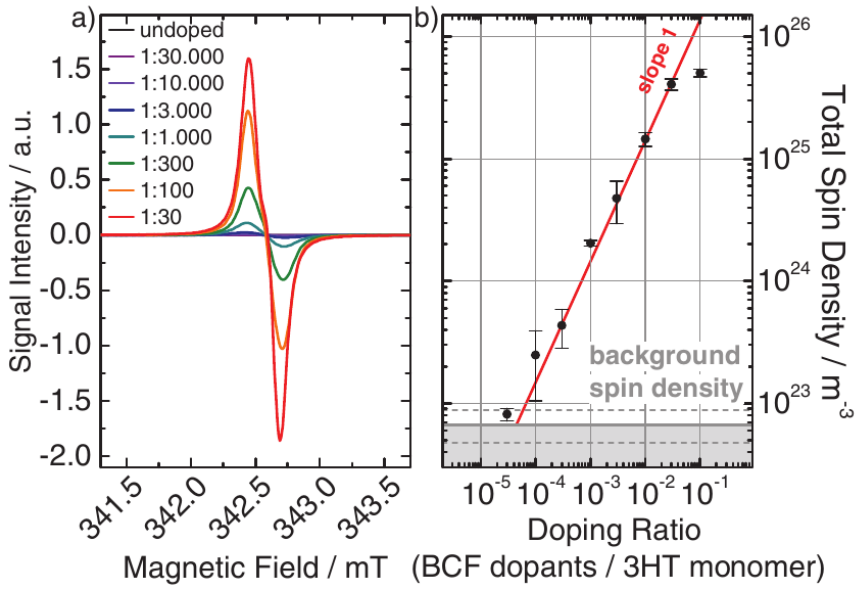

Figure 4.2.2: (a) EPR spectra of BCF-doped P3HT films with various doping concentrations at room temperature. (b) Total spin densities measured by quantitative EPR. The spin densities were calculated with our *spincounting toolbox* for Matlab (The MathWorks, Natick, MA). The densities consist of equal distributions of the polarons on P3HT and BCF. The spectral deconvolution is shown in Fig. 4.2.3. The background density was determined on pristine P3HT reference films. The error bars are based on the standard deviation of three independent doping series. Both plots are published in [FK5].

Spectral Deconvolution of the X-band Spectrum

One challenging question in our quantitative cwEPR analysis of the BCF doping mechanism is to distinguish between the contribution of the positive charges on P3HT and the negative charges on BCF. This deconvolution is described in the supplementary information of [FK5]. While the g-matrix of P^+ on P3HT has been reported several times, the g-matrix of a P^- on BCF has not been measured. In order to clarify whether the signal detected in X-band consists out of two species or just of the positive polaron on P3HT we perform high frequency measurements in W-band (95 GHz). The advantage of W-band in comparison to X-band EPR is the ten times higher g-resolution. This results from diminished relative line broadening in W-band compared to X-band

(9.6 GHz) frequencies, if the main broadening mechanism is based on hyperfine interactions. Figure 4.2.3a shows the W-band measurements on a 1:100 BCF:P3HT film sample together with simulations. The easyspin[98] simulation contains two uncoupled spin systems with an equal weight distribution. A spin species based on g-values reported in literature for P3HT (blue dashed line) and another one (green dashed line) is derived by fitting the complete spectrum (see red curve). The axial g-matrix, determined for the second unknown component, was attributed to the BCF anion. The simulation in Fig. 4.2.3b with the same set of parameters like in W-band proves that the signal, observed in our qEPR measurements, contains an equal contribution of a BCF anion and a P3HT cation. Therefore, we assumed for all quantitative measurements a spin count consisting out of an equal distribution of P^+ and P^-.

Abstract

"State-of-the-art p-type doping of organic semiconductors is usually achieved by employing strong π electron acceptors, a prominent example being tetrafluorotetracyanoquinodimethane (F_4TCNQ). Here, doping of the semiconducting model polymer poly(3-hexylthiophene), P3HT, using the strong Lewis acid tris(pentafluorophenyl)borane (BCF) as a dopant, is investigated by admittance, conductivity, and electron paramagnetic resonance measurements. The electrical characteristics of BCF- and F_4TCNQ-doped P3HT layers are shown to be very similar in terms of the mobile hole density and the doping efficiency. Ca. 18% of the employed dopants create mobile holes in either F_4TCNQ or BCF-doped P3HT, while the majority of doping-induced holes remain strongly Coulomb-bound to the dopant anions. Despite similar hole densities, conductivity and hole mobility are higher in BCF-doped P3HT layers than in F_4TCNQ-doped samples. This and the good solubility in many organic solvents render BCF very useful for p-type doping of organic semiconductors." cited from [FK5].

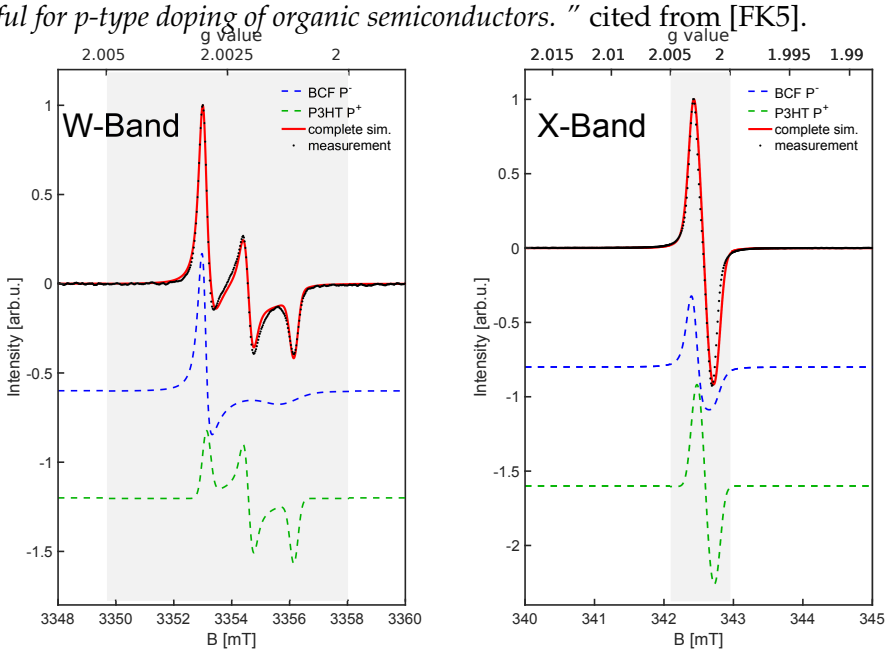

Figure 4.2.3: Field modulated cwEPR measurements at W-band (94 GHz) and X-band (9.6 GHz) of a 1:100 BCF doped P3HT film on an inner wall of an EPR tube at T=300 K. The simulation is performed with the easyspin[98] toolbox for Matlab for both both plots with the identical set of parameters except the line width. The W-band measurements enables the resolution of two different species P^- and P^+ which is not possible just from X-band data. Both plots are taken from the supplementary information of [FK5].

5 Conclusion and Outlook

This thesis involves several projects with an unifying theme: EPR techniques were used or developed to unravel uncertainties of processes in OSC materials. These projects can be summarized in three main directions (see Fig. 5.0.1):

I. *Charge separation in organic donor-acceptor materials*

II. *Exceeding the conventional efficiency limits of OSCs*

III. *Determining charge-carrier delocalizations and concentrations*

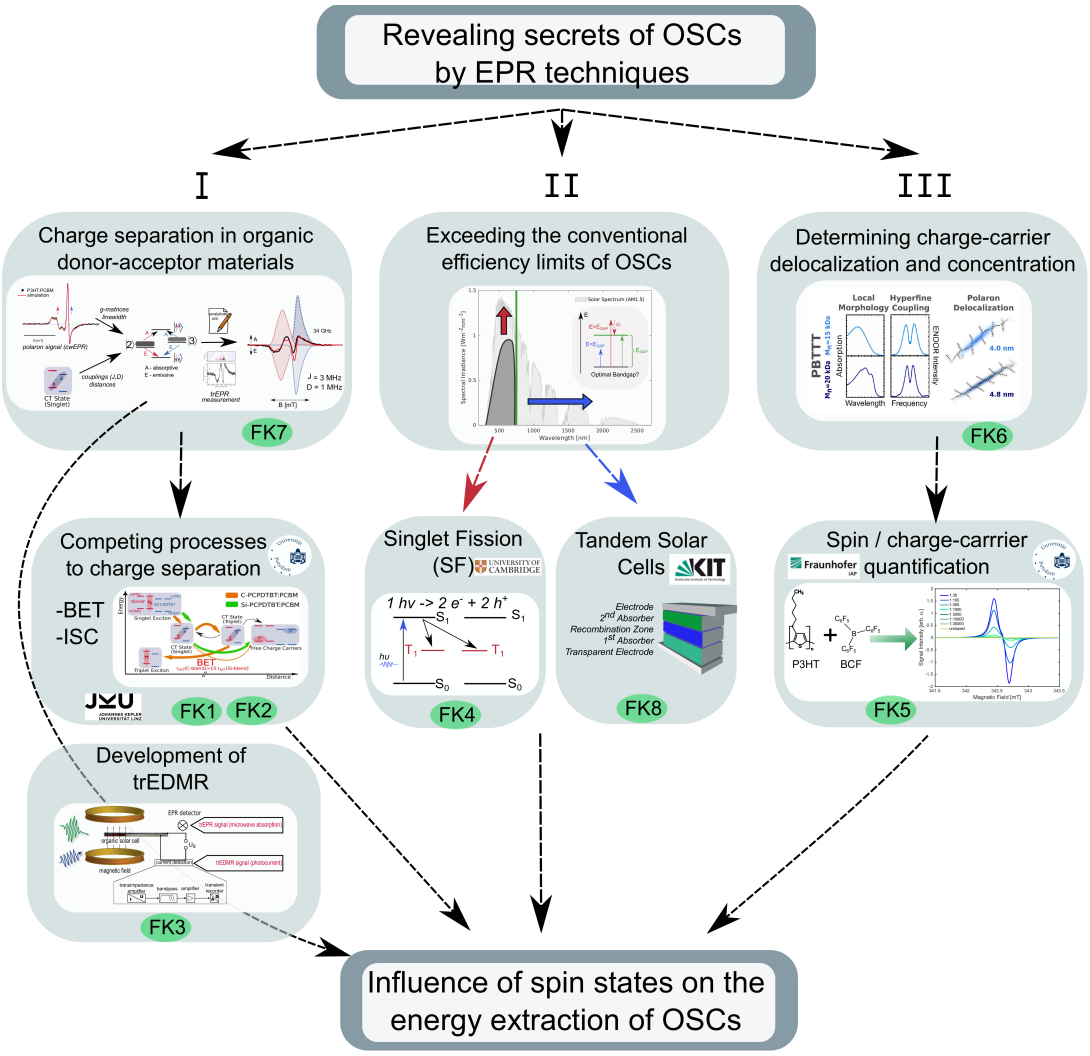

Figure 5.0.1: Concluding figure: Relations and connections of my different PhD projects. The green ellipsoids show to which field of research our publications contribute. The miniaturized table of content figures are partly reused from [FK1, FK3, FK6–FK8] to visualize the topics.

I. The first study of the charge-separation process in OSCs [FK1] illustrates a comprehensive picture of the charge separation in OSCs from an EPR point of view. This overview of the specific EPR signatures for most of the possible states and transfer process of OSCs shows that trEPR is a powerful tool to study OSCs. We investigated two structurally very similar low-bandgap polymers (C-PCPDTBT and Si-PCPDTBT), which reveal a difference in power-conversion efficiency by nearly a factor of two if blended with a fullerene acceptor ([60]PCBM). We observed that just the low efficiency polymer (C-PCPDTBT) exhibits extremely slow spin-lattice relaxation times for positive polarons which can be rationalized by deeply trapped polarons in defect states. Furthermore, we detected that only the low efficient polymer has a very intense triplet exciton generation yield within a blend with the acceptor. With dynamic spectral simulations we showed that triplet formation occurs through CT-state recombination (BET process). This reduces the probability of free charge-carrier formation via CT-state dissociation. In this case, the triplet formation acts as a loss mechanism within the charge-separation process, while triplet excitons can be also used to enhance the external quantum efficiency of a solar cell as we discuss below.[FK4]

   A consecutive study [FK7] complemented these experimental findings with theory. This study presented a development of a semi-analytical simulation code for the description of CT states in EPR. These simulations in combination with experimental multi-frequency EPR spectra allowed us to determine CT-state binding energies and hence information on the polaron pair wavefunction and delocalization. Our investigations demonstrated that it is often not sufficient to assume only dipolar couplings between weakly coupled radical pairs (CT state) but it is also necessary to consider exchange couplings.

   A further branch [FK1, FK2] targeted competing processes to efficient charge separation, e.g. BET or ISC, which can be distinguished by detailed spectral analysis. These studies showed that the knowledge about EPR signatures of triplet excitons and their decay dynamics are crucial to explain triplet population mechanisms and to clarify their precursor states.[FK1,FK4] These findings were important to interpret other time-dependent optical spectroscopy data, e.g. from transient-absorption spectroscopy[18] that are often ambiguous for the differentiation between CT states and triplet excitons. Furthermore, understanding signatures of triplet excitons helped to correlate triplet signals with their point of origin like interfaces or specific layers.[FK2] In addition, this knowledge was helpful to distinguish between triplets and higher spin states like quintet states.[FK4]

   Transient EPR alone is not able to link the observable microscopic spin processes to the macroscopic photocurrent of OSCs. To clarify the importance of free polarons, detected by trEPR, for the photocurrent of OSCs, we developed a transient electrical detection technique in [FK3]. In addition, this development contained a new design of a miniaturized fully-processed organic solar cell, which was also the foundation for subsequent projects (see [FK8]). In [FK3], we showed that the spin manipulation of CT states and free polarons influences the sample conductivity. This experiment connected the trEPR signatures with the photocurrent of the OSCs and opened the field for further studies. Additionally, it proved that both donor (P3HT) and acceptor ([60]PCBM) polaron-spin processes contribute to the photocurrent.

II. This thesis contains two projects about approaches to exceed the conventional absorption limit of OSCs by either using singlet fission [FK4] or a multi-junction

(tandem) solar cell [FK8]. In both studies we could apply our enhanced knowledge about OSC's triplet excitons probed by EPR. Within the singlet-fission project (cooperation with the University of Cambridge) we could prove the appearance of strongly exchange-coupled triplet pairs (quintet states) within a TIPS-tetracene film as well as a weakly coupled triplet exciton formed by the singlet-fission process. Additional pEPR experiments (Rabi nutations) clarified the assignment of the EPR signatures to doublets, triplets and quintets. In our most recent study about organic tandem solar cells (in cooperation with the Karlsruhe Institute of Technology) we used a similar approach (ED-Rabi nutations) to separate spectrally overlapping doublet and triplet exciton signatures. This project used the knowledge of building miniaturized OSCs gained in our trEDMR study [FK3] in combination with the expertise of generating efficient tandem solar cells from our collaborators. We demonstrated that triplet excitons occur within the absorber layer and influence the conductivity in fully-working organic tandem solar cells by a current-enhancing triplet-exciton polaron quenching process at low temperatures. Spectral analysis together with a recently developed ED-HYSCORE experiment helped to allocate various EDMR signatures to their originating layers within a complex device structure. In addition, spin dependent hopping transport was observed in the ZnO layer of the tandem solar cell. Our strategy provides a route to understand and separate the influence of various materials for the generation of triplet excitons within absorber or recombination layers of organic multi-layer solar cells. The electrical detection of the sample conductivity directly correlates the influence of these spin states on the photocurrent of OSCs.

III. The third theme contains two further projects that investigated organic semiconductor properties and their influence on the energy extraction of OSCs. One project, which is not included in this thesis, focused upon the hole delocalization in a semicrystalline conjugated polymer. We were able to measure hyperfine coupling between the polaron spins and the neighboring nuclear spins directly by pENDOR (pulsed electron nuclear double resonance) spectroscopy.[FK6] The study was supported by a pEPR analysis of a promising oligomer series and complemented by density functional theory (DFT) calculations performed by collaborators form the King Abdullah University of Science & Technology. The results showed that delocalization is strongly dependent on the molecular order and crystallinity of the semiconductor. For PBTTT (poly(2,5-bis(3-alkylthiophene-2-yl)thieno[3,2-b]thiophene)) we achieved polaron delocalization lengths between 4 nm to 4.8 nm in dependence on the molecular weight of the polymer. A yet unpublished study is about the relation between polaron delocalization and charge-carrier mobilities in various organic semiconductors. This study connects the delocalization of polarons in OSCs with the mobilities of charges in organic semiconductors and is based on a cooperation with the University of Potsdam.

Since the conductivity of a semiconductor is the product of its mobility and its charge-carrier concentration, we were also interested in chemically manipulating the charge-carrier density of organic semiconductors by doping. To measure this effect, we improved our spin-counting evaluation system to determine charge-carrier concentrations. We applied a multi-frequency EPR analysis to resolve g-matrices and to disentangle overlapping EPR signatures of electrons and holes, which is necessary for a reliable determination of charge-carrier concentrations. We performed several doping series for quantification and compared our results with optically and electrically determined charge-carrier concentrations by our

collaborators from the Potsdam University and the Fraunhofer IAP. The successful investigation of a new p-type dopant (BCF) for organic polymers based on a Lewis acid was published in [FK5]. The determined doping efficiency of BCF was about 18%, a comparably high doping efficiency for organic dopants. The procedure presented within this article paves the way for the quantification of other upcoming organic dopant series. Since the exact doping mechanism of BCF stayed unclear, further investigations will follow.

Outlook: This thesis contains several strategies to investigate new OSC materials. Especially for questions concerning the appearance of triplet excitons, CT states or for the determination of charge delocalization and doping efficiencies EPR should be considered as the method of choice if the process time-scale is suitable. But our studies also revealed that there are still some open questions.

To understand how a CT-state signature looks in a trEDMR spectrum a theoretical description of an EDMR experiment analogous to the developed semi-analytical CT-state simulation for trEPR spectra would be helpful. Therefore, a link between the CT-state population and the sample conductivity has to be found. Furthermore, the change of the dissociation probability for triplet and singlet CT states might be important. This theoretical description should be supported by further trEDMR experiments with other material compounds to gain a more detailed knowledge of possible EDMR spectra.

Also singlet-fission materials like TIPS-tetracene should be further investigated by trEDMR and pEDMR. These methods can validate whether triplet excitons generated by singlet fission really enhance the photocurrent generation in OSCs. Furthermore, it would be interesting to perform quantitative EPR measurements for singlet fission based solar cells to determine the charge-carrier generation influenced by the singlet-fission process.

Our study about the two PCPDTBT derivatives ([FK1]) revealed trapped positive polarons in C-PCPDTBT. Here, a pENDOR study like [FK6] could uncover the nuclear environment of the positive polarons and thus localize the origin of the traps.

In our organic tandem solar cell project, an investigation of the respective sub-cells could be used to study the process of triplet generation and to figure out under which conditions triplet excitons occur. Furthermore, it would be interesting to test other tandem OSCs with recombination layers that encounter hysteresis effects. These effects are discussed to stem from surface dipoles. If this is the case, spin manipulations of polarons at the interface would lead to a change of the spin-dependent electron-transfer probability and so of the sample conductivity.

Another open project is the investigation of CT states at ambient temperatures. These investigations were challenging so far since the dissociation processes become faster towards room temperature and the time resolution of our X-band and Q-band setups were limited. Our Q-band setup was improved during the last years and extended with a new IQ-mixer detection such that the RT measurements should now be possible.

In addition, the doping mechanism remains still unclear for most organic dopants. In order to further investigate these mechanisms, a temperature dependent quantitative EPR series can be performed to determine possible doping activation energies.

In general, this thesis shall demonstrate the versatility of OSC investigations by EPR spectroscopy and how many new insights into the charge-separation processes of OSCs could be gained.

A Experimental Details of EPR/EDMR Spectroscopy

The following sections are about the experimental setups used to achieve the presented results. The first section focuses upon the transient EPR and EDMR setup, because these are the most important one for my thesis. Moreover, the trEDMR setup was developed for the first time within this project. All relevant information about the instrumentations used for the shown results are reported within the specific publications.

A.1 Transient EDMR and EPR Setup

Within this thesis the transient spectrometer (ISAAK) of the AG Bittl is used to perform all trEPR and most of the cwEPR measurements shown in our publications. A schematic of the trEPR setup is visualized in Fig. A.1.1a. The whole setup is divided into an optical excitation component and a home built EPR spectrometer containing many Bruker and Varian devices. Our aim is to study light induced effects in OSCs, therefore the optical excitation system plays an important role. Our transient EPR setup includes several continuous diode laser with various wavelength and intensities as well three pulsed ND:YAG laser for time-resolved measurements. More information about the laser properties are reported below.

The general EPR setup relies mainly on an electromagnet that is used to create the main magnetic field up to 1.8 T to achieve a reasonable Zeeman splitting of the paramagnetic states. Furthermore, our setup contains three microwave bridges (two X-band bridges and a Q-band bridge), several microwave resonators, two types of microwave detectors and finally controlling and recording units. All these components of the transient spectrometer will be described in the following section.

In contrast to the trEPR setup the trEDMR one relies on a different detection system but uses the same optical-excitation and spin-manipulation system like EPR (see Fig. A.1.1b). The advantage of using the same excitation setup but independent detection components is that a simultaneous detection of trEPR and trEDMR signals is possible. The main difference of the detection is that a new sample design, including electrodes (see Fig. 2.3.1 and Sec. 2.3.1), is necessary and the photocurrent instead of the transient microwave absorption has to be acquired with the transient recorder. More detailed information about the development and the setting of the trEDMR setup are described in [FK3].

The following paragraphs name the instrumental details of the most necessary components.

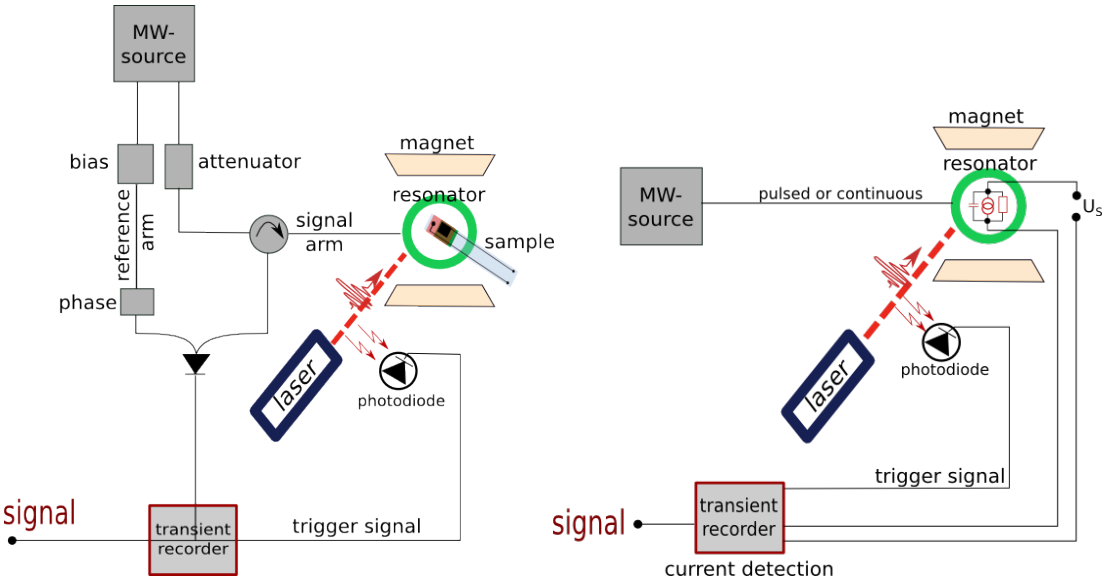

Figure A.1.1: Schematic setup for trEPR and trEDMR spectroscopy. The schematic visualizes the similarities and differences between both setups, which can be simultaneously installed and applied at the same spectrometer. Therefore, a two channel transient recorder is necessary to simultaneously record the transient microwave absorption and the photocurrent. Both setups use the same excitation system and microwave source. The main difference is the detection. a) Microwave absorption is detected by microwave diode or mixer. b) The transient conductivity change is detected via a current-voltage amplifier and the transient recorder.

Laser excitation: The laser excitation wavelength determines which electronic transition in the organic semiconductor is excited. In contrast, the laser intensity or pulse energy determines how many charges/electrons are excited.

Light induced cwEPR experiments are performed with continuous laser diodes (638 nm 110 mW *ML520G54* from *Mitsubishi Electronics*, 405 nm (40 mW) *SANYO DL-5146-101S*, 532 nm 10, 40 mW *Thorlabs DJ532-10/40*) mounted at a thermoelectric temperature-controlled diode-laser-mount *Thorlabs TED200C* or a stabilized DC driven white halogen cold light source either *Polytec DCR IV* or *Schott KL2500LCD*. The diode laser allows a stable continuous illumination of the sample at a constant laser power and a selective excitation of either the donor or acceptor material. In contrast the white-light source is preferred for a broad excitation of both the acceptor and donor.

To perform transient measurements a pulsed optical excitation is used. For different experiments we had to choose between three pulsed lasers:

- A ND:YAG $GCR-11$ laser from textitSpectra Physics with a pulse repetition rate of 10 Hz combined with a crystal for third harmonic generation (THG $\widehat{=}$ 355 nm) to pump an optical parametric oscillator (OPO) *OPTA BBO-355-vis/IR* (pulse width 4-9 ns). Due to nonlinear optics and birefringence the OPO splits the energy of the incident photon into two photons that had in summation the same energy as the initial one. That process enables the creation of photons in a continuous range between 410 nm and 700 nm while the second photon is dumped.

For direct excitation of the sample with 532 nm two diode-pumped 1-100 Hz ND-YAG lasers with a second harmonic generator are available:

- An actively Q-switched (using a Pockels cell) *Atum Titan AC 15 MM SHG* (pulse width 8ns)
- A passively switched (based on a saturable absorber inside the cavity) *Coherent Flare 532-40-100* (pulse width 2ns) laser.

The laser intensity is continuously recorded via a semi-transparent mirror and the *Soliton Gentec Maestro* energy meter. The triggering of the initial laser excitation is realized using a photodiode placed near to the laser beam line.

Electromagnet: A *Varian V-7301* electromagnet enables main magnetic fields between 20 mT and 1.8 T and is controlled by a *Bruker B-H 15* hall probe field controller and a *Varian V7900* power supply. In addition, the magnetic field is determined by a *Bruker NMR gaussmeter ER 035 M* to calibrate the magnetic field with an independent measurement system. For the field modulation additional coils are mounted to the resonator and connected to a lock-in detector from *Standford Research Systems SR 830 DSP* as well as a *Wavetek 80* function generator. The field modulation is necessary for cwEPR-measurements to increase the signal-to-noise ratio by lock-in detection.

Microwave generation and detection: The microwaves are generated inside the microwave bridge by a klystron (*Bruker ER 046 XK-T*) or gun diode (upgraded *Bruker ER 046 XK-T*) for all X-band (ca. 9.6 GHz) measurements. For Q-band (ca. 34 GHz) as well a gun diode inside the microwave bridge (*Bruker ER056 QRVM*) is used for all Q-band measurements. The frequency tuning and controlling is performed by a *Bruker microwave ER 048R* control panel while the reference frequency is measured with the *HP 5352B* frequency counter. During the measurement the samples are placed in a resonator which is mounted in a home-built Helium flow cryostat. The cryostat provides stable measurement temperatures between 5 K and 290 K. For the measurements different types of resonators are used: a *MD5* (*Bruker ER 4118x-MD5*), a laboratory-built Q-band resonator and a new designed laboratory-built MD5 resonator with two optical windows. The latter resonator allows also optical detected magnetic resonance or transient photo-luminescence measurements. In case of cwEPR measurements the signal of the diode detector is recorded by the lock-in detector. In case of trEPR and trEDMR the transients are recorded using a *LeCroy Wave Runner 104MXi* oscilloscope that is connected to a workstation. For electrical measurements an additional low noise current-voltage amplifier (*Femto DLPCA-200*) with a battery-based constant voltage source (*Stanford Research Systems SIM928*) or a combined voltage source and current amplifier (produced by the *Elektronik Manufaktur Mahlsdorf*) is placed between the sample and the transient recorder.

Resonator properties: The choice of the best resonator is an important part of an EPR measurement. Beside special resonator systems like ENDOR resonators, also for cwEPR or trEPR the resonator system has a big influence on the measurement. One has to choose between a high sensitivity or a high time resolution and bandwidth. The quality factor Q is the value that describes these properties and indicates the cavity efficiency for storing microwave energy:[92]

$$Q = \frac{2\pi \times (\text{energy stored})}{(\text{energy dissipated per cycle})}. \tag{A.1.1}$$

While the reaction time of a resonator is anti-proportional to the quality of the resonator, the signal intensity increases linearly with the quality factor. The quality factor

is dependent on the type of resonator, its bandwidth and the microwave frequency. Therefore, one uses also another definition of the Q-factor shown in Eq. A.1.2:

$$Q = \frac{\nu_{mw}}{\Delta\nu}, \tag{A.1.2}$$

with ν_{mw}, the microwave frequency and $\Delta\nu$, the band width. For X-band, dielectrical ring resonators have high quality factors such as the commonly used *MD5*. This resonator was chosen for the most measurements because of its sensitivity. It contains a transparent sapphire ring as dielectric medium. If a high time resolution is necessary a split-ring resonators can improve the measurement. One often uses split-ring resonators like the *MS3* from *Bruker* in combination with mixer detection, since mixer detection is faster than diode detection. The response time of a resonator depends on the resonator bandwidth:

$$\tau_{res} = \frac{1}{2\pi \cdot \Delta\nu}, \tag{A.1.3}$$

with τ_{res} being the response time of the resonator. The bandwidth of resonator can be tuned by changing the coupling of the microwave antenna to the microwave resonator. Critical coupling can lead to Q-values of about 10000 with a narrow bandwidth and a maximum of microwave absorption. Typically, cwEPR and trEPR measurements are performed with critically coupled resonators. For pEPR a high time resolution is necessary, so the resonators has to be overcoupled with Q-values between 100 and 300.[100] This results in a high bandwidth but with lower sensitivity. Low temperatures can also lead to higher quality factors, because of better performing resonator shields for screening.

A.2 Other EPR Instrumentations

Beside the trEPR/trEDMR setup (ISAAK) also several other spectrometer are used for cwEPR and pEPR/pEDMR measurements. All utilized spectrometer are listed with their most important equipment in Tab. A.2.1.

Table A.2.1: Overview of all EPR spectrometer utilized within this thesis. The microwave bands (mw-bands) stand for 3.4 GHz (S-band), 9.6 GHz (X-band), 34 GHz (Q-band) and 94 GHz (W-band). All spectrometer except the Magnettech MS5000 are equipped with a Helium flow cryostats (5-300 K). The following measuring mode "c" stands for continuous microwave and "p" for pulsed microwave radiation.

spectrometer name	model	mw-band	measuring modes	special equipment
ISAAK	laboratory-built cwEPR	X,Q	c	capable for all flex-line resonators, c- and p-laser excitation possible, *Spectra Physics GCR-11+OPTA BBO-355-vis/IR*, *Atum Titan AC 15 MM SHG*, *Coherent Flare 532-40-100* (portable), 4-channel transient recorder, two window cryostat, optical output for photo-luminescences spectroscopy
LYRA	laboratory-built cwEPR	X	c	equipped with a *Bruker SHQ* resonator, optimized for spin counting
X/Q	*Bruker Elexsys E580*	X, Q	c & p	capable for all flex-line resonators, 1 kW TWT mw amplifier, c- and p-laser excitation possible, *Spectra Physics, LAB150+OPTA BBO-355-vis/IR*, *Coherent Flare 532-40-100* (portable), Super-Q FT upgrade
X/W	*Bruker Elexsys E680*	X, W	c & p	capable for all flex-line resonators (X-band), 1 kW TWT mw amplifier, c- and p-laser excitation possible, *Coherent Flare 532-40-100* (portable)
S/W	*Bruker Elexsys E680*	S, W	c & p	0.4 W mw amplifier (W-band)
MS5000	*Magnettech MS5000*	X	c	Nitrogen flow cryostat (95-480 K)

B Publications

B.1 [FK1]: Charge Separation in PCPDTBT:PCBM Blends from an EPR Perspective

This section reprints [FK1] with permission from ACS.[1] *Copyright, 2014 American Chemical Society.*

F. Kraffert, R. Steyrleuthner, S. Albrecht, D. Neher, M. C. Scharber, R. Bittl, and J. Behrends. "Charge Separation in PCPDTBT: PCBM Blends from an EPR Perspective". In: *Journal of Physical Chemistry C* 118.49 (2014), pp. 28482–28493. DOI: 10.1021/jp509650v

[1] For copyright reasons, this article is not included in the online version of this thesis. An electronic version of the article is available (DOI: 10.1021/jp509650v).

B.2 [FK2]: Correlated Donor/Acceptor Crystal Orientation Controls Photocurrent Generation in All-Polymer Solar Cells (not attached)

The full-paper is not attached since it is not in the deeper focus of this cumulative thesis.

M. Schubert, B. A. Collins, H. Mangold, I. A. Howard, W. Schindler, K. Vandewal, S. Roland, J. Behrends, F. Kraffert, R. Steyrleuthner, Z. H. Chen, K. Fostiropoulos, R. Bittl, A. Salleo, A. Facchetti, F. Laquai, H. W. Ade, and D. Neher. "Correlated Donor/ Acceptor Crystal Orientation Controls Photocurrent Generation in All-Polymer Solar Cells". In: *Advanced Functional Materials* 24.26 (2014), pp. 4068–4081. DOI: 10.1002/adfm.201304216

B.3 [FK3]: Transient Electrically Detected Magnetic Resonance Spectroscopy Applied to Organic Solar Cells

This section reprints [FK3] with permission from AIP.[2] *Copyright, 2015 AIP Publishing LLC.*

F. Kraffert, R. Steyrleuthner, C. Meier, R. Bittl, and J. Behrends. "Transient electrically detected magnetic resonance spectroscopy applied to organic solar cells". In: *Applied Physics Letters* 107.4 (2015), 43302(1–5). DOI: 10.1063/1.4927446

[2]For copyright reasons, this article is not included in the online version of this thesis. An electronic version of the article is available (DOI: 10.1063/1.4927446).

B.4 [FK4]: Strongly Exchange-Coupled Triplet Pairs in an Organic Semiconductor

This section reprints [FK4] with permission from Springer Nature.[3] *Copyright, 2016 Macmillan Publishers Limited, part of Springer Nature.*

L. R. L. Weiss, S. L. S. Bayliss, F. Kraffert, K. K. J. Thorley, J. E. J. Anthony, R. Bittl, R. H. R. Friend, A. Rao, N. N. C. Greenham, and J. Behrends. "Strongly exchange-coupled triplet pairs in an organic semiconductor". In: *Nature Physics* 13 (2017), pp. 176–181. DOI: 10.1038/nphys3908

[3]For copyright reasons, this article is not included in the online version of this thesis. An electronic version of the article is available (DOI: 10.1038/nphys3908).

B.5 [FK5]: P-Type Doping of Poly(3-Hexylthiophene) with the Strong Lewis Acid Tris(Pentafluorophenyl)Borane

This section reprints [FK5] with permission from Wiley-VCH.[4] *Copyright, 2016 WILEY-VCH Verlag GmbH & Co KGaA, Weinheim.*

P. Pingel, M. Arvind, L. Kölln, R. Steyrleuthner, F. Kraffert, J. Behrends, S. Janietz, and D. Neher. "p-Type Doping of Poly(3-hexylthiophene) with the Strong Lewis Acid Tris(pentafluorophenyl)borane". In: *Advanced Electronic Materials* 2.10 (2016), 1600204(1–7). DOI: 10.1002/aelm.201600204

[4]For copyright reasons, this article is not included in the online version of this thesis. An electronic version of the article is available (DOI: 10.1002/aelm.201600204).

B.6 [FK6]: Impact of morphology on polaron delocalization in a semicrystalline conjugated polymer (not attached)

The full-paper is not attached since it is not in the deeper focus of this cumulative thesis.

R. Steyrleuthner, Y. Zhang, L. Zhang, F. Kraffert, B. P. Cherniawski, R. Bittl, A. Briseno, J.-L. Bredas, and J. Behrends. "Impact of Morphology on Polaron Delocalization in a Semicrystalline Conjugated Polymer". In: *Physical Chemistry Chemical Physics* 19.5 (2017), pp. 3627–3639. DOI: 10.1039/C6CP07485E

B.7 [FK7]: Spin-Correlated Doublet Pairs as Intermediate States in Charge Separation Processes

This section reprints [FK7] with permission from Taylor & Francis Group.[5] *Copyright, 2017 Informa UK Limited.*

F. Kraffert and J. Behrends. "Spin-correlated doublet pairs as intermediate states in charge separation processes". In: *Molecular Physics* 115.19 (2017), pp. 2373–2386. DOI: 10.1080/00268976.2016.1278479

[5]For copyright reasons, this article is not included in the online version of this thesis. An electronic version of the article is available (DOI: 10.1080/00268976.2016.1278479).

B.8 [FK8]: Transport-Related Triplet States and Hyperfine Couplings in Organic Tandem Solar Cells Probed by Pulsed Electrically Detected Magnetic Resonance Spectroscopy

This section reprints [FK8] with permission from Elsevier Inc.[6] *Copyright, 2017 Published by Elsevier Inc.*

F. Kraffert, D. Bahro, C. Meier, M. Denne, A. Colsmann, and J. Behrends. "Transport-related triplet states and hyperfine couplings in organic tandem solar cells probed by pulsed electrically detected magnetic resonance spectroscopy". In: *Journal of Magnetic Resonance* 282 (2017), pp. 10–17. DOI: 10.1016/j.jmr.2017.06.015

[6]For copyright reasons, this article is not included in the online version of this thesis. An electronic version of the article is available (DOI: 10.1016/j.jmr.2017.06.015).

B.9 Declaration of the Author's Contribution within the Publications

This declaration is in accordance with §7(2)b (last sentence) of the "Promotionsordnung" published in FU-Mitteilungen 34 (2013):

FELIX KRAFFERT is abbreviated in the following declaration the initials F.K.

1. F. Kraffert et al. [FK1] (see Appendix B.1): F.K. and J.B. wrote the manuscript with input from all authors. All authors discussed the results. F.K. and J.B. analyzed the data. F.K. carried out the experiments. M.C.S. provided the materials. R.S., S.A. and F.K. produced the samples.

2. M. Schubert et al. [FK2] (not included): The corresponding author of this article is D. Neher. M.S., F.K. and J.B. wrote the EPR content of the manuscript in the main article and in the EPR section in the supplementary. J.B. and F.K. contributed to the discussion of the whole manuscript. F.K. performed all EPR measurements contributing to this article.

3. F. Kraffert et al. [FK3] (see Appendix B.3): F.K. and J.B. wrote the manuscript with input from all authors. All authors discussed the results. F.K. analyzed the data. F.K. carried out the experiments. F.K. and R.S. produced the devices.

4. L. Weiss et al. [FK4] (see Appendix B.4): L.R.W. and S.L.B. wrote the manuscript with input from all authors. All authors discussed the results. L.R.W. and S.L.B. analyzed the data. F.K., J.B., L.R.W. and S.L.B. carried out the experiments. K.J.T. and J.E.A. provided the materials.

5. P. Pingel et al. [FK5] (see Appendix B.5): The corresponding author of this article is P. Pingel. F.K. and R.S. wrote the EPR content of the manuscript in the main article and in the EPR section in the supplementary. R.S., F.K. and J.B. contributed to the discussion of the whole manuscript. F.K. measured and analyzed the multi-frequency EPR approach to distinguish between polarons on the donor and acceptor. Charlotte Beck (Bachelor Student in AG Behrends), F.K. and R.S. performed all EPR measurements contributing to this article.

6. R. Steyrleuthner et al. [FK6] (not included): R.S. wrote the manuscript with input from all authors. All authors discussed the results. R.S. analyzed the data. R.S. carried out the experiments. F.K. and J.B. supported the experiments. L.Z., B.P.C. and A.L.B. provided the materials. R.S., Y.Z. and J.L.B. performed the simulations.

7. F. Kraffert et al. [FK7] (see Appendix B.7): F.K. and J.B. wrote the manuscript. All authors discussed the results. F.K. analyzed the data. F.K. carried out the experiments. F.K. produced the samples. F.K developed the simulation code.

8. F. Kraffert et al. [FK8] (see Appendix B.8): F.K. wrote the manuscript. All authors discussed the results. F.K. analyzed the data. F.K. carried out all EDMR experiments. C.M. support F.K. for the ED-HYSCORE experiments. D.B. and M.D. produced the samples.

Bibliography

[1] T. Stocker. *Climate change 2013: the physical science basis: Working Group I contribution to the Fifth assessment report of the Intergovernmental Panel on Climate Change*. Cambridge: Cambridge University press, 2014.

[2] S. Dale. *BP Statistical Review of World Energy, June 2017*. Tech. rep. http://www.bp.com/content/dam/bp/en/corporate/pdf/energy-economics/statistical-review-2017/bp-statistical-review-of-world-energy-2017-full-report.pdf. British Petrol, 2017, p. 4.

[3] H. C. Gils, Y. Scholz, T. Pregger, D. L. de Tena, and D. Heide. "Integrated modelling of variable renewable energy-based power supply in Europe". In: *Energy* 123 (2017), pp. 173–188. DOI: 10.1016/j.energy.2017.01.115.

[4] C. L. Benson and C. L. Magee. "On improvement rates for renewable energy technologies: Solar PV, wind turbines, capacitors, and batteries". In: *Renewable Energy* 68.0 (2014), pp. 745–751. DOI: 10.1016/j.renene.2014.03.002.

[5] N. Stern. *Stern Review: The economics of climate change*. Cambridge: Cambridge University press, 2006.

[6] U. D. of Energy. *Annual Energy Outlook 2017*. Tech. rep. Washington DC: U.S. Energy Information Adminstration, 2017, p. 3. DOI: DOE/EIA-0383(2012)U.S..

[7] M. A. Green. *Third Generation Photovoltaics: Advanced Solar Energy Conversion*. Berlin, Heidelberg, New York: Springer-Verlag Berlin Heidelberg, 2006.

[8] K. Yoshikawa, H. Kawasaki, W. Yoshida, T. Irie, K. Konishi, K. Nakano, T. Uto, D. Adachi, M. Kanematsu, H. Uzu, and K. Yamamoto. "Silicon heterojunction solar cell with interdigitated back contacts for a photoconversion efficiency over 26%". In: *Nature Energy* 2.5 (2017), p. 17032. DOI: 10.1038/nenergy.2017.32.

[9] P. Jackson, D. Hariskos, E. Lotter, S. Paetel, R. Wuerz, R. Menner, W. Wischmann, and M. Powalla. "New world record efficiency for Cu(In,Ga)Se2 thin-film solar cells beyond 20%". In: *Progress in Photovoltaics: Research and Applications* 19.7 (2011), pp. 894–897. DOI: 10.1002/pip.1078.

[10] J. Zhao, A. Wang, M. A. Green, and F. Ferrazza. "19.8% Efficient "Honeycomb" Textured Multicrystalline and 24.4% Monocrystalline Silicon Solar Cells". In: *Applied Physics Letters* 73.14 (1998), pp. 1991–1993. DOI: 10.1063/1.122345.

[11] M. Neophytou, W. Cambarau, F. Hermerschmidt, C. Waldauf, C. Christodoulou, R. Pacios, and S. A. Choulis. "Inkjet-printed polymer–fullerene blends for organic electronic applications". In: *Microelectronic Engineering* 95 (2012), pp. 102–106. DOI: 10.1016/j.mee.2012.02.005.

[12] POLYERA CORPORATION. *The World's First Flexible Display Product*. www.polyera.com. 2017.

[13] OLED-Info. *Mobile phones and smartphones with OLED screens*. 2017.

[14] C. Jahnel. *Heliatek sets new Organic Photovoltaic world record efficiency of 13.2% - Heliatek – The future is light*. 2016.

[15] NREL. *Reference Solar Spectral Irradiance (Accessed Feb/2017)*. http://rredc.nrel.gov/solar/spectra/am1.5/. 2017.

[16] BELECTRIC OPV GmbH. *Organische Photovoltaik-Module von BELECTRIC OPV und Merck erhalten Innovationspreis Architecture + Building*. http://www.solarserver.de/. 2017.

[17] Heliatek GmbH. *Die weltweit erste Rolle-zu-Rolle-Produktion unter Vakuum*. http://www.heliatek.com/. 2017.

[18] M. C. Scharber, M. Koppe, J. Gao, F. Cordella, M. A. Loi, P. Denk, M. Morana, H.-J. J. Egelhaaf, K. Forberich, G. Dennler, R. Gaudiana, D. Waller, Z. Zhu, X. Shi, and C. J. Brabec. "Influence of the bridging atom on the performance of a low-bandgap bulk heterojunction solar cell." In: *Advanced materials (Deerfield Beach, Fla.)* 22.3 (2010), pp. 367–70. DOI: 10.1002/adma.200900529.

[19] B. Fan, K. Zhang, X. F. Jiang, L. Ying, F. Huang, and Y. Cao. "High-Performance Nonfullerene Polymer Solar Cells based on Imide-Functionalized Wide-Bandgap Polymers". In: *Advanced Materials* 29.21 (2017), p. 1606396. DOI: 10.1002/adma.201606396.

[20] Z. Zheng, O. M. Awartani, B. Gautam, D. Liu, Y. Qin, W. Li, A. Bataller, K. Gundogdu, H. Ade, and J. Hou. "Efficient Charge Transfer and Fine-Tuned Energy Level Alignment in a THF-Processed Fullerene-Free Organic Solar Cell with 11.3% Efficiency". In: *Advanced Materials* 29.5 (2017), pp. 3–8. DOI: 10.1002/adma.201604241.

[21] W. Zhao, S. Zhang, and J. Hou. "Realizing 11.3% efficiency in fullerene-free polymer solar cells by device optimization". In: *Science China Chemistry* 59.12 (2016), pp. 1574–1582. DOI: 10.1007/s11426-016-0198-0.

[22] C. Piliego and M. A. Loi. "Charge transfer state in highly efficient polymer–fullerene bulk heterojunction solar cells". In: *Journal of Materials Chemistry* 22.10 (2012), p. 4141. DOI: 10.1039/c2jm15027a.

[23] A. D. Chepelianskii, J. Wang, and R. H. Friend. "Low-temperature transport properties of photogenerated charges in organic materials". In: *Physical Review Letters* 112.12 (2013), p. 126802. DOI: 10.1103/PhysRevLett.112.126802.

[24] A. A. Bakulin, A. Rao, V. G. Pavelyev, P. H. M. van Loosdrecht, M. S. Pshenichnikov, D. Niedzialek, J. Cornil, D. Beljonne, and R. H. Friend. "The Role of Driving Energy and Delocalized States for Charge Separation in Organic Semiconductors". In: *Science* 335.6074 (2012), pp. 1340–1344. DOI: 10.1126/science.1217745.

[25] H. Bässler and A. Köhler. ""Hot or cold": how do charge transfer states at the donor–acceptor interface of an organic solar cell dissociate?" In: *Physical Chemistry Chemical Physics* 17.43 (2015), pp. 28451–28462. DOI: 10.1039/C5CP04110D.

[26] T. Hahn, J. Geiger, X. Blase, I. Duchemin, D. Niedzialek, S. Tscheuschner, D. Beljonne, H. Bässler, and A. Köhler. "Does Excess Energy Assist Photogeneration in an Organic Low-Bandgap Solar Cell?" In: *Advanced Functional Materials* 25.8 (2015), pp. 1287–1295. DOI: 10.1002/adfm.201403784.

[27] A. C. Jakowetz, M. L. Böhm, J. Zhang, A. Sadhanala, S. Huettner, A. A. Bakulin, A. Rao, and R. H. Friend. "What Controls the Rate of Ultrafast Charge Transfer and Charge Separation Efficiency in Organic Photovoltaic Blends". In: *Journal of the American Chemical Society* 138.36 (2016), pp. 11672–11679. DOI: 10.1021/jacs.6b05131.

[28] I. a. Howard, R. Mauer, M. Meister, and F. Laquai. "Effect of morphology on ultrafast free carrier generation in polythiophene:fullerene organic solar cells." In: *Journal of the American Chemical Society* 132.42 (2010), pp. 14866–76. DOI: 10.1021/ja105260d.

[29] D. Caruso and A. Troisi. "Long-range exciton dissociation in organic solar cells". In: *Proceedings of the National Academy of Sciences of the United States of America* 109.11 (2012), pp. 13498–13502. DOI: 10.1073/pnas.1206172109.

[30] G. Grancini, M. Maiuri, D. Fazzi, A. Petrozza, H.-J. Egelhaaf, D. Brida, G. Cerullo, and G. Lanzani. "Hot exciton dissociation in polymer solar cells". In: *Nature Materials* 12.1 (2012), pp. 29–33. DOI: 10.1038/nmat3502.

[31] S. D. Dimitrov, A. A. Bakulin, C. B. Nielsen, B. C. Schroeder, J. Du, H. Bronstein, I. McCulloch, R. H. Friend, and J. R. Durrant. "On the Energetic Dependence of Charge Separation in Low-Band-Gap Polymer/Fullerene Blends". In: *Journal of the American Chemical Society* 134.44 (2012), pp. 18189–18192. DOI: 10.1021/ja308177d.

[32] B. R. Gautam, A. Barrette, C. Mai, L. Yan, Q. Zhang, E. Danilov, W. You, H. Ade, and K. Gundogdu. "Direct Optical Observation of Stimulated Emission from Hot Charge Transfer Excitons in Bulk Heterojunction Polymer Solar Cells". In: *The Journal of Physical Chemistry C* 119.34 (2015), pp. 19697–19702. DOI: 10.1021/acs.jpcc.5b06557.

[33] A. P. Arndt, M. Gerhard, A. Quintilla, I. A. Howard, M. Koch, and U. Lemmer. "Time-Resolved Charge-Transfer State Emission in Organic Solar Cells: Temperature and Blend Composition Dependences of Interfacial Traps". In: *The Journal of Physical Chemistry C* 119.24 (2015), pp. 13516–13523. DOI: 10.1021/acs.jpcc.5b03507.

[34] S. Albrecht, K. Vandewal, J. R. Tumbleston, F. S. U. Fischer, J. D. Douglas, J. M. J. Fréchet, S. Ludwigs, H. Ade, A. Salleo, and D. Neher. "On the Efficiency of Charge Transfer State Splitting in Polymer:Fullerene Solar Cells". In: *Advanced Materials* 26.16 (2014), pp. 2533–2539. DOI: 10.1002/adma.201305283.

[35] K. Vandewal, S. Albrecht, E. T. Hoke, K. R. Graham, J. Widmer, J. D. Douglas, M. Schubert, W. R. Mateker, J. T. Bloking, G. F. Burkhard, A. Sellinger, J. M. J. Fréchet, A. Amassian, M. K. Riede, M. D. McGehee, D. Neher, and A. Salleo. "Efficient charge generation by relaxed charge-transfer states at organic interfaces". In: *Nature Materials* 13.1 (2013), pp. 63–68. DOI: 10.1038/nmat3807.

[36] J. Lee, K. Vandewal, S. R. Yost, M. E. Bahlke, L. Goris, M. a. Baldo, J. V. Manca, and T. Van Voorhis. "Charge transfer state versus hot exciton dissociation in polymer-fullerene blended solar cells." In: *Journal of the American Chemical Society* 132.34 (2010), pp. 11878–80. DOI: 10.1021/ja1045742.

[37] S. Gélinas, T. S. v. d. Poll, G. C. Bazan, and R. H. Friend. "Ultrafast Long-Range Charge Photovoltaic Diodes". In: *Science* 343 (6170 2014), pp. 512–517. DOI: 10.1126/science.1246249.

[38] D. Moses, A. Dogariu, and A. J. Heeger. "Ultrafast photoinduced charge generation in conjugated polymers". In: *Chemical Physics Letters* 316.5 (2000), pp. 356–360. DOI: 10.1016/S0009-2614(99)01316-0.

[39] K. Tvingstedt, K. Vandewal, A. Gadisa, F. Zhang, J. Manca, and I. Olle. "Electroluminescence from Charge Transfer States in Polymer Solar Cells". In: *Journal of the American Chemical Society* 131.33 (2009), pp. 11819–11824. DOI: 10.1021/ja903100p.

[40] M. Hallermann, S. Haneder, and E. Da Como. "Charge-transfer states in conjugated polymer/fullerene blends: Below-gap weakly bound excitons for polymer photovoltaics". In: *Applied Physics Letters* 93.5 (2008), p. 053307. DOI: 10.1063/1.2969295.

[41] K. Hasharoni, M. Keshavarz-K., a. Sastre, R. Gonzalez, C. Bellavia-Lund, Y. Greenwald, T. Swager, F. Wudl, and a. J. Heeger. "Near IR photoluminescence in mixed films of conjugated polymers and fullerenes". In: *The Journal of Chemical Physics* 107.7 (1997), p. 2308. DOI: 10.1063/1.474607.

[42] D. Jarzab, F. Cordella, J. Gao, M. Scharber, H. J. Egelhaaf, and M. A. Loi. "Low-temperature behaviour of charge transfer excitons in narrow-bandgap polymer-based bulk heterojunctions". In: *Advanced Energy Materials* 1.4 (2011), pp. 604–609. DOI: 10.1002/aenm.201100083.

[43] M. Gerhard, A. P. Arndt, I. A. Howard, A. Rahimi-Iman, U. Lemmer, and M. Koch. "Temperature- and Energy-Dependent Separation of Charge-Transfer States in PTB7-Based Organic Solar Cells". In: *The Journal of Physical Chemistry C* 119.51 (2015), pp. 28309–28318. DOI: 10.1021/acs.jpcc.5b09842.

[44] N. Sariciftci and L. Smilowitz. "Photoinduced electron transfer from a conducting polymer to buckminsterfullerene". In: *Science* 258.5087 (1992), pp. 1474–1476. DOI: 10.1126/science.258.5087.1474.

[45] P. Hore, D. Hunter, C. McKie, and A. Hoff. "Electron paramagnetic resonance of spin-correlated radical pairs in photosynthetic reactions". In: *Chemical Physics Letters* 137.6 (1987), pp. 495–500. DOI: 10.1016/0009-2614(87)80617-6.

[46] D. Stehlik, C. H. Bock, and J. Petersen. "Anisotropic Electron-Spin Polarization of Correlated Spin Pairs in Photosynthetic Reaction Centers". In: *Journal of Physical Chemistry* 93.4 (1989), pp. 1612–1619. DOI: 10.1021/j100341a084.

[47] D. E. Budil and M. C. Thurnauer. "The Chlorophyll Triplet-State as a Probe of Structure and Function in Photosynthesis". In: *Biochimica et Biophysica Acta - Bioenergetics* 1057.1 (1991), pp. 1–41. DOI: 10.1016/S0005-2728(05)80081-7.

[48] M. D. E. Forbes, K. E. Dukes, T. L. Myers, H. D. Maynard, C. S. Breivogel, and H. B. Jaspan. "Time-resolved electron paramagnetic resonance spectroscopy of organic free radicals anchored to silica surfaces". In: *The Journal of Physical Chemistry* 95.26 (1991), pp. 10547–10549. DOI: 10.1021/j100179a008.

[49] A. Maniero, A. Barbon, M. Bortolus, and M. Brustolon. "Dyes included in channels: effects of the confinement on the photoexcited triplets". In: *Synthetic Metals* 147.1-3 (2004), pp. 127–131. DOI: 10.1016/j.synthmet.2004.05.026.

[50] C. E. Lee, D. K. Oh, J. I. Jin, and B. K. Nam. "EPR study of the PPV conducting polymers". In: *Synthetic Metals* 69.1-3 (1995), pp. 425–426. DOI: 10.1016/0379-6779(94)02513-X.

[51] A. Aguirre, G. Janssen, E. Goovaerts, K. Colladet, D. Vanderzande, and L. Lutsen. "Optical and EPR spectroscopy in pure and blended films of a novel low band gap polymer". In: *European Physical Journal-Applied Physics* 36.3 (2006), pp. 285–287. DOI: 10.1051/epjap:2006143.

[52] A. Aguirre, G. Janssen, E. Goovaerts, K. Colladet, D. Vanderzande, and L. Lutsen. "Optical and EPR spectroscopy in pure and blended films of a novel low band gap polymer". In: *European Physical Journal-Applied Physics* 36.3 (2006), pp. 285–287. DOI: 10.1051/epjap:2006143.

[53] G. Janssen, A. Aguirre, E. Goovaerts, P. Vanlaeke, J. Poortmans, and J. Manca. "Optimization of morphology of P3HT/PCBM films for organic solar cells: effects of thermal treatments and spin coating solvents". In: *European Physical Journal-Applied Physics* 37.3 (2007), pp. 287–290. DOI: 10.1051/Epjap:2007002.

[54] E. A. Thomsen, D. J. Keeble, B. Lochab, P. L. Burn, H. El-Mkami, and I. D. W. Samuel. "Photoinduced charge separation in poly(1,4-phenylenevinylene) derivatives studied by electron paramagnetic resonance". In: *Organic Electronics* 9.5 (2008), pp. 809–815. DOI: 10.1016/j.orgel.2008.05.020.

[55] V. I. Krinichnyi and E. I. Yudanova. "Light-Induced EPR Study of Charge Transfer in P3HT/PC_{71}BM Bulk Heterojunctions". In: *The Journal of Physical Chemistry C* 116.16 (2012), pp. 9189–9195. DOI: 10.1021/jp2120516.

[56] L. Franco, A. Toffoletti, M. Ruzzi, L. Montanari, C. Carati, L. Bonoldi, and R. Po'. "Time-resolved EPR of photoinduced excited states in a semiconducting polymer/PCBM blend". In: *Journal of Physical Chemistry C* 117.4 (2013), pp. 1554–1560. DOI: 10.1021/jp306278v.

[57] A. Aguirre, P. Gast, S. Orlinskii, I. Akimoto, E. J. J. Groenen, H. El Mkami, E. Goovaerts, and S. Van Doorslaer. "Multifrequency EPR analysis of the positive polaron in I2-doped poly(3-hexylthiophene) and in poly[2-methoxy-5-(3,7-dimethyloctyloxy)]-1,4-phenylenevinylene." In: *Physical Chemistry Chemical Physics* 10.47 (2008), pp. 7129–38. DOI: 10.1039/b811419f.

[58] J. Niklas, K. L. Mardis, B. P. Banks, G. M. Grooms, A. Sperlich, S. Beaupr, V. Dyakonov, S. Beaupré, M. Leclerc, T. Xu, L. P. Yu, O. G. Poluektov, S. Beaupre, M. Leclerc, T. Xu, L. P. Yu, and O. G. Poluektov. "Highly-efficient charge separation and polaron delocalization in polymer-fullerene bulk-heterojunctions: a comparative multi-frequency EPR and DFT study". In: *Physical Chemistry Chemical Physics* 15.24 (2013), pp. 9562–9574. DOI: 10.1039/c3cp51477c.Highly-Efficient.

[59] A. Sperlich, H. Kraus, C. Deibel, H. Blok, J. Schmidt, and V. Dyakonov. "Reversible and Irreversible Interactions of Poly(3-hexylthiophene) with Oxygen Studied by Spin-Sensitive Methods". In: *The Journal of Physical Chemistry B* 115.46 (2011), pp. 13513–13518. DOI: 10.1021/jp2077215.

[60] J. Behrends, A. Sperlich, A. Schnegg, T. Biskup, C. Teutloff, K. Lips, V. Dyakonov, and R. Bittl. "Direct Detection of Photoinduced Charge Transfer Complexes in Polymer:Fullerene Blends". In: *Physical Review B* 85.12 (2012), p. 125206. DOI: 10.1103/PhysRevB.85.125206.

[61] J. Niklas, S. Beaupré, M. Leclerc, T. Xu, L. Yu, A. Sperlich, V. Dyakonov, and O. G. Poluektov. "Photoinduced Dynamics of Charge Separation: From Photosynthesis to Polymer–Fullerene Bulk Heterojunctions". In: *The Journal of Physical Chemistry B* 119.24 (2015), pp. 7407–7416. DOI: 10.1021/jp511021v.

[62] S. Väth, K. Tvingstedt, A. Baumann, M. C. Heiber, A. Sperlich, J. A. Love, T. Q. Nguyen, and V. Dyakonov. "Triplet Excitons in Highly Efficient Solar Cells Based on the Soluble Small Molecule p-DTS(FBTTh2)2". In: *Advanced Energy Materials* 7 (2017), p. 1602016. DOI: 10.1002/aenm.201602016.

[63] M. J. Y. Tayebjee, S. N. Sanders, E. Kumarasamy, L. M. Campos, M. Y. Sfeir, and D. R. McCamey. "Quintet multiexciton dynamics in singlet fission". In: *Nature Physics* 13 (Oct. 2017), pp. 182–189. DOI: 10.1038/nphys3909.

[64] E. A. Lukina, A. A. Popov, M. N. Uvarov, E. A. Suturina, E. J. Reijerse, and L. V. Kulik. "Light-induced charge separation in a P3HT/PC70BM composite as studied by out-of-phase electron spin echo spectroscopy". In: 18.41 (2016), pp. 28585–28593. DOI: 10.1039/C6CP05389K.

[65] L. Franco, M. Ruzzi, and C. Corvaja. "Time-resolved electron paramagnetic resonance of photoinduced ion pairs in blends of polythiophene and fullerene derivatives". In: *Journal of Physical Chemistry B* 109.28 (2005), pp. 13431–13435. DOI: 10.1021/jp0514877.

[66] B. Z. Tedlla, F. Zhu, M. Cox, J. Drijkoningen, J. Manca, B. Koopmans, and E. Goovaerts. "Understanding triplet formation pathways in bulk heterojunction polymer:fullerene photovoltaic devices". In: *Advanced Energy Materials* 5.2 (2015), pp. 1–11. DOI: 10.1002/aenm.201401109.

[67] C. Boehme, D. R. McCamey, K. J. van Schooten, W. J. Baker, S.-Y. Lee, S.-Y. Paik, and J. M. Lupton. "Pulsed electrically detected magnetic resonance in organic semiconductors". In: *physica status solidi (b)* 246.11-12 (2009), pp. 2750–2755. DOI: 10.1002/pssb.200982357.

[68] M. Eckardt, J. Behrends, D. Münter, and W. Harneit. "Compact electrically detected magnetic resonance setup". In: *AIP Advances* 5.4 (2015), p. 047139. DOI: 10.1063/1.4919247.

[69] A. J. Kupijai, K. M. Behringer, F. G. Schaeble, N. E. Galfe, M. Corazza, S. A. Gevorgyan, F. C. Krebs, M. Stutzmann, and M. S. Brandt. "Bipolar polaron pair recombination in polymer/fullerene solar cells". In: *Physical Review B* 92.24 (2015), p. 245203. DOI: 10.1103/PhysRevB.92.245203.

[70] R. Miller, K. J. van Schooten, H. Malissa, G. Joshi, S. Jamali, J. M. Lupton, and C. Boehme. "Morphology effects on spin-dependent transport and recombination in polyfluorene thin films". In: *Physical Review B* 94.21 (2016), p. 214202. DOI: 10.1103/PhysRevB.94.214202.

[71] C. Deibel and V. Dyakonov. "Polymer–fullerene bulk heterojunction solar cells". In: *Reports on Progress in Physics* 73.9 (2010), pp. 1–39. DOI: 10.1088/0034-4885/73/9/096401.

[72] N. S. Sariciftci, L. Smilowitz, A. J. Heeger, and F. Wudl. "Semiconducting polymers (as donors) and buckminsterfullerene (as acceptor): photoinduced electron transfer and heterojunction devices". In: *Synthetic Metals* 59.3 (1993), pp. 333–352. DOI: 10.1016/0379-6779(93)91166-Y.

[73] I. W. Hwang, D. Moses, and A. J. Heeger. "Photoinduced carrier generation in P3HT/PCBM bulk heterojunction materials". In: *Journal of Physical Chemistry C* 112.11 (2008), pp. 4350–4354. DOI: 10.1021/jp075565x.

[74] A. Koehler and H. Baessler. *Electronic Processes in Organic Semiconductors*. Weinheim: Wiley-VCH Verlag GmbH & Co. KGaA, 2015.

[75] S. Albrecht. "Generation , Recombination and Extraction of Charges in Polymer : Fullerene Bulk Heterojunction Solar Cells". https://publishup.uni-potsdam.de/files/7228/albrecht_diss.pdf. PhD thesis. 2014.

[76] J. Zhao, A. Wang, M. A. Green, and F. Ferrazza. "19.8% Efficient "Honeycomb" Textured Multicrystalline and 24.4% Monocrystalline Silicon Solar Cells". In: *Applied Physics Letters* 73.14 (1998), pp. 1991–1993. DOI: 10.1063/1.122345.

[77] C. Honsberg and S. Bowden. *Silicon Solar Cell Parameters*. http://www.pveducation.org/pvcdrom/design/solar-cell-parameters. 2017.

[78] M. Pope and C. E. Swenberg. *Electronic Processes in Organic Crystals and Polymers*. 2nd ed. Oxford: Oxford University press, 1999, p. 1360.

[79] C. L. Braun. "Electric Field Assisted Dissociation of Charge Transfer States as a Mechanism of Photocarrier Production". In: *The Journal of Chemical Physics* 80.9 (1984), pp. 4157–4161. DOI: 10.1063/1.447243.

[80] L. Onsager. "Initial recombination of ions". In: *Physical Review* 54.8 (1938), pp. 554–557. DOI: 10.1103/PhysRev.54.554.

[81] A. G. Lee. *Membrane studies using fluorescence spectroscopy*. Techniques in Lipid and Membrane Biochemistry. Elsevier Scientific Publishers Ireland, 1982.

[82] V. Gold. *Compendium of Chemical Terminology*. Ed. by A. D. McNaught and A. Wilkinson. 2nd ed. Blackwell Scientific Publications, Oxford, 1997, p. 1670. DOI: 10.1351/goldbook.I03352.

[83] D. R. McCamey, S. Y. Lee, S. Y. Paik, J. M. Lupton, and C. Boehme. "Spin-dependent dynamics of polaron pairs in organic semiconductors". In: *Physical Review B - Condensed Matter and Materials Physics* 82.12 (2010). DOI: 10.1103/PhysRevB.82.125206.

[84] S. Sankararaman, K. B. Yoon, T. Yabe, and J. K. Kochi. "Control of back electron transfer from charge-transfer ion pairs by zeolite supercages". In: *Journal of the American Chemical Society* 113.4 (1991), pp. 1419–1421. DOI: 10.1021/ja00004a057.

[85] W. Lubitz, F. Lendzian, and R. Bittl. "Radicals, Radical Pairs and Triplet States in Photosynthesis". In: *Accounts of Chemical Research* 35.5 (2002), pp. 313–320. DOI: 10.1021/ar000084g.

[86] A. Distler, P. Kutka, T. Sauermann, H. J. Egelhaaf, D. M. Guldi, D. Di Nuzzo, S. C. J. Meskers, and R. A. J. Janssen. "Effect of PCBM on the photodegradation kinetics of polymers for organic photovoltaics". In: *Chemistry of Materials* 24.22 (2012), pp. 4397–4405. DOI: 10.1021/cm302623p.

[87] A. Rao, P. C. Y. Chow, S. Gélinas, C. W. Schlenker, C.-Z. Z. Li, H.-L. L. Yip, A. K.-Y. Y. Jen, D. S. Ginger, R. H. Friend, S. Gelinas, C. W. Schlenker, C.-Z. Z. Li, H.-L. L. Yip, A. K.-Y. Y. Jen, D. S. Ginger, and R. H. Friend. "The role of spin in the kinetic control of recombination in organic photovoltaics". In: *Nature* 500.7463 (2013), pp. 435–440. DOI: 10.1038/nature12339.

[88] M. B. Smith and J. Michl. "Singlet Fission". In: *Chemical Reviews* 110.11 (2010), pp. 6891–6936. DOI: 10.1021/cr1002613.

[89] A. Rao, M. W. B. Wilson, J. M. Hodgkiss, S. Albert-Seifried, H. Bässler, and R. H. Friend. "Exciton Fission and Charge Generation via Triplet Excitons in Pentacene/C_{60} Bilayers". In: *Journal of the American Chemical Society* 132.36 (2010), pp. 12698–12703. DOI: 10.1021/ja1042462.

[90] J. A. Weil and J. R. Bolton. *EPR: Elementary Theory and Practical Applications*. Hoboken: John Wiley & Sons, Inc., 2007.

[91] N. M. Atherton. *Advanced EPR: Applications in biology and biochemistry*. Ed. by A. J. Hoff. Vol. 28. 8. Elsevier Scientific Publishers, 1990, pp. 737–737. DOI: 10.1002/mrc.1260280816.

[92] G. R. Eaton, S. S. Eaton, D. P. Barr, and R. T. Weber. *Quantitative EPR*. Springer Verlag Wien, 2010, p. 197. DOI: 10.1016/0020-7519(79)90055-9.

[93] K. M. Salikhov. *Schweiger, A., Jeschke, G.:Principles of pulse electron paramagnetic resonance*. Vol. 22. 2. Oxford University press, 2002, pp. 319–319. DOI: 10.1007/BF03166113.

[94] H. A. Lorentz and P. Zeeman. *Nobel Lecture - Light Radiation in a Magnetic Field*. http://www.nobelprize.org/nobel_prizes/physics/laureates/1902/zeeman-lecture.html. 1903.

[95] Stern, Otto. *Nobel Lecture - The Method of Molecular Rays*. http://www.nobelprize.org/nobel_prizes/physics/laureates/1943/stern-lecture.html. 1944.

[96] V. Dyakonov, G. Zoriniants, M. Scharber, C. Brabec, R. Janssen, J. Hummelen, and N. Sariciftci. "Photoinduced charge carriers in conjugated polymer–fullerene composites studied with light-induced electron-spin resonance". In: *Physical Review B* 59.12 (1999), pp. 8019–8025. DOI: 10.1103/PhysRevB.59.8019.

[97] A. J. Hoff, P. Gast, S. A. Dzuba, C. R. Timmel, C. E. Fursman, and P. P. J. Hore. "The nuts and bolts of distance determination and zero- and double-quantum coherence in photoinduced radical pairs". In: *Spectrochimica Acta Part A: Molecular and Biomolecular Spectroscopy* 54.14 (1998), pp. 2283–2293. DOI: 10.1016/S1386-1425(98)00211-X.

[98] S. Stoll and A. Schweiger. "EasySpin, a comprehensive software package for spectral simulation and analysis in EPR". In: *Journal of Magnetic Resonance* 178.1 (2006), pp. 42–55. DOI: 10.1016/j.jmr.2005.08.013.

[99] J. Behrends, A. Sperlich, A. Schnegg, T. Biskup, C. Teutloff, K. Lips, V. Dyakonov, and R. Bittl. "Direct detection of photoinduced charge transfer complexes in polymer fullerene blends". In: *Physical Review B* 85.12 (2012). DOI: 10.1103/PhysRevB.85.125206.

[100] C. D. Buckley, D. a. Hunter, P. J. Hore, and K. a. McLauchlan. "Electron spin resonance of spin-correlated radical pairs." In: *Chemical Physics Letters* 135.3 (1987), pp. 307–312. DOI: 10.1016/0009-2614(87)85162-X.

[101] V. I. Krinichnyi and H. K. Roth. "EPR study of spin and charge dynamics in slightly doped poly(3-octylthiophene)". In: *Applied Magnetic Resonance* 26.3 (2004), pp. 395–415. DOI: 10.1007/BF03166811.

[102] O. Poluektov, S. Filippone, N. Martin, A. Sperlich, C. Deibel, and V. Dyakonov. "Spin signatures of photogenerated radical anions in polymer-[70]fullerene bulk heterojunctions: High frequency pulsed EPR spectroscopy". In: *Journal of Physical Chemistry B* 114.45 (2010), pp. 14426–14429. DOI: 10.1021/jp1012347.

[103] V. I. Krinichnyi, E. I. Yudanova, and N. G. Spitsina. "Light-Induced Electron Paramagnetic Resonance Study of Poly(3-alkylthiophene)/ Fullerene Composites". In: *The Journal of Physical Chemistry C* 114.39 (2010), pp. 16756–16766. DOI: 10.1021/jp105873r.

[104] E. A. Thomsen, D. J. Keeble, B. Lochab, P. L. Burn, H. El-Mkami, and I. D. W. Samuel. "Photoinduced charge separation in poly(1,4-phenylenevinylene) derivatives studied by electron paramagnetic resonance". In: *Organic Electronics* 9.5 (2008), pp. 809–815. DOI: 10.1016/j.orgel.2008.05.020.

[105] J. Schmidt and I. Solomon. "Photoconductivity modulation in Si at low temperatures by electron paramagnetic resonance of shallow impurities". In: *Comptes Rendus des Seances de l'Academie des Sciences* 263.2 (1966), pp. 169–172.

[106] R. Maxwell and A. Honig. "Neutral-impurity scattering experiments in silicon with highly spin-polarized electrons". In: *Physical Review Letters* 17.4 (1966), pp. 188–190. DOI: 10.1103/PhysRevLett.17.188.

[107] M. Stutzmann, M. S. Brandt, and M. W. Bayerl. "Spin-dependent processes in amorphous and microcrystalline silicon: a survey". In: *Journal of Non-Crystalline Solids* 266-269 (2000), pp. 1–22. DOI: 10.1016/S0022-3093(99)00871-6.

[108] C. Meier. "Multi-Frequency EDMR Studies of Light-Activated Paramagnetic Centers in µc-Si:H Thin-Film Solar Cells". http://www.diss.fu-berlin.de/diss/receive/FUDISS_thesis_000000096876. PhD thesis. Freie Universtität Berlin, 2013.

[109] J. Behrends. "Spin-dependent Transport and Recombination in Solar Cells studied by Pulsed Electrically Detected Magnetic Resonance". http://www.diss.fu-berlin.de/diss/receive/FUDISS_thesis_000000017458. PhD thesis. Freie Universität Berlin, 2009.

[110] C. Boehme and H. Malissa. "Electrically Detected Magnetic Resonance Spectroscopy". In: *eMagRes*. John Wiley & Sons, Ltd, 2017. DOI: 10.1002/9780470034590.emrstm1525.

[111] J. Niklas and O. G. Poluektov. "Charge Transfer Processes in OPV Materials as Revealed by EPR Spectroscopy". In: *Advanced Energy Materials* 7.10 (2017), p. 1602226. DOI: 10.1002/aenm.201602226.

[112] H. Yan, Z. Chen, Y. Zheng, C. Newman, J. R. Quinn, F. Dötz, M. Kastler, and A. Facchetti. "A high-mobility electron-transporting polymer for printed transistors". In: *Nature* 457.7230 (2009), pp. 679–686. DOI: 10.1038/nature07727.

[113] W. Shockley and H. J. Queisser. "Detailed balance limit of efficiency of p-n junction solar cells". In: *Journal of Applied Physics* 32.3 (1961), pp. 510–519. DOI: 10.1063/1.1736034.

[114] C. Deibel, T. Strobel, and V. Dyakonov. "Role of the charge transfer state in organic donor-acceptor solar cells." In: *Advanced materials* 22.37 (2010), pp. 4097–4111. DOI: 10.1002/adma.201000376.

List of Abbreviations

BCF	tris(pentafluorophenyl)borane
BET	back electron-transfer
CT state	charge-transfer state
cwEDMR	continuous wave EDMR
cwEPR	continuous wave electron paramagnetic resonance
daf	delay after flash
ED-HYSCORE	electrically detected hyperfine sublevel correlation experiment
EDMR	electrically detected magnetic resonance
EPR	electron paramagnetic resonance
EQE	external quantum efficiency
FSE	field-sweep echo
HOMO	highest occupied molecular orbital
ISC	intersystem crossing
ITO	indium tin oxide
li-cwEPR	light induced continuous wave EPR
LUMO	lowest unoccupied molecular orbital
mw	microwave
OPV	organic photovoltaic
OSC	organic solar cell
OSCs	organic solar cells
pEDMR	pulsed electrically detected magnetic resonance
pENDOR	pulsed electron nuclear double resonance
pEPR	pulsed electron paramagnetic resonance
TCO	transparent conductive oxide
trEDMR	transient electrically detected magnetic resonance
trEPR	transient electron paramagnetic resonance

List of Oral and Poster Presentations

Most of the results were presented as oral presentations or poster at different conferences or workshops.

[P FK1] F. Kraffert. "Transient EDMR measurements: Current status". In: *SPP1601 – Young researchers workshop*. **Oral Presentation**. Berlin, 2013.

[P FK2] F. Kraffert, J. Behrends, and R. Bittl. "Spin-polarized charge transfer states studied by trEPR and pEPR". In: *6th EFEPR School on EPR*. **Poster**. Weizmann Institut, Israel, 2013.

[P FK3] F. Kraffert, R. Steyrleuthner, R. Bittl, and J. Behrends. "Photoinduced Charge Transfer States in Polymer:Fullerene Blends probed by Transient EPR". In: *ICEL 10*. **Poster (Prize Winner)**. Köln, 2014.

[P FK4] F. Kraffert and J. Behrends. "Transient EDMR: Recent Progress and Challenges Ahead". In: *SPP1601 Annual meeting*. **Oral Presentation**. Schwerte, 2014.

[P FK5] F. Kraffert, R. Steyrleuthner, R. Bittl, and J. Behrends. "Photoinduced Charge Transfer States in Polymer:Fullerene Blends probed by Transient EPR". In: *CECAM Workshop*. **Poster**. 2014.

[P FK6] F. Kraffert, R. Steyrleuthner, S. Albrecht, D. Neher, M. C. Scharber, R. Bittl, and J. Behrends. "Charge Separation in PCPDTBT:PCBM Blends from an EPR Perspective". In: *Next Generation Organic Photovoltaics II*. **Oral Presentation**. Groningen, Niederlanden, 2015.

[P FK7] F. Kraffert, R. Steyrleuthner, S. Albrecht, D. Neher, M. C. Scharber, R. Bittl, and J. Behrends. "Charge Separation in PCPDTBT:PCBM Blends from an EPR Perspective". In: *Invited Talk Groupseminar S. Stoll*. **Oral Presentation**. Seattle, USA, 2015.

[P FK8] F. Kraffert and J. Behrends. "Transient Electrically Detected Magnetic Resonance Spectroscopy applied to Organic Solar Cells". In: *GDCh FGMR 37th*. **Oral Presentation**. Darmstadt, 2015.

[P FK9] F. Kraffert, R. Steyrleuthner, and J. Behrends. "Transient Electrically Detected Magnetic Resonance Spectroscopy applied to Organic Solar Cells". In: *Hybrid-Photovoltaics 2015 Symposium*. **Oral Presentation**. Berlin, 2015.

[P FK10] F. Kraffert, R. Steyrleuthner, S. Albrecht, D. Neher, M. C. Scharber, R. Bittl, and J. Behrends. "Charge Separation in PCPDTBT:PCBM Blends from an EPR Perspective". In: *FPi 12*. **Oral Presentation**. Seattle, USA, 2015.

[P FK11] F. Kraffert, R. Steyrleuthner, U. Yasin, and J. Behrends. "Transient Electrically Detected Magnetic Resonance Spectroscopy applied to Organic Solar Cells". In: *SPP1601 –Young researcher meeting 2016*. **Oral Presentation** (**Prize Winner**). Konstanz, 2016.

[P FK12] F. Kraffert, R. Steyrleuthner, and J. Behrends. "Simultaneous Detection of Transient Electrically and classical Transient Magnetic Resonance Signals from Organic Solar Cells". In: *Rocky Mountain Conference*. **Oral Presentation**. Breckenridge, USA, 2016.

[P FK13] F. Kraffert, R. Steyrleuthner, and J. Behrends. "Transient EDMR: Recent Progress and Challenges Ahead". In: *SPP1601 Annual meeting Meeting*. **Oral Presentation**. Hirschegg, 2016.

[P FK14] F. Kraffert, R. Steyrleuthner, R. Bittl, and J. Behrends. "Excited States and Charge Separation in Organic Solar Cells studied by Spin-sensitive Techniques". In: *MRS Fall Meeting*. **Oral Presentation**. Boston, USA, 2016.

[P FK15] F. Kraffert, R. Steyrleuthner, R. Bittl, and J. Behrends. "Spin-Correlated Polaron Pairs and High-Spin States in Organic Solar Cells". In: *Joint ISMAR and RMC*. **Oral Presentation**. Québec, Canada, 2017.

Danksagung

An dieser Stelle möchte ich mich bei den Menschen bedanken, die einen besonderen Anteil am Gelingen dieser Arbeit hatten.

Allen voran danke ich Jan Behrends, meinen Betreuer. Zum einem bedanke ich mich für die Möglichkeit in deiner noch junger Gruppe meine Arbeit anzufertigen, zum anderen für das große Vertrauen und die intensive Betreuung, die du mir entgegen gebracht hast. Die vielen Gestaltungsmöglichkeiten, die du mir in den Projekten eingeräumt hast, und die tollen Erfahrungen, die ich auf den zahlreichen Konferenzreisen sammeln durfte, um unsere Forschungsergebnisse vorzustellen, weiß ich sehr zu schätzen.

Ich danke Martin Weinelt für die Bereitschaft das Zweitgutachten zu übernehmen.

Mein besonderer Dank gilt auch Robert Bittl, der meine Masterarbeit betreute und mir somit den Einstieg in die EPR ermöglichte. Seine anregenden Ideen, die konstruktive Kritik an meinen Theorien und sein Enthusiasmus für die Physik ermöglichten es mir erst die oft komplizierten Zusammenhänge der EPR richtig zu verstehen.

Weiterhin danke ich auch allen aktuellen und ehemaligen Mitgliedern der Arbeitsgruppen Bittl und Behrends für die tolle Arbeitsatmosphäre, die großen Hilfsbereitschaft und für die schönen Gruppenfeiern. Ich möchte hier besonders Robert S. danken für die schöne Zeit, die vielen wissenschaftlichen und auch privaten Diskussionen und für das große Wissen über die organische Photovoltaik, das er mir vermittelt hat. Aber auch Christian, Christopher, Ula und Christoph möchte ich hier explizit nennen, ihr ward immer bereit mir zu helfen, wenn ich eine neue Methode lernen wollte oder wir wieder ein Gerät reparieren mussten. Das gemeinsame Tüfftteln war mir stets eine Freude. Danke, Roswitha, Richard und Susanne für die vielen schönen Gespräche und die vielen spannenden Spieleabende, die wir zusammen verbracht haben. Auch danke ich Birgit für die Unterstützung bei der Überwindung der bürokratischen Hürden.

Auch danke ich den vielen Bachelor und Masterstudenten, die meine Doktorarbeit begleitet haben: Christian N., Charlotte, Helen, Kelvin, Audrey, Sebastian, Adrià, Ilia, Johann und Daria.

Mein Dank gilt auch unseren Kooperationspartnern aus der Gruppe von Dieter Neher: Steve Albrecht, Patrick Pingel, Marcel Schubert und Jona Kurpiers; der Gruppe von Alexander Colsmann: Daniel Bahro und Maximilian Dene; der Gruppe von Richard Friend: Leah Weiss und Sam Bayliss und der Gruppe von Klaus Lips, Joscha Nehrkorn und Jannik Möser, sowie Markus Scharber für die gute Zusammenarbeit und die vielen fachlichen Diskussionen die wir miteinander geführt haben. Klaus, vielen Dank für deine Motivation für unsere Themen und deine schön gestalteten Vorträge, von denen ich viel lernte.

Das Entstehen einer Dokotorarbeit ist natürlich auch immer mit vielen Verbesserungen, Korrekturen und konstruktiver Kritik verbunden bei denen mir besonders Katrin, Kai, Kai, Christopher und Sam geholfen haben. Vielen Dank dafür, ohne euch wäre die Arbeit nie so geworden wie sie heute ist.

Abschließend möchte ich noch meiner Familie danken für die Unterstützung während meines Studiums und der Promotion. Das gilt natürlich auch für meine langjährigen Freunde Arne, Kai, Henryk, Julius und ganz besonders dir Katrin, die mich immer wieder motiviert und für viel Spaß fernab der Universität gesorgt haben.

Erklärung

Ich, M. Sc. Ken Felix KRAFFERT, erkläre hiermit, dass die Arbeit mit dem Titel "Charge Separation and Transport in Organic Solar Cells Studied by Electron Paramagnetic Resonance Spectroscopy" von mir selbstständig angefertigt wurde. Ich bestätige,

- dass die Arbeit komplett im Rahmen meiner Promotion an dieser Universität durchgeführt wurde.
- dass ich die Arbeit in keinen anderen Promotionsverfahren eingereicht habe oder hatte.
- dass ich alle wörtlich oder inhaltlich übernommen Textstellen als solche gekennzeichnet habe.
- dass ich keine anderen als die angegeben Hilfsmittel verwendet habe.

Felix Kraffert

Berlin, den 12.04.2018